NONLINEAR DYNAMICS OF REGULAR AND CHAOTIC MAGNETIC FIELDS

By
SUBHA SAMANTA
PHYS05201404009

Saha Institute of Nuclear Physics, Kolkata

A thesis submitted to the

Board of Studies in Physical Sciences

In partial fulfillment of requirements
for the Degree of
DOCTOR OF PHILOSOPHY
of
HOMI BHABHA NATIONAL INSTITUTE

May, 2019

Homi Bhabha National Institute

Recommendations of the Viva Voce Committee

As members of the Viva Voce Committee, we certify that we have read the dissertation prepared by **Subha Samanta** entitled **"Nonlinear Dynamics of Regular and Chaotic Magnetic Fields"** and recommend that it may be accepted as fulfilling the thesis requirement for the award of Degree of Doctor of Philosophy.

N. Chakrabarti — 9th July, 2019

Chairman - Prof. Nikhil Chakrabarti — **Date:**

M. S. Janaki — 9.7.2019.

Guide/Convener - Prof. M. S. Janaki — **Date:**

Animesh Kuley — 9th July, 2019.

Examiner - Prof. Animesh Kuley — **Date:**

S. Mukhopadhyay — 9th July 2019

Member 1 - Prof. Supratik Mukhopadhyay — **Date:**

Sandip Sarkar — 9th July, 2019

Member 2 - Prof. Sandip Sarkar — **Date:**

B. Ghosh — 9/7/2019

Member 3 - Prof. Basudev Ghosh — **Date:**

A N Sekar Iyengar — 9 July 2019

Technology Adviser - Prof. A. N. S. Iyengar — **Date:**

Final approval and acceptance of this thesis is contingent upon the candidate's submission of the final copies of the thesis to HBNI.

I hereby certify that I have read this thesis prepared under my direction and recommend that it may be accepted as fulfilling the thesis requirement.

Date: 9th July, 2019

Place: KOLKATA.

M. S. Janaki

Prof. M. S. Janaki, **Guide**

STATEMENT BY AUTHOR

This dissertation has been submitted in partial fulfillment of requirements for an advanced degree at Homi Bhabha National Institute (HBNI) and is deposited in the Library to be made available to borrowers under rules of the HBNI.

Brief quotations from this dissertation are allowable without special permission, provided that accurate acknowledgement of source is made. Requests for permission for extended quotation from or reproduction of this manuscript in whole or in part may be granted by the Competent Authority of HBNI when in his or her judgment the proposed use of the material is in the interests of scholarship. In all other instances, however, permission must be obtained from the author.

Subha Samanta

DECLARATION

I, hereby declare that the investigation presented in the thesis has been carried out by me. The work is original and has not been submitted earlier as a whole or in part for a degree / diploma at this or any other Institution / University.

Subha Samanta

List of Publications arising from the thesis

Journal

1. "Energization of charged particles in regular and chaotic magnetic fields",
   Subha Samanta, P. K. Shaw, M. S. Janaki, B. Dasgupta, *Physics of Plasmas*, **2017**, *24*, 054506-1—054506-4.

2. "Characterization of magnetic field lines in connection with their transport in Beltrami magnetic fields",
   Subha Samanta, M. S. Janaki, A. K. Ram, B. Dasgupta, *Physics of Plasmas*, **2018**, *25*, 122308-1—122308-7.

3. "Stickiness in double-curl Beltrami magnetic fields",
   Subha Samanta, M. S. Janaki, *Chaos*, **2018**, *28*, 123115-1—123115-8.

4. "Order to chaos transitions in damped KdV equation modeled as a jerk equation",
   Subha Samanta, P. K. Shaw, M. S. Janaki, A. N. S. Iyengar, *Physica Scripta*, **2019**, *94*, 045602-1—045602-9.

Chapters in books and lecture notes

NIL

Conferences

1. **Poster Presentation** at the 30th National Symposium on Plasma Science and Technology, Saha Institute of Nuclear Physics, Kolkata, December 1-4, 2015, "Investigations on chaotic magnetic fields that are obtained as Vlasov-Maxwell equilibria", **Subha Samanta**, P. K. Shaw, M. S. Janaki, A. N. S. Iyengar.

2. **Poster Presentation** at the National Conference on Plasma Physics and Nonlinear Dynamics, JIS University, Agarpara, Kolkata, March 23-24, 2017, "Ener-

gization of charged particles in chaotic magnetic fields", **Subha Samanta**, M. S. Janaki.

3. **Oral Presentation** at Prof. M. R. Gupta Memorial 2nd National Seminar, Jadavpur University, Kolkata, August 3, 2018, "Study of stickiness phenomena in magnetic field lines governed by Beltrami magnetic fields", **Subha Samanta**, M. S. Janaki, B. Dasgupta.

4. **Oral Presentation** at the 3rd Regional Science and Technology Congress, Southern Region, Bidhannagar College, Kolkata, December 18-19, 2018, "Study of stickiness phenomena in magnetic field lines in connection with their transport in Beltrami magnetic fields", **Subha Samanta**, M. S. Janaki.

5. **Oral Presentation** at the West Bengal State Science and Technology Congress, Science City, Kolkata, February 28-March 1, 2019, "Study of stickiness phenomena in magnetic field lines in connection with their transport in Beltrami magnetic fields", **Subha Samanta**, M. S. Janaki.

Others

Nil.

Subha Samanta

ACKNOWLEDGEMENTS

This thesis is a result of four years of work and during this time, I am benefited from many people with whom I came in contact with. First of all, I would like to express my sincere gratitude to Madam, my supervisor, Prof. M.S. Janaki whose contribution spans the entire period of my research work. Without her guidance and assistance, it would have never been possible to complete this thesis. She has given me numerous suggestions, read through my papers, suggested improvements, and corrected the mistakes. Her influence will be felt all over my life.

I want to express my gratitude to the doctoral committee members Prof. Nikhil Chakrabarti, Prof. Supratik Mukhopadhyay, Prof. Sandip Sarkar, Prof. Basudev Ghosh, and Prof. A.N.S. Iyengar for making the yearly evaluation of my work and providing me valuable suggestions regarding this. Besides this, it is always a pleasure to acknowledge all my teachers who influenced my understanding about various subjects that made it possible to carry out the research work. I have learned equally extensively through discussions with my friends and seniors over the years and I am grateful to all of them. Finally I extend my heartiest thanks to all the members of Plasma Physics Division who have made my research days enjoyable.

Contents

Summary

Magnetic fields play an important role in a wide variety of astrophysical and laboratory plasmas. Observations indicate that such fields exist in regular as well as chaotic states with scale lengths ranging from small to large values.

The thesis describes the dynamical behavior of regular and chaotic magnetic fields by studying the properties of chaotic magnetic field lines in the context of three dimensional Beltrami magnetic fields as well as the diffusion characteristics of field lines and charged particles in presence of such fields. Many coupled nonlinear equations describing magnetic fields in plasmas exhibit chaotic solutions under certain conditions. Energization of charged particles by external electric fields in presence of chaotic magnetic fields forms another subject of study in this thesis. A well known equation describing the nonlinear evolution of magnetic fields is the KdV equation. The conditions under which the KdV equation gives rise to chaotic solutions is also explored in the thesis.

Three dimensional Beltrami fields constitute simple models for the magnetic fields exhibiting chaotic field lines with regular field strengths. The phase space of some configurations of Beltrami magnetic fields consist of some islands embedded into the chaotic sea, whereas the field lines for certain profiles of Beltrami magnetic fields are chaotic over the entire space. The islands in the phase space cause dynamical trapping of the chaotic trajectories so that the field lines stay around such flux tubes for a long time. This phenomena is called stickiness which is characterized by various statistical properties like distribution of a chaotic field line in the spirit of central limit theorem, distribution

of finite distance Lyapunov exponents, recurrence length statistics etc. Moreover, in a mixed phase space, the indication of long coherent displacements is observed. The presence of islands in the phase space has profound implication on the transport of chaotic field lines which is found to be anomalous rather than usual normal or Gaussian diffusion which happens in most cases of random fluctuations.

Regular and chaotic magnetic fields in which the fluctuations are transverse to a locally uniform mean magnetic field and vary only in the direction along that mean field have been considered in the present thesis to study the energization of charged particles in presence of an external electric field. Here, the fluctuating magnetic fields are obtained from coupled nonlinear equations varying in one dimension. Such study reveals that the energy gain of an ensemble of charged particles decreases with the increase in the RMS values of fluctuation when the overall profile of the chaotic magnetic field changes. On the other hand, the same increase in RMS values by changing the amplitude of fluctuation for inhomogeneous regular magnetic fields leads to an increase in energy gain.

Finally the dynamical properties of regular and chaotic magnetic fields are studied considering a KdV equation in presence of dissipative effects. Under the traveling wave ansatz, the equation can not be reduced to a second order one and hence it is treated as a third order ordinary differential equation known as the jerk equation. The key finding of this study points to the existence of chaotic solutions for left moving traveling waves.

List of Figures

CHAPTER 1

Introduction

1.1 Study of magnetic fields in plasma

Plasma is a complex system consisting of a large number of interacting particles. The charged particles in a plasma generate electric and magnetic fields. These internally created fields together with the externally applied fields govern the behavior of a plasma. So magnetic fields form an important part of plasmas. There are various approaches for the theoretical description of plasma behavior. When the plasma density is very low such as can be found in cosmic rays, solar corona etc., the single particle theory can be used for predicting the plasma behavior. In this approach, the motion of each charged particle is studied in presence of specified fields. Although this theory is very much simple, it provides some insight that helps to understand the plasma phenomena. For high density plasmas, the study of single particle motion becomes impractical because to get an understanding of plasma behavior, actually one needs to solve a self-consistent problem in which the particles generate fields and the fields cause the particles to move. It is observed that the majority of plasma phenomena can be explained by the model of fluid theory. In this method, the plasma is considered as a mixture of two or more fluids depending on the number of species present in a plasma. Now we neglect the identity of individual particle and consider only the motion of each fluid element. In contrast to the ordinary fluid in which collisions control the fluid behavior, plasma behavior is dominated by the long range effects due to the electromagnetic forces. The fluid equations based on conservation of mass, momentum and energy together with Maxwell's equations can provide a self-consistent description for the plasma phenomena. In the study of macroscopic equilibrium and stability of a plasma, the length and time scales associated with the underlying phenomena are large compared to the Debye length and the time scale of ion dynamics respectively. In such cases the whole plasma can be considered as a single fluid and the corresponding model is known as magnetohydrodynamics (MHD). Besides the long wavelength and low frequency phenomena described by the single fluid MHD theory, in some situations, the ion dynamics dominates in a two fluid electron-ion plasma and such situations are handled by making the assumption of zero mass for the electrons while keeping the mass of the ions finite. This approximation is called Hall-magnetohydrodynamics (Hall-MHD) approximation. On the other hand, the electron dynamics dominated situations are handled by assuming the ion mass infinite but the electron mass finite. Such approximation leads to another model known as electron-magnetohydrodynamics (EMHD) model.

Many magnetic configurations in plasmas can be obtained as a result of self-organization [1] which is the spontaneous generation of coherent structures in complex systems. Equilibrium magnetic field in several plasma environments has been postulated as a result of relaxation process that leads to the so-called Taylor's minimum energy relaxed state [2] given by $\nabla \times \mathbf{B} = \lambda \mathbf{B}$. Later, the idea of self-organization gave rise to a lot of other magnetic configurations that are obtained from alternative relaxation models [3,4] other than that of Taylor. Such magnetic fields are eigenfunctions of double or higher curl operator. The relaxed states emerge from standard variational principles [5] for fluid models.

Several phenomena in plasmas can be explained considering plasma equilibria. Although many equilibrium magnetic field configurations can be explained in the framework of fluid theory, in some cases it is found to be inadequate. The processes with time scales much shorter than the collision times require a different description of plasma in terms of kinetic theory based on the concept of single particle distribution function. When collisions are neglected and the plasma is described by the self-consistent electromagnetic fields, the distribution functions satisfy a partial differential equation known as Vlasov equation. Stationary solutions of Vlasov equation for a magnetized plasma can be constructed by choosing functions that depend on the invariants of single particle motion. A well-known equilibria obtained from the Vlasov equation is the Harris current sheet [6] whose magnetic field profile shows tangential discontinuities. Certain combination of invariants of single particle motion chosen as steady state solution describing the Vlasov-Maxwell equilibria, can lead to coupled nonlinear differential equations governing the evolution of magnetic fields [7]. Vlasov-Maxwell equilibrium solutions contain exponential Maxwellian distribution function multiplied by other chosen functions of constants of motion. The evolution equation of magnetic fields are obtained from the relations between the current and the vector potential.

A plasma system is associated with various waves and instabilities. The study of small amplitude waves in plasmas can be performed using linear perturbation theory in which we assume the variations in plasma parameters in presence of waves to be much smaller than the undisturbed parameters. Linear phenomena can be described by equations in which dependent variable appears in first power only. But in many experiments, the observed phenomena can not be described by a linear theory. In the fluid description of a plasma, the set of electron and ion equations together with Maxwell's equations enables to cast the magnetic field equations in the form of nonlinear equations. However, one of the extensively treated popular nonlinear equations to deal with propagation of weakly nonlinear waves is the Korteweg-de Vries (KdV) equation. The KdV equation with its well known soliton solution was originated to represent water waves. Soliton is a localized structure that maintains its shape while it propagates at a constant velocity. KdV equation can be derived based on various approaches of fluid theory and the soliton can explain the formation of localized concentrations of magnetic fields in a plasma. Formation of nonlinear structures in magnetic fields is frequently observed in many space plasma environments like planetary magnetosheaths, cometary environments, interplanetary coronal mass ejections etc. Examples are magnetic holes with significant magnetic field reduction or a magnetic field upsurge, opposite to the magnetic hole. The local formation of the small-scale magnetic structures can be explained using KdV equation. Later various modifications of KdV equation have been derived such as the modified KdV, KdV-Burgers (KdVB) equation etc. to model different physical phenomena in various branches of science. For example, plasma shock wave which is a popular nonlinear phenomenon can be obtained as a solution of KdV-Burgers equation.

Magnetic fields originating in a plasma can be described by solutions of various linear and nonlinear equations. Such solutions can exhibit regular or chaotic behavior. In the following sections, we present a brief description of various magnetic fields that are considered in the present thesis.

1.1.1 The Beltrami magnetic fields

Magnetic fields in regions of low plasma pressure and large currents are force-free in the sense that Lorentz force vanishes. The study of force-free magnetic fields originates from astrophysics. Lüst and Schlüter [8] initially pointed out that cosmic magnetic fields might be force-free. In plasma regions of high electrical conductivity, large currents may flow. The prevailing pressure gradients or gravitational or inertial forces cannot balance a Lorentz force that arises from such current flow [9, 10]. Consequently, the Lorentz force vanishes which constraints the current to flow parallel to the magnetic field. The force-free magnetic field obeys

$$\nabla \times \mathbf{B} = \lambda \mathbf{B} \tag{1.1}$$

where λ is in general an arbitrary function of position. The corresponding situation is the Beltrami flow [11] where the vortex field is parallel to the velocity field everywhere. For turbulent flows, some numerical simulations [12] and experimental observations [13] indicate that in certain regimes, the velocity and vorticity vectors have a tendency to align. Consequently among various chaotic flows, Beltrami flow has attracted special attention by various researchers.

Equation (1.1.1) for arbitrary λ, appears as a MHD force balance condition in equilibrium under low beta situation i.e. when plasma kinetic pressure is much smaller than the magnetic pressure. The class of force-free Beltrami magnetic fields with constant λ has been studied extensively in many publications. Such fields can be obtained from a variational principle that minimizes magnetic energy of a closed system keeping the magnetic helicity constant [14]. Chandrasekhar [9] presented the solution to equation (1.1.1) in terms of the Bessel functions when $\mathbf{B}$ has a symmetry about an axis and when λ is constant. Studies of force-free fields on different domains in $\mathbb{R}^3$ were reported in various works [15–17] that use representation of Beltrami fields in terms of Bessel and Legendre functions. Magnetic fields in different astrophysical and laboratory plasma environments such as coronal-arcades [18], twisted magnetic flux ropes through the coronal mass ejections [19], reversed-field pinches [2] and spheromaks [15] can be described by the solutions of single curl force-free equation under assumption of various symmetries.

In three dimensional $(3-D)$ Cartesian coordinate system, the solution of linear single curl Beltrami equation with constant λ is exactly known. The class of solutions is commonly referred to as Arnold-Beltrami-Childress (ABC) field [20] which is a well known helical steady solution of Euler equations for ideal incompressible flows.

But structures obtained as solutions of the single curl force-free equation suffer from several limitations. They are incapable of describing states with high plasma beta or the formation of fusion related topologies such as tokamaks and field-reversed configurations. So, the force-free states have limited interest in fusion, since significant plasma pressure is needed in a practical system. Besides, force-free states appear experimentally only in certain arrangements like reversed-field pinch and spheromak. The need for describing a wide class of magnetic fields in plasmas where the current is not aligned with the magnetic field or the plasma beta is high enough necessitates to extend the search for the alternative models of magnetic fields. The simplest model that describes non force-free magnetic fields is the double curl Beltrami equation. Chandrasekhar [10] first proposed the double curl equation in the form

$$\nabla \times \nabla \times \mathbf{B} = \Lambda \mathbf{B} \tag{1.2}$$

with constant Λ, in the context of dissipative plasmas where the system is driven to a state of minimum dissipation under conditions of constant magnetic energy. The nature of the double curl equation indicates that for the double curl magnetic fields, the Lorentz force cannot vanish. Besides the double curl equation given in equation (1.2), more general double curl equation [21] was derived later considering the strong coupling of the fluid kinetic and magnetic aspects of the plasma. The general double curl equation is given by

$$\nabla \times \nabla \times \mathbf{B} + \alpha \nabla \times \mathbf{B} + \beta \mathbf{B} = 0 \tag{1.3}$$

where α and β represent arbitrary complex numbers. Double curl equation can help to model high-pressure confining, highly compact magnetic configurations in the laboratory that are currently deriving lot of attention.

Various aspects of Beltrami fields have been studied in the existing literature. But most of the solutions are obtained by exploiting various symmetries of the configurations to model different realistic systems. Linear Beltrami equations admit exact solutions in $3-D$ Cartesian coordinate system. Now, field lines are the most useful graphical tool for the representation of field strength distributions. The field lines for $3-D$ Beltrami fields exhibit chaotic behavior and their characteristics are studied in the present thesis. This is important in connection with the transport of the field lines and has not been paid much attention till now.

1.1.2 Regular and chaotic magnetic fields governed by coupled nonlinear equations

Nonlinear equations can give rise to a variety of magnetic configurations showing periodic as well as chaotic behavior. Although some nonlinear equations admit analytical solution which can be expressed in terms of known standard mathematical functions, in most of the cases we need to invoke numerical procedure. For collisionless plasmas, magnetic field fluctuations can be governed by simple coupled nonlinear equations varying in $1-D$. Depending on the parameter of the equations, the inhomogeneous magnetic fields obtained from such equations can show either regular or chaotic behavior.

In the present thesis, we consider the description of regular and chaotic magnetic fields obtained by solving coupled nonlinear equations numerically. Then energization of charged particles is studied in presence of such regular and chaotic fields varying in $1 - D$ in presence of a constant electric field.

1.1.3 Regular and chaotic magnetic fields obtained from KdV type equation

The well-known KdV equation is given by

$$u_\tau + uu_\xi + u_{\xi\xi\xi} = 0 \tag{1.4}$$

where $u = u(\tau, \xi)$, with u, τ, ξ being real variables. u represents the amplitude of the fluctuation and τ and ξ denote time and space like variables respectively. The subscript denotes the derivative with respect to the variable.

The modeling of various physical phenomena in many practical situations requires a modification of the KdV equation to include terms arising due to the presence of dissipative effects in the medium or due to an external perturbation. Such additional terms modifying the KdV equation occur in the context of fluid dynamics [22] or plasmas in the form of viscous or collisional effects [23]. Weakly nonlinear dispersive waves in presence of viscous damping can be modeled by KdVB equation

$$u_\tau + uu_\xi + u_{\xi\xi\xi} + \nu u_{\xi\xi} = 0 \tag{1.5}$$

where ν is a real parameter.

Both KdV and KdVB equation can be treated as second order ordinary differential equations considering traveling wave solution that depends on $\xi - v\tau$,with v representing the velocity of propagation of the disturbance.

In presence of dissipative effects represented by a Burger and a linear term, the KdV equation

$$u_\tau + uu_\xi + u_{\xi\xi\xi} + \nu u_{\xi\xi} + \alpha u = 0 \tag{1.6}$$

should be treated as a third order ordinary differential equation under consideration of traveling wave solution. The linear term involving α destroys the possibility of reducing the equation to a second order one, as is done conventionally. Now, the simplest ordinary differential equation in single variable that is capable of exhibiting chaos is a third order equation.

In the present thesis, it is observed that the third order ordinary differential equation obtained from equation (1.6) with suitable choice of parameters can give rise to chaos for a left moving traveling wave. Nonlinear fluctuations in a plasma may be associated with chaotic magnetic fields which can be obtained from KdV equation in presence of Burger and a linear term.

1.2 Methods and statistical properties used for the description of magnetic fields

To characterize the behavior of magnetic fields, we make use of various methods and calculate several quantities which are mentioned briefly in the following sections. We will discuss their applicability in the respective situations.

1.2.1 Poincaré surface of section

Global properties of any system can be predicted by plotting Poincaré sections. For a space with dimension higher than *two*, the trajectories are complex and it is hard to see if they have any regularity or not. Interesting information about the motion can be obtained by finding a way to sample the trajectories in lower dimensions by exploiting the constants of motion and studying the points where the trajectories pass through some plane. This plane is known as Poincaré section.

1.2.2 Lyapunov exponent

In case of chaotic dynamics, the trajectories must exhibit sensitive dependence on initial conditions. Then two nearby trajectories starting very close together will rapidly diverge from each other, making their futures totally different. The exponential divergence of two initially close trajectories, which is one characteristic of chaotic dynamics, is quantified by Lyapunov exponents. For an N dimensional system, there are N different Lyapunov exponents. We consider only the largest Lyapunov exponent, since it represents the dominant divergence rate. There are two different sets of Lyapunov exponents: one is finite time Lyapunov exponent which is calculated after a short time of evolution of a trajectory and the other one is asymptotic time Lyapunov exponent which requires a much longer time of evolution of the trajectory for its evaluation.

1.2.3 Probability distribution

Probability distribution gives a clear description of any statistical event by providing the probabilities of occurrence of different possible outcomes of a random phenomenon, i.e., the observed set of all possible outcomes of an event specify the distribution function. A distribution may consist of a single peak or two or more peaks. Single peak indicates that a particular outcome appears most often which implies the uniformity of any dynamics. On the other hand a bimodal distribution consisting of two peaks indicates the existence of two different types of dynamics in a system. Sometimes a distribution has a long tail with a significant number of occurrences far from the central part of the distribution. The long tailed distribution suggests many important aspects of the dynamics of a system.

1.2.4 Fourier transform

The Fourier transform of any function of an independent variable enables us to observe the corresponding representation in the inverse domain of that independent variable. The presence of discrete peaks in the Fourier spectrum indicates that the system dynamics is regular, while a broadband structure in the spectrum implies chaotic dynamics.

1.2.5 Recurrence statistics

Recurrence time is the time interval between two consecutive moments when a system visits a particular state. The distribution of all such times serves as an excellent test to understand the global behavior of the system. In case of random dynamics, all the recurrence times are of the same order and the set of recurrence times exhibits a rapidly decaying distribution. On the other hand, if the system involves some coherent dynamics associated with memory effect, the recurrence time distribution consists of a long tail.

1.2.6 Variance

Variance gives a measure of the spread of a set of random numbers away from their average or mean value and based on the second central moment of a distribution. This quantity plays a key role in statistics. The study of diffusion characteristics of any entity can be performed by computing the variance of associated displacements considering an ensemble of that entity. In order to get a quantitative idea about the nature of diffusion, the numerically calculated variance is to be fitted with the transport law $\sigma^2 \sim t^\alpha$, where σ^2 represents variance and t is the independent variable of the system. The exponent α characterizes the random walk law of the entity under consideration. Gaussian diffusion corresponds to $\alpha = 1$, whereas for anomalous diffusive regime, $\alpha \neq 1$ with $\alpha < 1$ in case of subdiffusion and $\alpha > 1$ in case of superdiffusion.

1.2.7 Kurtosis

In statistics, kurtosis is another important quantity that provides a description of the shape of a probability distribution and is a measure of the 'tailedness' of the distribution of random variables. Computation of kurtosis is based on the fourth moment of the data. The diffusion characteristics of an entity as obtained by computing the variance, can be evidenced by calculating the kurtosis.

1.2.8 Linear stability analysis

For nonlinear systems, the possibility of finding the trajectories analytically is quite small. In such cases, first we find the equilibrium or fixed points where the flow of the system is zero and then analyze the stability of the equilibrium points. The classification of the fixed points can be made easily on determining the eigenvalues of the corresponding Jacobian matrix at the fixed point. In order to know the nature of the trajectories near these equilibria, we approximate the trajectories near the fixed points by that of a corresponding linear system.

1.2.9 Bifurcation diagram

To visualize the long term behavior of a system for all values of associated parameters, specially to detect the period doubling bifurcation of the system, we plot bifurcation diagram. Bifurcation is the change in the qualitative structure of the dynamics of a system and in a period doubling bifurcation, slight change in the system's parameter value leads the system to switch to a different behavior in which the period of the system is doubled. When the period of a system get doubled, the system repeats itself after twice as many iterations as before. The bifurcation diagram is a magnificent picture and an icon of nonlinear dynamics. This diagram shows the characteristic values (e.g. the local maxima or minima of oscillation) of a system as a function of bifurcation parameter when the system approaches asymptotically to its eventual behavior for each parameter values. A single point in the bifurcation diagram for a particular value of the parameter indicates that the attractor has a single period. At some parameter value, the single branch get split into two branches indicating a period doubling bifurcation. Then each branches for the two period cycle split simultaneously, yielding a four period cycle and a cascade of period doubling bifurcations occurs so on as the value of the parameter increases. Finally the number of points for a parameter value becomes infinite and the system becomes chaotic.

1.3 Dynamics of magnetic field lines in the context of Beltrami fields

Magnetic field lines are tangential to the magnetic field at any spatial point. In general magnetic field lines are determined by the equations of a $3-D$ dynamical system. The equations governing the evolution of magnetic field lines of Beltrami fields are nonlinear in nature. The force-free equation is known to have non-integrable field lines [24, 25] in $3-D$ for constant values of λ independent of space. The streamlines corresponding to the ABC flows have a complicated Lagrangian structure that has been studied by Dombre et al. [26] with dynamical system tools. When one of the coordinates becomes cyclic, the field lines become integrable. Evolution of magnetic field lines following the double curl equation was also observed to be non-integrable. It was observed that while the phase spaces of ABC fields show a mixture of regular and chaotic regions, certain solutions of double curl equation reveal a phase space that is totally chaotic [27].

To explore the long term behavior of the magnetic field lines, it is meaningful to study their diffusion characteristics that preserve the full nonlinear properties of the field line equations. One of the areas in which the transport properties of magnetic field lines has received the most attention in past years is turbulence. In any real system, turbulent magnetic fields may coexist with a large scale mean field. Different transport regimes for the field line motion can be obtained depending on the strength of the fluctuations compared with the mean field. Because of random fluctuations in the magnetic fields, adjacent field lines random walk away from each other [28]. Theoretical concepts of field line random walk [29, 30] have been developed considering the magnetostatic turbulence to be much weaker than the large-scale mean field [31] or for the transverse turbulence [32, 33] with fluctuations being perpendicular to the unperturbed field. Zimbardo et al. [34, 35] have numerically studied the transport properties of magnetic field lines in $3-D$ turbulent magnetic fluctuations in presence of a uniform magnetic field for a wide range of fluctuation level. Such study reveals that at low or moderate fluctuation levels, the system exhibits weak chaos accompanied by closed magnetic surfaces and the transport is anomalous where mean square displacement follows a nonlinear relationship in evolution parameter. With increase in fluctuation levels, stochastic behavior increases and the transport approaches Gaussian diffusion in which mean square displacement is proportional to the independent variable. The existence of different transport regimes and the transitions between them is therefore closely related to the stochastic behavior of magnetic field lines.

Sometimes it may be of interest to study the dynamics of field lines and the nature of their transport in a situation where the magnetic fields are deterministic. Field line equations of deterministic Beltrami fields being non-integrable in $3-D$ have some similarities with that of turbulent magnetic fields. Diffusion characteristic of the field lines of ABC magnetic field was studied by Ram et al. [36] revealing that the transport in $3-D$ chaotic magnetic fields is sometimes different from the usual ordinary diffusion. Field lines of ABC field are seen to undergo superdiffusion in space. This anomalous transport property of chaotic field lines leads to the necessity of characterizing the behavior of single field lines.

In the context of diffusion of charged particles in turbulent magnetized plasma, an important issue was to understand the change in the transport properties when the level of magnetic turbulence is increased [37, 38] and also when the mean field vanishes. In the light of such studies, another pertinent question would be to study the diffusion characteristics of field lines when the mean field is much smaller [39] or zero [40] and much larger than the amplitude of fluctuation.

The Poincaré section for the magnetic field lines of ABC flows, consists of islands of regular field lines embedded into the chaotic sea [26]. The dynamical behavior of the field lines can be characterized by monitoring the largest Lyapunov exponents (LLE). Exploring the dependence of the LLE on the initial conditions of the system, one can identify the areas with different dynamical behavior in phase space, i.e. where the dynamics is chaotic, and those showing regular, periodic or quasiperiodic dynamics. The regular islands in the phase space cause dynamical trapping [41] of the chaotic trajectories so that the field lines stay around such flux tubes for a long time. This phenomena is called stickiness which can be characterized by various statistical properties like probability distribution of a chaotic field line in the spirit of central limit theorem, probability distribution of finite distance Lyapunov exponents, recurrence length statistics etc. Moreover, in a mixed phase space, sometimes there is indication of long coherent displacements which can be detected by the long tails in the displacement probability distribution. The presence of nonchaotic islands in the phase space has profound implication on the transport of chaotic field lines which is found to be anomalous rather than usual normal or Gaussian diffusion which happens in most cases of random fluctuations.

Characteristics of a chaotic trajectory has been studied extensively in the context of standard map which is a convenient model for studying chaotic behavior of Hamiltonian systems. A chaotic trajectory moving in a mixed phase space has parts that are almost regular. The characteristics of such trajectories are quite different from that moving in a completely chaotic phase space. The phenomena of stickiness and its impact on transport properties of a system have been extensively studied in the context of area preserving maps [42–47]. Various techniques such as finite time Lyapunov exponent, distribution of a trajectory, recurrence time statistics have been employed for this purpose. Szezech et al. [48] have studied the finite time Lyapunov spectrum for chaotic orbits of non-integrable Hamiltonian systems. Zaslavsky and Tippet [49] have shown that the transition from normal to anomalous transport is accompanied by a corresponding change of the distribution of recurrence time statistics from exponential to power law.

1.4 Dynamics of charged particles

The properties of magnetic field lines influence the behavior of magnetized particles. The motion of charged particles in complex magnetic fields exhibit interesting dynamical properties. In spatially homogeneous magnetic fields, charged particles gyrate about the magnetic field lines. But in spatially inhomogeneous magnetic fields, particle orbits drift off the field lines because of gradient and curvature drifts [50]. Also, the variation of magnetic field strength along a field line causes reflection of the particles from regions of higher field strength to the regions of lower field strength. These effects cause significant differences between the dynamics of field lines and the motion charged particles in such magnetic fields. The dynamics of charged particles can be chaotic even in regular magnetic fields [51]. The equations describing charged particle motion in a magnetic field form a Hamiltonian system. A Hamiltonian system with N degrees of freedom is integrable if and only if there exist N constants of motion that are in involution. A nonzero value of the Poisson bracket for any one pair of constants of motion leads the system to possess nonintegrable stochastic orbits. However, in a chaotic magnetic field, the most important feature of particles is their spatial diffusion across the ambient large scale magnetic field. The concept of perpendicular particle diffusion via collisions is the most evident notion and can be easily understood if collisions between the charged particles and the neutral atoms in a plasma are taken into account. However chaotic magnetic field lines also lead to diffusion of charged particles across the large scale field. In presence of uniform magnetic fields, charged particles perform helical motion around the field direction and they are completely confined in the perpendicular direction. But the presence of chaotic field lines causes the particles to experience perpendicular scattering. Such scattering leads to the perpendicular diffusion of charged particles.

The study of the dynamics of charged particle motion in complex electric and magnetic fields is interesting owing to its relevance in the acceleration of particles in many space and laboratory plasma systems. Investigation of charged particle transport and acceleration in a $2-D$ system with a uniform electric field and stationary magnetic fluctuations has been carried out by Shustov et al. [52], to obtain the dependence of transport and acceleration on properties of magnetic field fluctuations. The motion of charged particles in the vicinity of magnetic null configurations that are solutions of kinetic steady state, resistive MHD equations have been investigated by Gascoyne [53] to understand the role of sheared and torsional magnetic fields on particle motion and energization. Cohen et al. [54] have studied the role of chaotic orbits in field reversed configurations in ion heating by application of rotating magnetic fields. The spatial diffusion and energization of charged particles in ABC type magnetic fields have been investigated [55] to show that for an initial distribution of particles whose velocity is uniformly distributed within some interval, the probability density function of kinetic energy at late times is close to a Gaussian with steeper tails. The study of charged particle acceleration in various descriptions of electromagnetic fields motivates the search for charged particle energization in a uniform electromagnetic field together with stationary inhomogeneous magnetic fluctuations that can be obtained from simple nonlinear equations.

1.5 Organization of the thesis

The thesis describes the dynamical behavior of regular and chaotic magnetic fields. In chapter 2, we study the characteristics of magnetic field lines in connection with their transport properties considering $3-D$ solutions of single and double curl Beltrami equations. Global qualitative properties of magnetic field lines are observed by plotting Poincaré sections and the study of characterization of single chaotic field line involves various statistical properties like probability distribution of a chaotic field line, distribution of finite distance Lyapunov exponents, recurrence length statistics etc. Chapter 3 consists of the study of the dynamics of magnetic field lines of a double curl Beltrami field in presence of a uniform magnetic field. In this chapter, the chosen solution of double curl equation is different from that presented in chapter 2. In presence of a uniform magnetic field, the most relevant study consists of the search of diffusion characteristics perpendicular to the mean field. The study of diffusion properties of the field lines is extended in chapter 4 taking the same magnetic field configuration as in chapter 3. Here, the characteristics of the chaotic trajectories are studied through the statistical properties like variance, kurtosis, and probability distribution of their displacements followed by the numerical results revealing the effect of field line transport on the diffusion of charged particles. Now, we consider different description of magnetic fields obtained from nonlinear equations. Such description can lead to magnetic fields (varying in $1-D$) that are chaotic in magnitude unlike $3-D$ Beltrami magnetic fields that are regular in strength. In chapter 5, we choose a simple coupled nonlinear equation for the description of magnetic fields and study the dynamics of charged particles addressing their energization in presence of a constant electric field. Then, we study the dynamical aspects of magnetic fields governed by KdV type equation in chapter 6. The KdV equation in presence of a Burger and a linear term can give rise to chaotic solutions for suitable choice of parameters and the left moving traveling wave solutions of the equation are studied numerically using bifurcation diagram, Lyapunov exponents etc. Finally, in chapter 7, we conclude with a discussion of the results obtained in the thesis.

CHAPTER 2

The Beltrami magnetic fields: Characterization of field lines in connection with their transport

In this chapter, we introduce Beltrami magnetic fields to deal with various dynamical properties of the magnetic field lines. After presenting the solutions of single and double curl Beltrami equations in $3-D$ Cartesian coordinate system, the spatial evolution pattern and diffusion of magnetic field lines governed by these fields will be shown. Subsequent sections of the present chapter consist of the study of characterization of single chaotic field lines of two different magnetic fields by various statistical properties like probability distribution of a chaotic field line in the spirit of central limit theorem, distribution of finite distance Lyapunov exponents, recurrence length statistics etc.

2.1 Introduction

Many magnetized plasma configurations in laboratory as well as astrophysical environments shape into existence out of turbulent fluctuations through free relaxation mechanisms that help the system to get rid of its excess energy. Evidence of relaxation has been found in many laboratory plasmas, starting from the pinch experiments of early days to fusion devices such as reversed field pinches, spheromaks, field reversed configurations, sawtooth relaxation in tokamak plasmas. In space and astrophysical plasmas, the magnetic topologies owe their existence to self-organization and reconnection events that leave their footprints in various observed phenomena.

The study of self-organization and relaxation in magnetohydrodynamic plasmas originated in the work of Woltjer [14] who derived the following Beltrami condition

$$\nabla \times \mathbf{B} = \lambda \mathbf{B} \tag{2.1}$$

by invoking an intuitively obvious variational principle of minimizing magnetic energy. In equation (2.1), λ playing the role of Lagrange multiplier, is a scalar field satisfying $\mathbf{B} \cdot \nabla \lambda = 0$ since $\mathbf{B}$ is a solenoidal field. While deriving equation (2.1), Woltjer considered an ideal MHD plasma, wherein the local magnetic helicity $\int \mathbf{A} \cdot \mathbf{B} dV$ associated with each flux tube is a conserved quantity. For a low-beta plasma, where forces due to plasma pressure can be neglected, and flows are absent, equation (2.1) is also the MHD force-balance condition in equilibrium. The inhomogeneous nature of λ, brings in dependence on initial conditions, so that equation (2.1), when obtained under conditions of infinite plasma conductivity, is not in confirmation with the properties of relaxed states. Taylor [2, 56] resolved this inconsistency, by introducing a variational principle for a slightly resistive plasma, wherein all the local helicity constraints relax, leaving only the global helicity to serve as a constraint in the minimization of magnetic energy. Relaxed states [57] obtained by such minimization satisfy $\nabla \times \mathbf{B} = \lambda \mathbf{B}$, where now λ is a constant. Such

Beltrami states, also called Woltjer-Taylor states, have the property that their existence is independent of the initial conditions.

The paradigm of understanding relaxed states in a plasma through variational principles was extensively extended by Mahajan and his coworkers over a series of papers [5, 21, 58–60] spanning over various MHD models, multifluid plasmas including relativistic fluids leading to double, triple and multi-Beltrami states.

Recent works on magnetofluid unification using the minimal coupling prescription of incorporating the electromagnetic fields in particle dynamics have extended the scope of force-free fields. The dynamics of hot relativistic charged fluids in electromagnetic fields is described by the unification of flow field and the electromagnetic fields [61]. New concepts of force-free fields arise for homentropic fluids upon using such unified magnetofluid fields. Following the ideas of magnetofluid unification, a new electro-vortical field has been constructed [62] that unifies all macroscopic forces into a single grand force that is the weighed sum of electromagnetic and the inertial/thermal forces. In the context of all these models, it is possible to delineate a whole class of solutions of magnetic fields and flows that can appropriately describe various physical systems. The double and higher Beltrami states also can be shown to be force-free states if one considers generalized forces.

The simplest among the several higher curl Beltrami equations, developed to describe relaxation in a magnetofluid, is the double curl equation,

$$\nabla \times \nabla \times \mathbf{B} + \alpha \nabla \times \mathbf{B} = \Lambda \mathbf{B} \tag{2.2}$$

This two-parameter, double curl system of equations can describe the equilibrium magnetic (velocity) field in an ideal coupled magnetofluid [21]. In a two-fluid plasma, equation (2.2) also arises [5] through a mathematically well-posed variational principle by minimizing enstrophy with the constants of motion adjusted through a weakly dissipative process. The double Beltrami states of a two-fluid plasma are capable of capturing small scales [63] that plays an important role in various phenomena such as coronal heating [64]. The conventional force-free field equation $\nabla \times \mathbf{B} = \lambda \mathbf{B}$ is a special case of the above equation with $\alpha = 0$ and $\Lambda > 0$. The general solutions of force-free equation in $3-D$ with constant λ are known as Arnold-Beltrami-Childress (ABC) fields [24,25]. For constant values of λ, α and Λ, both single and double curl equations are linear, so that the solutions of the latter can be written as a linear superposition of the ABC fields. The general and richer double Beltrami system allows a much wider class of solutions that are qualitatively different from the constant-λ single-Beltrami magnetic fields besides also containing the solutions of the single curl equation as a subset.

2.2 Arnold-Beltrami-Childress (ABC) Magnetic fields

For constant λ, the ABC solutions of equation (2.1) in Cartesian coordinate system can be written as

$$B_x = A_1 \sin \lambda z + C_1 \cos \lambda y$$

$$B_y = B_1 \sin \lambda x + A_1 \cos \lambda z$$

$$B_z = C_1 \sin \lambda y + B_1 \cos \lambda x \tag{2.3}$$

where λ is interpreted as the eigenvalue of the curl operator and signifies a length scale over which the B-fields vary appreciably. The solution of equation (2.2) can be written as a linear superposition of the above solutions and is given by

$$B_x = A_1 \sin \lambda_+ z + C_1 \cos \lambda_+ y + A_2 \sin \lambda_- z + C_2 \cos \lambda_- y$$

$$B_y = B_1 \sin \lambda_+ x + A_1 \cos \lambda_+ z + B_2 \sin \lambda_- x + A_2 \cos \lambda_- z$$

$$B_z = C_1 \sin \lambda_+ y + B_1 \cos \lambda_+ x + C_2 \sin \lambda_- y + B_2 \cos \lambda_- x \tag{2.4}$$

where $\lambda_\pm = [-\alpha \pm \sqrt{\alpha^2 + 4\Lambda}]/2$ and $A_1, B_1, C_1, A_2, B_2, C_2$ are arbitrary constants. The values of $\lambda_\pm$ vary with the variation in the parameters α and Λ and can take both real and complex values. In the present work, we choose only real values of $\lambda_\pm$.

Magnetic field lines are tangential to the magnetic field $\mathbf{B}(\mathbf{r})$ at any spatial point $\mathbf{r}$. The field line equations are thus obtained as [36],

$$\frac{d\mathbf{r}}{ds} = \frac{\mathbf{B}(\mathbf{r})}{|\mathbf{B}(\mathbf{r})|} \tag{2.5}$$

where $\mathbf{B} = B_x\hat{\mathbf{i}} + B_y\hat{\mathbf{j}} + B_z\hat{\mathbf{k}}$, $\mathbf{r} = x\hat{\mathbf{i}} + y\hat{\mathbf{j}} + z\hat{\mathbf{k}}$, $|\mathbf{B}(\mathbf{r})|$ is the magnitude of $\mathbf{B}$ and s is the length along the field line.

To integrate equation (2.5) numerically, dimensionless variables are used where distances are normalized by constant λ for the single curl field and by constant λ_+ for the double curl field. Magnetic field $\mathbf{B}$ is normalized by a constant magnetic field B_0'. A specially significant situation for ABC field is the case with zero value of one of the three real parameters A_1, B_1 or C_1. In this case, the ABC magnetic field does not depend on one coordinate. Here the equations are integrated numerically using fourth order Runge-Kutta scheme [49] with fixed step size guaranteeing desired accuracy for the preservation of conservation of the quantity $(C_1 \sin y + B_1 \cos x)$, when one coordinate z is made cyclic. The normalized parameters for the magnetic fields are chosen [26] as $A_1 = A_2 = 1$, $B_1 = B_2 = \sqrt{2/3}$, $C_1 = C_2 = \sqrt{1/3}$ and $\lambda = \lambda_+ = 1$, $\lambda_- = -0.5$. The choice of such parameters enables to differentiate a mixed phase space from a fully chaotic one.

2.3 Spatial structure and diffusion of magnetic field lines

Global properties of the system can be predicted by plotting Poincaré sections. For

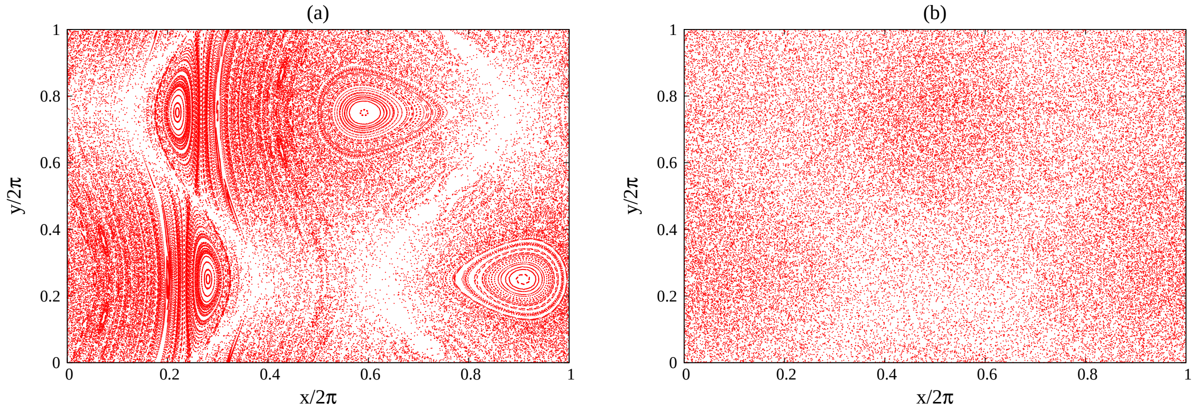

Figure 2.1: The $z = 0$ Poincaré surface-of-section of the magnetic field lines for (a) single curl and (b) double curl magnetic field.

a three dimensional phase space, the trajectories are complex. Qualitative information about the field lines can be obtained by finding a way to sample the trajectories in lower dimensions. The dimensionality of phase space is lowered down by one by studying the points where the trajectories pass through some plane. This plane is known as Poincaré section. Figure 2.1 depicts the $z = 0$ Poincaré surface of section which shows the existence of regular islands in the chaotic sea in case of single curl field unlike that for the double curl field with the chosen parameters where the field lines are seen to be chaotic over the entire space. Since the magnetic fields are periodic in each spatial dimension with period 2π, the modulus of the spatial variables by this period is taken.

To explore the long term behavior of the magnetic field lines, it is meaningful to study their diffusion characteristics that preserve the full nonlinear properties of the field line equation. For studying the spatial diffusion, we consider the evolution of an ensemble of magnetic field lines along the length s of the trajectories. All the field lines in the ensemble are located initially in the chaotic part of the phase space. The choice of initial conditions can be made by inspecting figure 2.1. One point on the chaotic part of the phase space is chosen as a reference point which is the initial position of a reference field line and the initial positions of other field lines are taken from the close vicinity of the reference line. Following the ensemble of magnetic field lines along s, we compute the variance σ^2 of spatial distances of chaotic trajectories from the reference one as a function of path length s:

$$\sigma^2(s) = \frac{1}{N}\sum_{i=1}^{N}(\Delta_i(s) - \mu_B(s))^2 \tag{2.6}$$

where

$$\mu_B(s) = \frac{1}{N}\sum_{i=1}^{N}\Delta_i(s)$$

and

$$\Delta_i(s) = |\mathbf{r}_i(s) - \mathbf{r}_0(s)|.$$

$\Delta_i(s)$ is the distance between the i-th and the reference field line (designated by subscript zero) after a distance s along each field line. Total number of field lines that are evolved to study diffusion is $N+1$ where N number of field lines are initially located in close proximity of the reference line such that $|\mathbf{r}_i - \mathbf{r}_0| = 0.01$ for $i = 1, 2, ..., N$. Fig. 2.2 shows

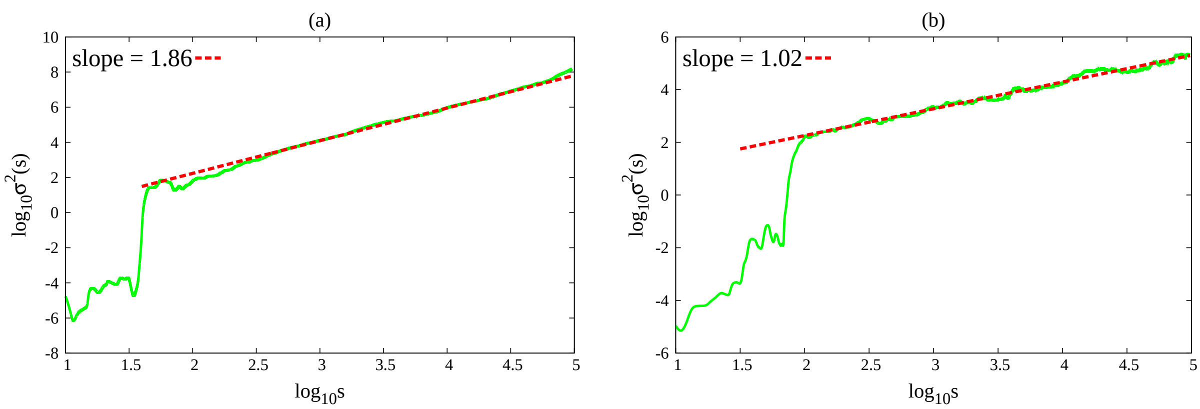

Figure 2.2: Fit of the variance of spatial distances between all field lines and a reference field line as a function of s for (a) single curl and (b) double curl magnetic field.

the plots of $log_{10}^{\sigma^2}$ as a function of $log_{10}s$ along with their least square fits for single curl and double curl field. The variance is calculated by considering 1001 field lines including the reference line and the results will not change on taking more number of trajectories. The least square fits of the variances indicate that the field lines of the single curl field are superdiffusive, whereas for the double curl field, it is close to Gaussian.

Now, in connection with the transport properties, we characterize single field lines of two different magnetic fields in section 2.4.

2.4 Characterization of single field line trajectories

Figure 2.3(a1) shows the surface plot of a chaotic trajectory for the single curl field where

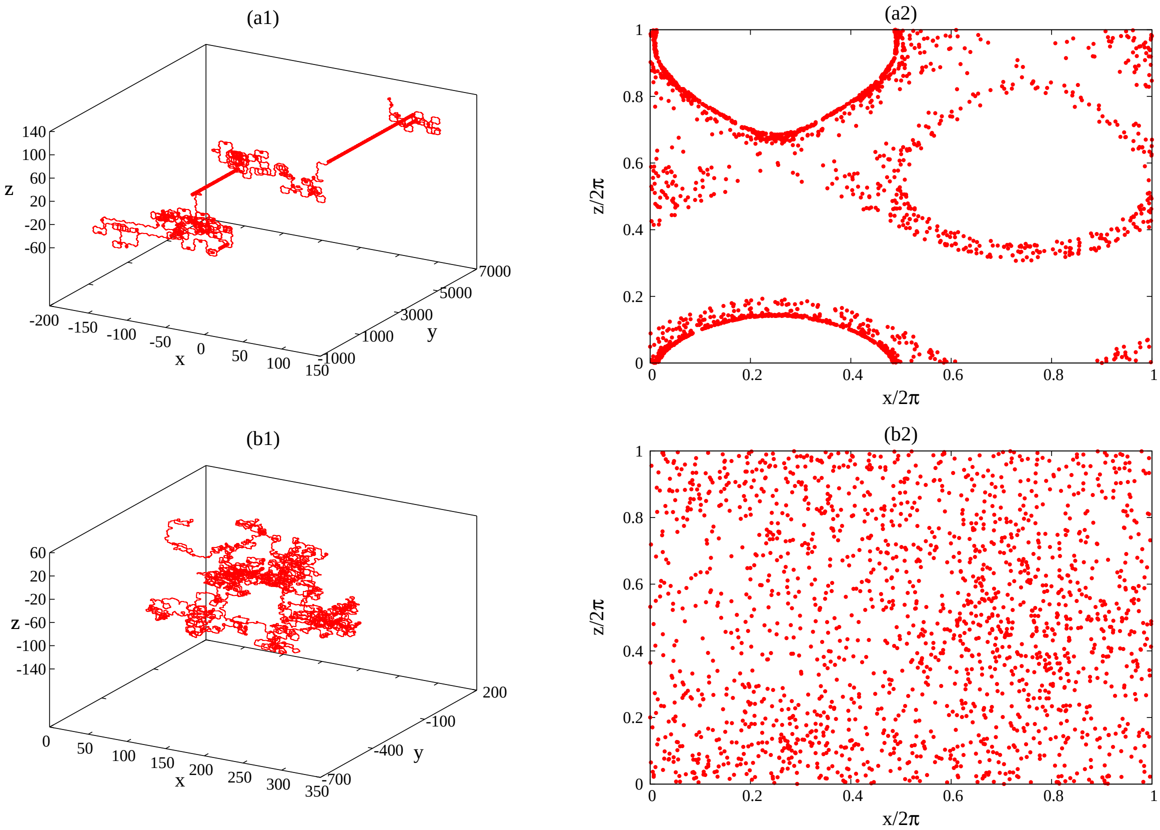

Figure 2.3: Trajectory of a chaotic field line for (a1) single curl, (b1) double curl magnetic field and corresponding $y = 0$ surface of section of the chaotic field line for (a2) single curl, (b2) double curl magnetic field.

we see the presence of long flights during the evolution of the trajectory. That means, in the dynamics of a chaotic trajectory, long regular motions are present during which one coordinate increases linearly while the other two get trapped (i.e their mean position remain the same). Figure 2.3(a2) shows the points that belongs to the same trajectory in the $y = 0$ surface of section. Vacant regions where there are no points on the Poincaré section correspond to integrable regions where a chaotic trajectory cannot enter or might also arise when field lines move parallel to the plane of the figure. The boundary of some islands has a dark area with larger accumulation of points indicating that the trajectory spends a longer time there. This phenomena is called stickiness which appears as a result of the trapping suffered by the trajectory in the neighborhood of the island. Trajectory of a chaotic field line of double curl field is shown in figure 2.3(b1). This trajectory looks almost random where large scale regularity is absent. Figure 2.3(b2) shows that a chaotic field line of the double curl field can sample the whole space almost uniformly.

The difference between the two parts of a chaotic trajectory, one maintaining oscillation about a fixed mean value (trapped or sticky part) and the other looking random (random or chaotic part), of single curl field can be illustrated by spatial Fourier transform. Figure 2.4(a2) and (b2) show the plots of the spectrum of power against the

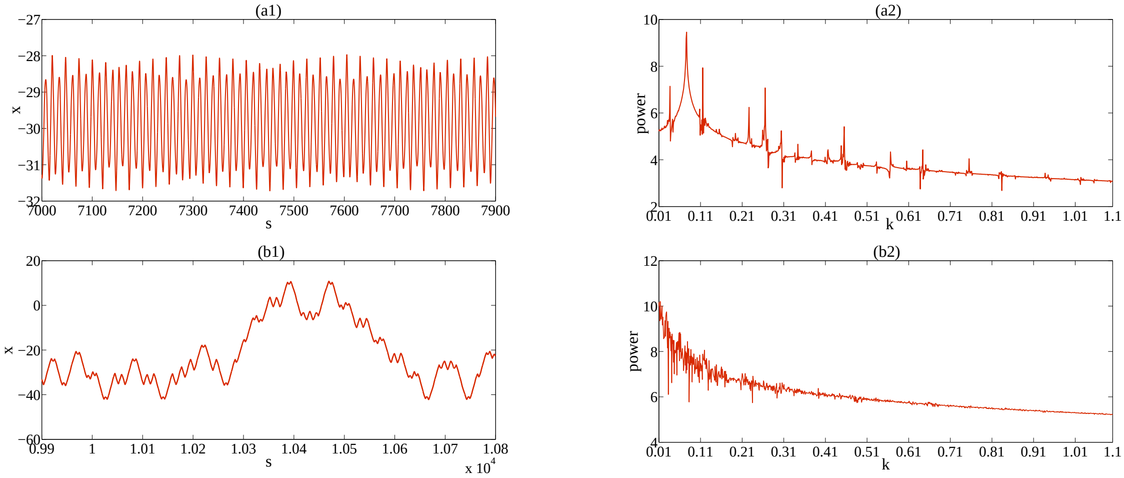

Figure 2.4: Spatial evolution of the x component of a chaotic field line of single curl field for (a1) sticky, (b1) chaotic part and corresponding power spectrum for (a2) sticky, (b2) chaotic part.

Fourier variable k. The spatial evolution patterns of the x component of the field line for two different parts of the chaotic trajectory are shown in figure 2.4(a1) and (b1) respectively. The sticky part of a chaotic field line of single curl field has some spatial regularity and corresponding FFT consists of some discrete peaks in contrast to the other part consisting of a broadband structure in FFT. The broadband structure implies that this part of the trajectory is spatially chaotic.

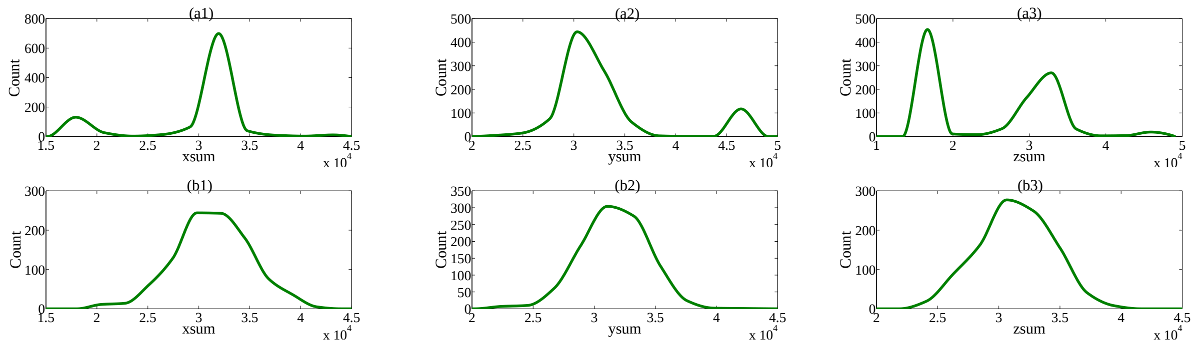

Figure 2.5: Distribution of a single chaotic trajectory: (a1) x, (a2) y, (a3)z component for single curl and (b1) x, (b2) y, (b3) z component for double curl magnetic field in the spirit of CLT.

Another way to characterize a trajectory is by studying its distribution. The behavior of random variables can be studied using the central limit theorem (CLT) by calculating their sums [65]. Figure 2.5(a1), (a2), and (a3) show the distribution of the three coordinates of a chaotic trajectory for single curl field in the spirit of CLT. The trajectory is evolved over 10^7 length steps and the sum is calculated over consecutive length windows of size 10^4. In this way, we treat the point at the beginning of every length window as a new initial condition and repeat this process 1000 times to obtain as many sums as required for reliable statistics. The size of the length window is such that it contain a significant part of the trajectory. Here the modulus of the spatial variables by the period of the magnetic field is taken. Although the sum of a large number of random numbers is a variable with Gaussian probability distribution, exceptions arise when long jumps in the trajectories are observed. Due to the presence of two different types of dynamics during the evolution of a chaotic trajectory of the single curl field, the distribution is bimodal. One peak appears due to chaotic motion and the other due to regular motion. The peaks due to the regular motion appear in different positions in three cases depending on the accessible range of values between 0 and 2π during regularity. On the other hand, the single peaked distributions shown in figure 2.5(b1), (b2), and (b3) indicate that the dynamics is almost same throughout the evolution of a chaotic field line of double curl magnetic field.

Dynamical traps of a chaotic orbit can be characterized by finite distance Lyapunov

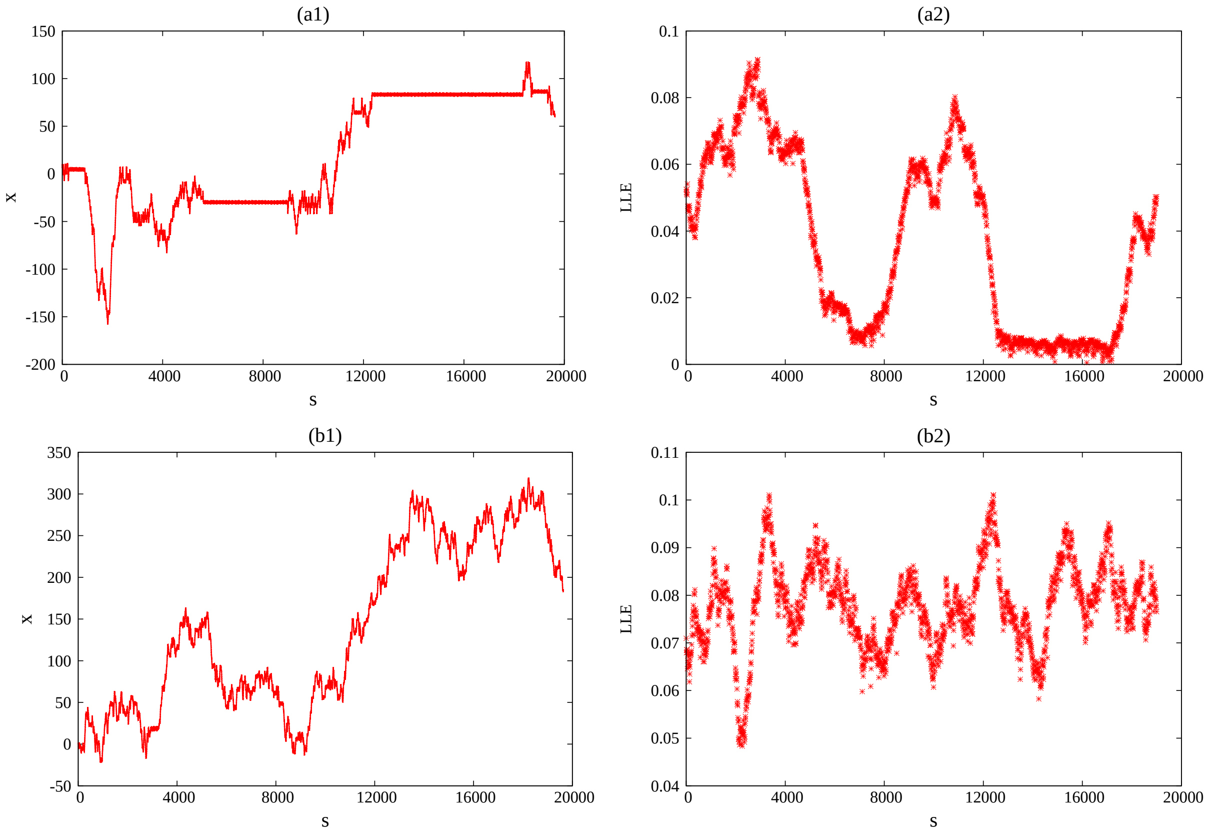

Figure 2.6: Spatial evolution of x component of a single chaotic field line for (a1) single curl, (b1) double curl magnetic field and spatial evolution of finite distance LE of the chaotic field line for (a2) single curl, (b2) double curl magnetic field.

exponent (LE) which is the local rate of divergence of two nearby trajectories during finite intervals of length along a field line. Since the largest LE (LLE) represents the dominant divergence rate, only the LLE is considered here. Figure 2.6(a2) shows the values of finite distance LE for different parts of a chaotic field line of single curl magnetic field. Here a single chaotic trajectory is evolved for 2×10^6 number of steps. To compute the finite distance LE, the spatial positions along the trajectory are taken as initial conditions and each initial condition is evolved for finite number of steps compared to the total number of steps of evolution of the whole trajectory. The Gram-Schmidt orthnormalization process is carried out at each step, while calculating the values of finite distance LE. The spatial evolution pattern of the x component of the field line, in figure 2.6(a1), is shown to relate different types of dynamics with its corresponding finite distance LE values. When the trajectory gets trapped near some island, the values of finite distance

LE corresponding to that part are small compared to the values when the trajectory is in the bulk of the chaotic sea. Figure 2.6(b2) shows the finite distance LE values for different parts of a chaotic trajectory in case of double curl field and corresponding x component of the trajectory is shown in figure 2.6(b1). In this case large scale regularity is absent but there may be some small scale regularity due to which finite distance LE attain some small values relative to the mean of its values. However, such small values appear over a very short length of the trajectory. Distribution of finite distance LEs of

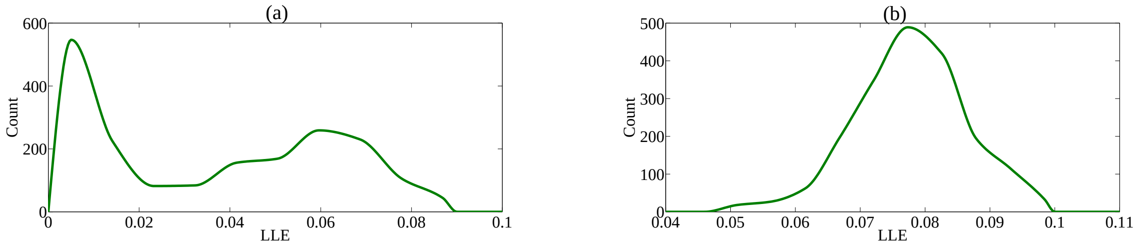

Figure 2.7: Distribution of finite distance LEs for (a) single curl and (b) double curl magnetic field.

a chaotic trajectory for single curl field is bimodal which is shown in figure 2.7(a). The maxima near zero appears due to the stickiness of the chaotic trajectory and the values around the other peak arise due to the chaotic motion in the bulk of chaotic sea. While for the case of double curl field, stickiness phenomena is absent. The distribution of finite distance LEs in this case appears with a single peak with small asymmetry due to some short scale regularity.

2.5 Recurrence length distribution

The recurrence length is the length a trajectory takes to return to a small region in space (epsilon vicinity of a given point which is chosen from a chaotic region away from the boundary of any regular island) starting from the same region. During the evolution of the trajectory, it will come several times to this particular region and recurrence length is the difference between two consecutive moments when the trajectory falls in the epsilon vicinity of that particular point. This local test gives information about

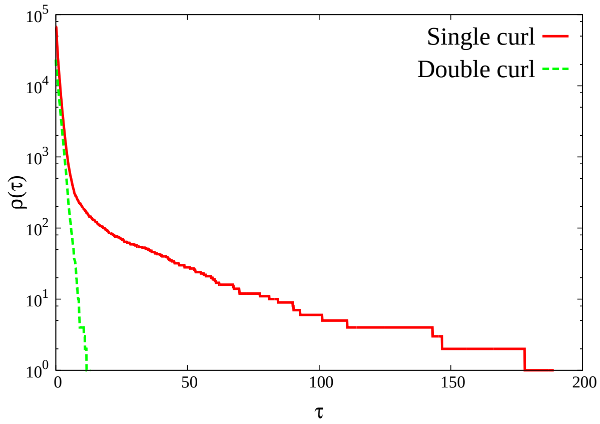

Figure 2.8: Cumulative distribution of mean recurrence lengths.

the global behavior of the trajectory. The cumulative distribution of mean recurrence lengths $\rho(\tau)$ defined by

$$\rho(\tau) = \sum_{\tau'=\tau}^{\infty} \rho(\tau')$$

is shown in figure 2.8. Here we take an ensemble of field lines containing 100 trajectories that are located initially within a circle of radius 0.01. The center of the circle is located on the chaotic sea of the $z = 0$ Poincaré section shown in figure 2.1. Then we choose another point from the chaotic part of phase space and consider the recurrence of the trajectories in the sphere of radius 0.5 centered about the point. A large number of trajectories is considered to achieve good statistical properties. Distribution of mean recurrence lengths has a long tail in case of single curl field, while that for a double curl field decays very quickly. A sticky trajectory of single curl field gets trapped for long times around regular islands and then escape to the stochastic region which leads to longer recurrence lengths compared to the case of double curl field where there is almost uniform stochastic regions everywhere in space.

2.6 Summary

In this work, we characterize the chaotic field lines of both single and double curl fields. The single curl ABC magnetic field has a mixed phase space which is neither entirely regular, nor entirely chaotic. Certain solutions of the double curl equation lead to field lines that are uniformly chaotic over the entire phase space. In the domains of mixed phase space, parts of chaotic trajectories are almost regular in spite of the full trajectory being chaotic. Anomalous diffusion in such systems can be related to the dynamical traps of chaotic orbits in the neighborhood of regular regions in phase space. In contrast to the chaotic trajectories of single curl field, the field lines of certain solutions of double curl equation are almost diffusive in nature. Statistics of single field line trajectories are studied in order to differentiate the transport properties of magnetic field lines for different types of deterministic magnetic fields. A single chaotic field line is characterized by its sum distribution and the distribution of finite distance Lyapunov exponents for different parts of the trajectory. The distributions are observed to be bimodal for ABC field in contrast to the chosen double curl field, for which the considered distributions consist of single peaks.

A complete $3-D$ view of the trapping domains as well repetitive effects for various trajectories is hard to visualize. The global behavior of the field lines can be quantified through a local test by using recurrence statistics. The test provides a long-tailed distribution for the field lines of ABC field showing a mixed phase space, while a rapidly decaying distribution for the field lines of the chosen double curl field associated with uniform spatial chaoticity.

CHAPTER 3

Dynamics of magnetic field lines of a double curl Beltrami field in presence of a mean field

In the previous chapter, we have discussed some dynamical features of the magnetic field lines considering single curl and double curl Beltrami fields. In the present chapter, we consider a different solution of the double curl equation in presence of a uniform background magnetic field. The spatial evolution of the field lines of such chosen magnetic fields governed by the double curl equation will be shown by the plots of Poincaré sections, contours of asymptotic distance Lyapunov exponents, recurrence length distribution etc. It is well known that in presence of a steady background field, the turbulent fluctuations introduce random motions perpendicular to the mean field. We attempt to analyze the perpendicular transport characteristics of the field lines in connection with their nonlinear dynamical properties considering a fluctuating deterministic field.

3.1 Double curl Beltrami magnetic fields

We consider a double curl equation of the form

$$\nabla \times \nabla \times \mathbf{B} = \Lambda \mathbf{B}. \tag{3.1}$$

This double curl equation, in the presence of certain symmetries, helps us to understand a variety of structures generated in plasmas. Bhattacharyya et al. [66] have shown that a relaxation mechanism based on the principle of minimum dissipation of energy, which is involved in the formation of field-reversed configuration, yields this double curl Euler-Lagrange equation. The solutions of equation (3.1) for non constant Λ will vary with the choice of its profiles and become, in general, too complicated to consider in the present study. For constant Λ, one solution of equation (3.1) in $3-D$ Cartesian coordinate system can be written as

$$B_x = a_1 \sin \lambda z + c_2 \sin \lambda y$$

$$B_y = b_1 \sin \lambda x + a_2 \sin \lambda z$$

$$B_z = c_1 \sin \lambda y + b_2 \sin \lambda x \tag{3.2}$$

where a_i, b_i, c_i $(i = 1, 2)$ are arbitrary constants and $\Lambda = \Lambda^2$. Since each component of the magnetic field consists of two *sine* functions, the solution represented by equation (3.2) will henceforth be referred to as double-sine field.

Here we take the magnetic field $\mathbf{B}$ to be the sum of a background field given by $\mathbf{B}_0 = B_0\hat{\mathbf{k}}$ and a static magnetic fluctuation $\delta\mathbf{B}(\mathbf{r})$ i.e.

$$\mathbf{B} = \delta B_x(\mathbf{r})\hat{\mathbf{i}} + \delta B_y(\mathbf{r})\hat{\mathbf{j}} + (\delta B_z(\mathbf{r}) + B_0)\hat{\mathbf{k}}. \tag{3.3}$$

The fluctuating part of the magnetic field is given by the double-sine field, presented in equation (3.2).

Now magnetic field lines are tangential to the magnetic field $\mathbf{B}(\mathbf{r})$ at any spatial point $\mathbf{r}$. The field line equations are thus obtained as [40] ,

$$\frac{d\mathbf{r}}{ds} = \frac{\mathbf{B}(\mathbf{r})}{|\mathbf{B}(\mathbf{r})|} \tag{3.4}$$

where $\mathbf{r} = x\hat{\mathbf{i}} + y\hat{\mathbf{j}} + z\hat{\mathbf{k}}$, $|\mathbf{B}(\mathbf{r})|$ is the magnitude of $\mathbf{B}$ and s is the length along the field line.

To integrate equation (3.4) numerically, dimensionless variables are used where distances are normalized by constant λ and magnetic field $\mathbf{B}$ is normalized by arbitrary unit B_0'. The equations are integrated numerically using fourth order Runge-Kutta scheme [39] with fixed step size. The normalized parameters for the double-sine field are chosen as $a_1 = a_2 = a = 1$, $b_1 = b_2 = b = \sqrt{2/3}$, $c_1 = c_2 = c = \sqrt{2/3}$ and the field line length s is used as the integration parameter. Under this choice of the coefficients, the final solution looks like the single curl ABC field with the *cosine* terms being replaced by *sine* functions. Also the system is isotropic with respect to x and y coordinates which will be shown graphically later in section 3.3. Here we keep the background field constant at $B_0 = \sqrt{7/3}$ and scale the fluctuating double curl field.

$$\mathbf{B} = \alpha(\delta\mathbf{B}(\mathbf{r})) + \mathbf{B}_0 \tag{3.5}$$

This allows us to identify different behaviors that the double-sine field introduces in presence of a background field. The r.m.s value of the fluctuating double-sine field $\delta\mathbf{B}(\mathbf{r})$ is equal to $\sqrt{a^2 + b^2 + c^2}$. We have taken the value of B_0 to be equal to this r.m.s value and hence α specify the ratio of the fluctuation (taking into account the corresponding multiplication factor α) δB to B_0. So, we vary only the value of α to obtain the desired values of the fluctuation level $\delta B/B_0$.

In section 3.2, before considering the mean field, let us first study the structure of the field lines of double-sine field alone.

3.2 Spatial evolution of magnetic field lines in absence of a mean field

Figure 3.1 depicts the $z = 0$ Poincaré section for the double-sine field, which shows

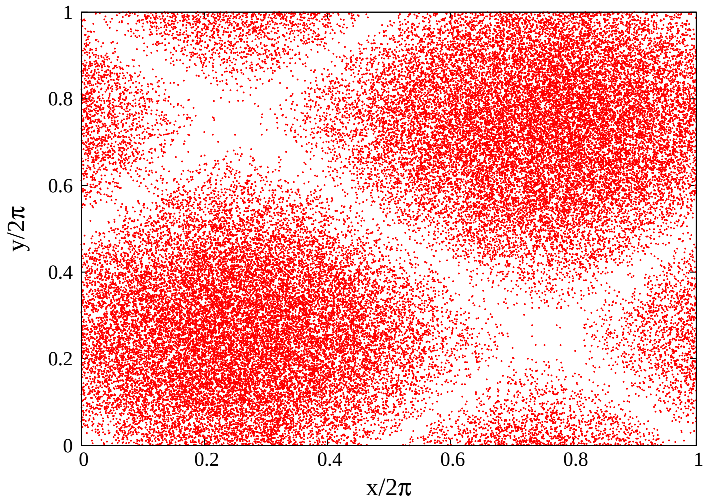

Figure 3.1: The $z = 0$ Poincaré surface-of-section of the magnetic field lines for double-sine magnetic field.

that the field lines are chaotic over the entire space in contrast to the single curl ABC magnetic fields that show mixture of regular and chaotic regions. Since the magnetic fields are periodic in each spatial dimension with period 2π, the modulus of the spatial variables by this period is taken.

3.3 Spatial evolution of magnetic field lines in presence of a mean field

Now we introduce a steady mean field in the z direction and see how the phase space changes with increasing the fluctuation level $\delta B/B_0$. Figure 3.2 shows the Poincaré section for different fluctuation levels. In absence of any mean field, the double-sine field represents a fully chaotic system without any closed magnetic surfaces. The mean field

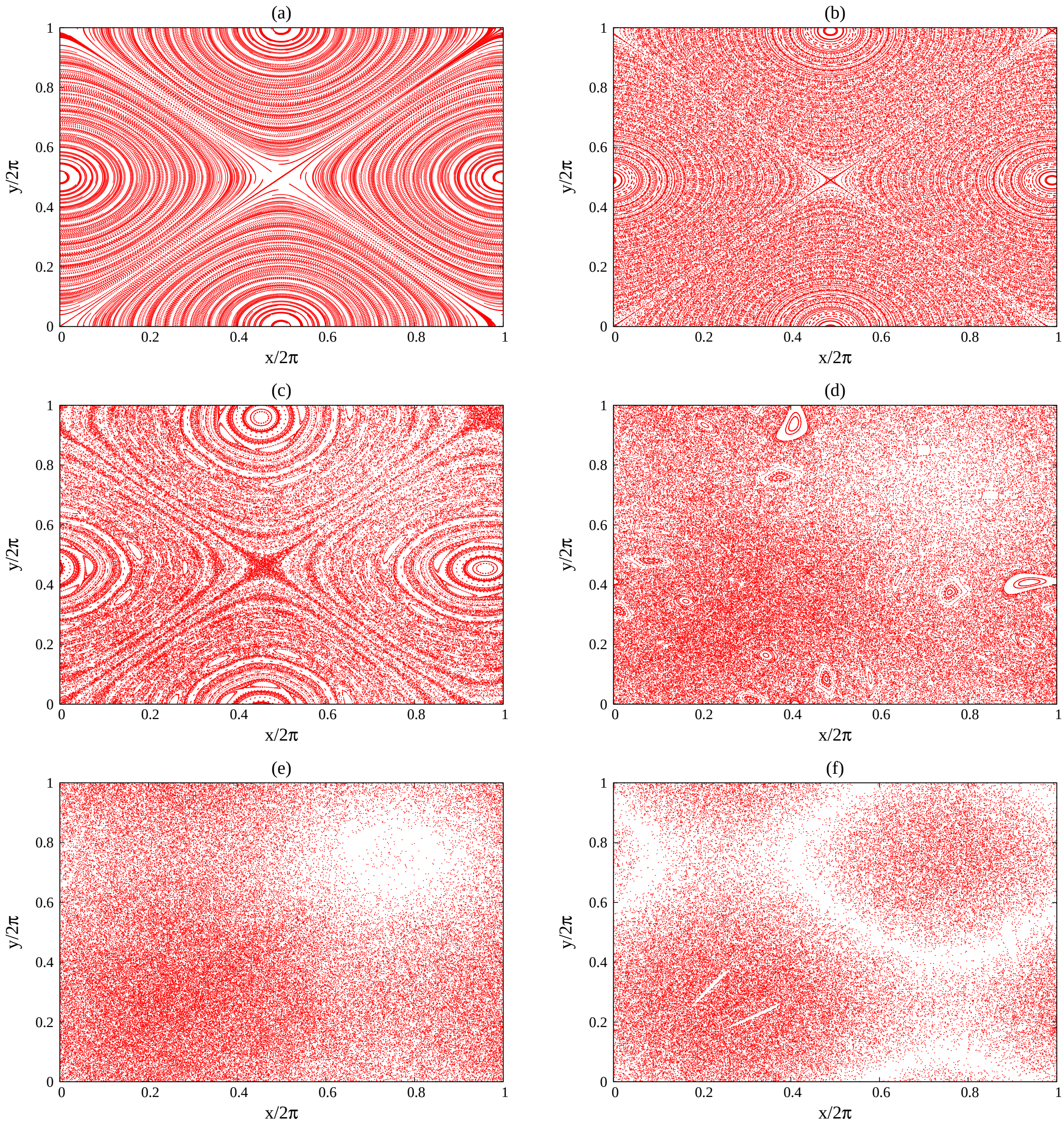

Figure 3.2: The $z = 0$ Poincaré surface-of-section of the magnetic field lines for (a) $\delta B/B_0 = 0.01$, (b) $\delta B/B_0 = 0.1$, (c) $\delta B/B_0 = 0.4$, (d) $\delta B/B_0 = 0.7$, (e) $\delta B/B_0 = 1.0$, and (f) $\delta B/B_0 = 4.0$.

introduces some regular islands in the system when the strength of the fluctuating field is small compared to the mean field. When $\delta B/B_0 = 0.01$, almost all the magnetic surfaces are regular i.e. non chaotic, which is shown in figure 3.2(a). Subsequent figures show that the width of the chaotic layer between the closed loops increases with increasing the fluctuation level and finally all the magnetic surfaces are destroyed which corresponds to global chaoticity. Figure 3.2(e) and (f) correspond to such globally chaotic scenario.

The white regions on the Poincaré section arise when the field lines move parallel to the plane of the figure.

Figure 3.2(a) provides an easy way to check the accuracy of the RK4 algorithm used to integrate field line equations by comparing the numerical results with the analytic solution obtained from the linear stability analysis about the fixed points. For $B/B_0 = 0.01$, B_z and $|\mathbf{B}|$ can be approximated to B_0. Then

$$\begin{aligned}\frac{dx}{ds} &= \frac{a\sin z + c\sin y}{B_0}\\ \frac{dy}{ds} &= \frac{b\sin x + a\sin z}{B_0}\\ \frac{dz}{ds} &= 1.\end{aligned} \tag{3.6}$$

When $z \simeq 0$, $\dot{x}$ and $\dot{y}$ vanish for $(x, y) = (\pi, 0), (0, \pi), (\pi, \pi)$. The points $(\pi, 2\pi)$ and $(2\pi, \pi)$ are equivalent to $(\pi, 0)$ and $(0, \pi)$ respectively. Linearization approximates the trajectories by closed orbits around the elliptic points $(\pi, 0)$ and $(0, \pi)$ (the eigenvalues of the Jacobian corresponding to the points are purely imaginary), whereas the trajectories resembles hyperbolas near the hyperbolic point (π, π) (the eigenvalues of the Jacobian corresponding to the point are real with opposite signs). Such nature of trajectories is also observed in the Poincaré section shown in figure 3.2(a) with $\delta B/B_0 = 0.01$.

However, in connection with the change of chaoticity of phase space with the fluctuation level, we consider two representative examples to understand the global behavior of the field lines. The Poincaré section for $\delta B/B_0 = 0.6$ is depicted in figure 3.3(a) which corresponds to a mixed phase space. As a second example, the fluctuating field is taken to be greater than the mean field with $\delta B/B_0 = 2.0$ where regions of global chaoticity is reached and is shown in figure 3.3(b).

The chaoticity of the phase space can be measured through the asymptotic-distance Lyapunov exponents (LE) of the magnetic field lines. As mentioned in chapter 2, again

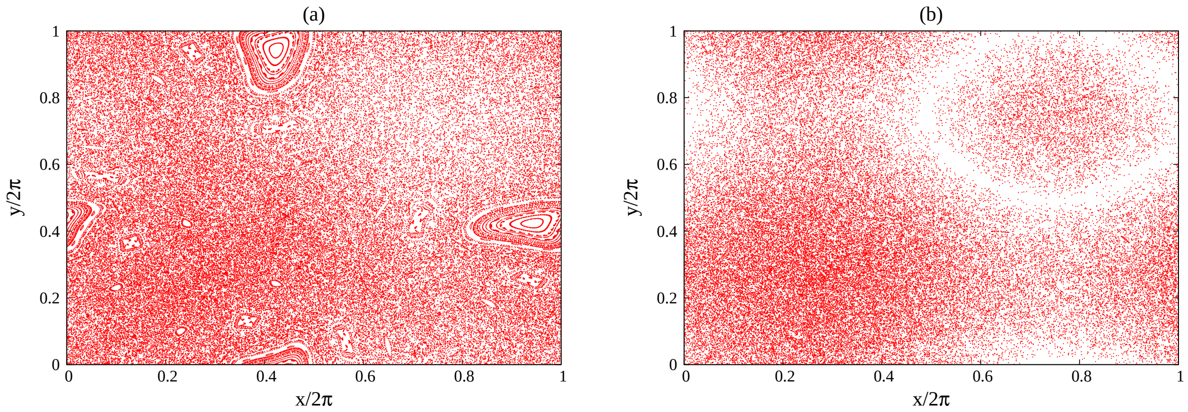

Figure 3.3: The $z = 0$ Poincaré surface-of-section of the magnetic field lines for (a) $\delta B/B_0 = 0.6$ and (b) $\delta B/B_0 = 2.0$.

we consider only the LLE. The asymptotic-distance LEs are evaluated using the Gram-Schmidt orthnormalization process at each step of evolution of the trajectory and the results are plotted after 10^6 such normalizations. Figure 3.4 is a contour plot of the

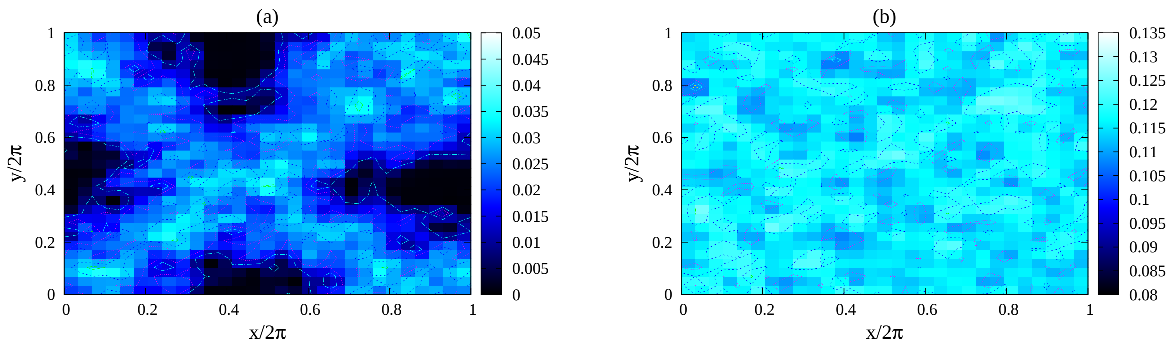

Figure 3.4: Contours of the largest asymptotic-distance Lyapunov exponents for the magnetic field lines for (a) $\delta B/B_0 = 0.6$ and (b) $\delta B/B_0 = 2.0$.

largest asymptotic-distance LEs for two different fluctuation levels as a function of initial conditions which are uniformly distributed in the $x-y$ plane. This figure helps to find a correlation with the Poincaré section plots. In regions where the magnetic field lines are regular, the magnitude of the asymptotic-distance LLE is smaller by at least one order of magnitude than that corresponding to the chaotic regions. Also the maximum value of the LLE for higher fluctuation level is greater than the corresponding maximum value associated with the smaller fluctuation level.

After getting information about the global structure of the phase space, it is necessary to visualize the spatial evolution pattern of a single chaotic field line. The behavior of a chaotic field line gets affected by the structure of the entire phase space. Figure

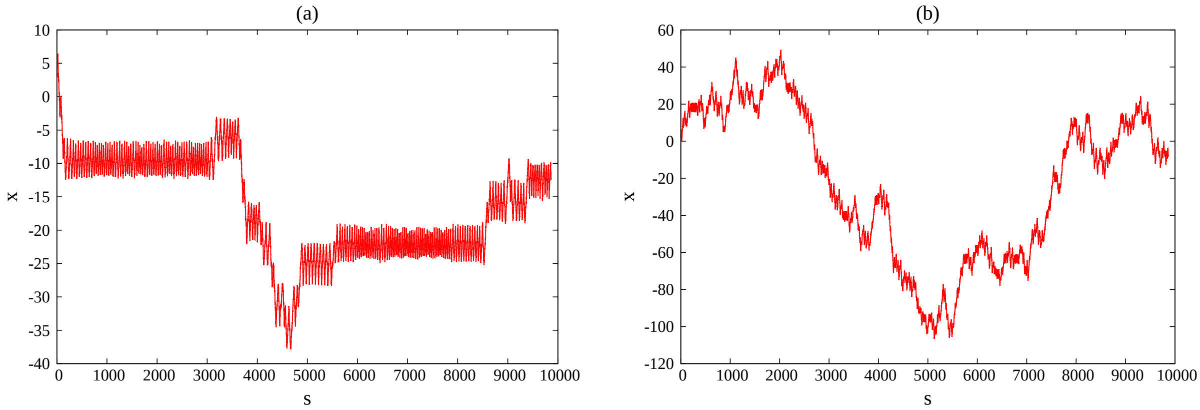

Figure 3.5: x component of a chaotic field line for (a) $\delta B/B_0 = 0.6$ and (b) $\delta B/B_0 = 2.0$.

3.5(a) shows the spatial evolution pattern of the x component of a chaotic trajectory for $\delta B/B_0 = 0.6$. Since the system is isotropic with respect to the perpendicular coordinates x and y, y component has similar pattern of spatial evolution. Furthermore z component increases linearly with distance because of the presence of a steady field along z direction and is of no relevance here. Now, it is clearly seen from figure 3.5(a) that for large values of the mean field B_0 compared to the fluctuating field, the chaotic trajectory consists of oscillations about a fixed mean value over some certain length intervals during its evolution, whereas for the fluctuation level $\delta B/B_0 = 2.0$, the trajectory looks almost random as depicted in figure 3.5(b).

Now, to get some quantitative information about the global behavior of a chaotic field line, we study recurrence length statistics. The cumulative distribution of mean recurrence lengths $\rho(\tau)$, as defined in section 2.5, is shown in figure 3.6. Distribution of mean recurrence lengths has a long tail in case of smaller fluctuation level with $\delta B/B_0 = 0.6$, while that for a larger fluctuation level, $\delta B/B_0 = 2.0$, decays very quickly.

In order to visualize the dynamics of a chaotic trajectory corresponding to the largest

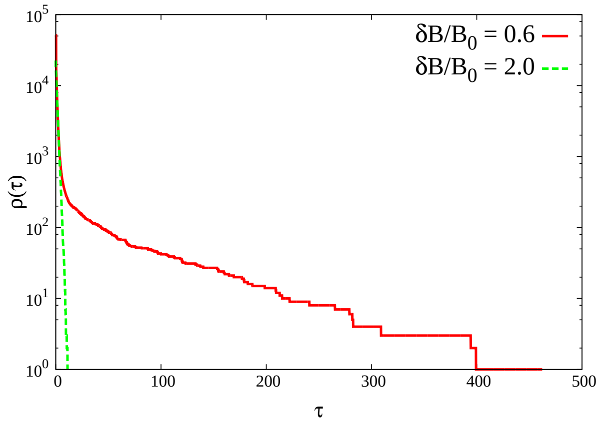

Figure 3.6: Cumulative distribution of mean recurrence lengths.

recurrence length, the Poincaré section and the spatial evolution of x component of the trajectory is plotted again during the concerned length interval. Figure 3.7(a) gives

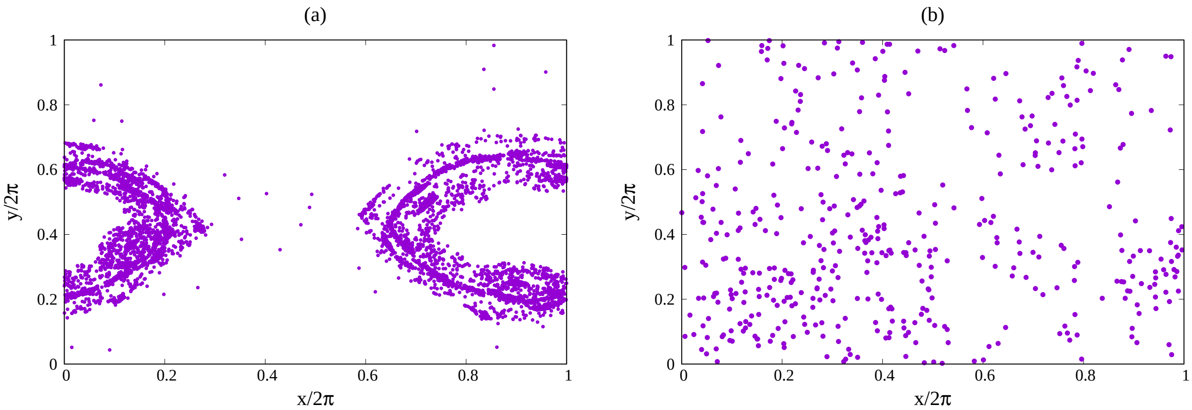

Figure 3.7: The $z = 0$ Poincaré surface-of-section for single chaotic field line in the length interval which corresponds to the largest recurrence length for (a) $\delta B/B_0 = 0.6$ and (b) $\delta B/B_0 = 2.0$.

some qualitative information about the chaotic trajectory during the length interval corresponding to the largest recurrence length for fluctuation level $\delta B/B_0 = 0.6$. The surface of section contains some dark area with larger accumulation of points indicating that the trajectory spends a longer time there. This phenomena may be called stickiness, which appears as a result of the trapping suffered by the trajectory in the neighborhood of island like regions. On the other hand, a chaotic trajectory for the fluctuation level $\delta B/B_0 = 2.0$ can uniformly sample almost the whole space during the corresponding largest length interval. Then the spatial evolution pattern of the x component of the

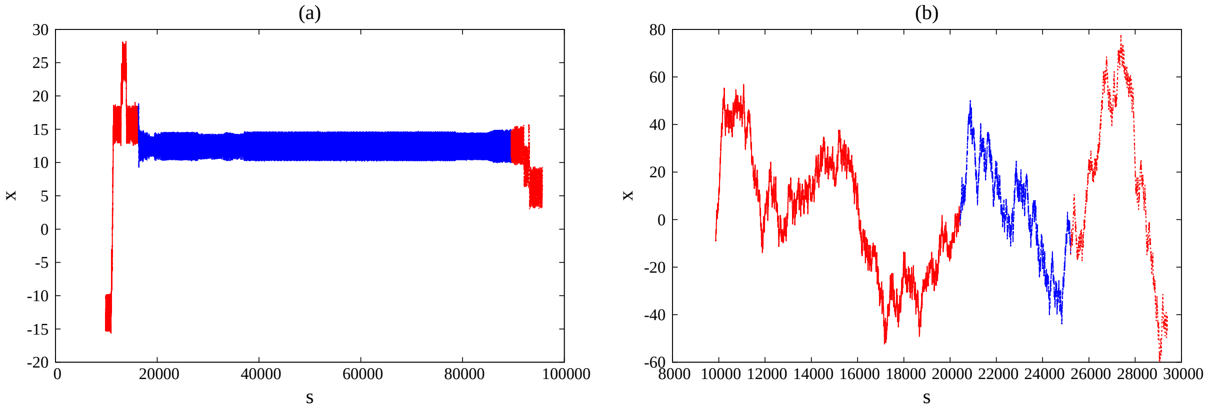

Figure 3.8: x component of a chaotic field line for (a) $\delta B/B_0 = 0.6$ and (b) $\delta B/B_0 = 2.0$.

trajectory for fluctuation level $\delta B/B_0 = 0.6$ is shown in figure 3.8(a) in which the length interval corresponding to the largest recurrence length is plotted in blue. The major part of the trajectory during this length interval consists of oscillations about a fixed mean value. Such oscillations about a fixed mean corresponds to stickiness phenomena. Similar plot for the fluctuation level $\delta B/B_0 = 2.0$ is shown in figure 3.8(b) where the trajectory oscillates in a random fashion without maintaining a fixed mean value over the concerned length interval plotted in blue.

Finally, we investigate the effect of stickiness on the transport properties of the field lines in the perpendicular plane. But before going into such study, we first look into the spatial evolution of the ensemble-averaged position of the magnetic field lines considering the two perpendicular coordinates x and y. For this purpose, we consider the evolution of an ensemble of magnetic field lines consisting of $N = 1001$ trajectories, along the length s of the field lines. The trajectories in the ensemble are chosen according to the considerations as mentioned in section 2.3. The results remain unaffected if we consider more number of field lines. Figure 3.9 is a plot of the mean spatial position

$$< x(s) >= \frac{1}{N+1}\sum_{i=0}^{N} |x_i(s)|; < y(s) >= \frac{1}{N+1}\sum_{i=0}^{N} |y_i(s)| \tag{3.7}$$

as a function of s along the field line for the ensemble of trajectories mentioned above,

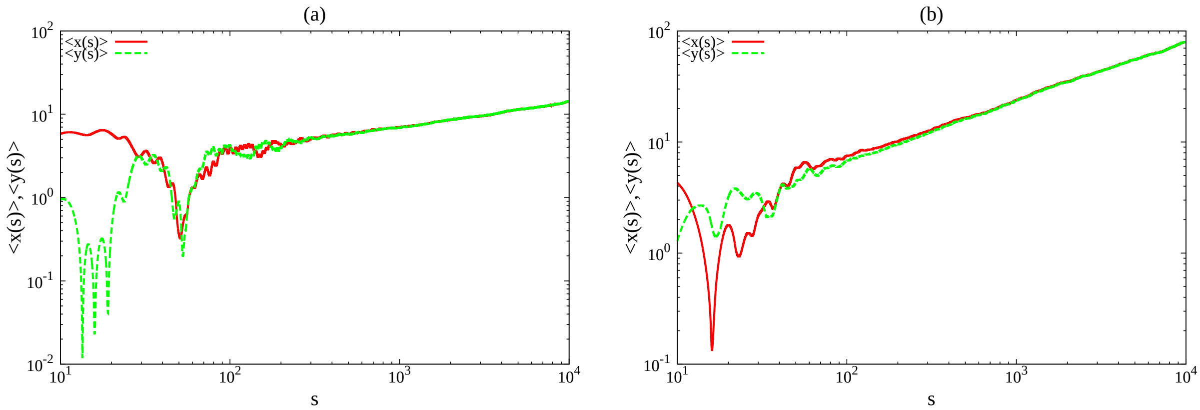

Figure 3.9: Mean spatial position as a function of length along the field line for (a) $\delta B/B_0 = 0.6$ and (b) $\delta B/B_0 = 2.0$.

with two different fluctuation levels. Initially, the two perpendicular coordinates evolves anisotropically. But as the length along the field line increases, the ensemble averaged perpendicular coordinates follow each other. For the fluctuation level $\delta B/B_0 = 0.6$, the initial anisotropy persists upto a longer length compared to that for the higher fluctuation level with $\delta B/B_0 = 2.0$. So, the larger the fluctuation level, the smaller will be the length to start a isotropic evolution of the field lines in terms of two perpendicular coordinates.

Now we evaluate the diffusive aspect of the field lines in the regime of isotropic evolution. Also, it is enough to consider one perpendicular coordinate only for studying the transport properties. In order to get sense of spatial diffusion, we compute the variance σ_x^2 as a function of s following the same ensemble of magnetic field lines as appeared in the previous chapter. The only difference is that, here we compute the displacements considering the x component of the position vector of a trajectory, instead of taking all the components.

$$\sigma_x^2(s) = \frac{1}{N}\sum_{i=1}^{N}(\Delta x_i(s) - \mu_B(s))^2 \tag{3.8}$$

where

$$\mu_B(s) = \frac{1}{N}\sum_{i=1}^{N}\Delta x_i(s)$$

and

$$\Delta x_i(s) = |x_i(s) - x_0(s)|.$$

$\Delta x_i(s)$ is the x component of the displacement of i-th field line from the reference one (designated by subscript zero) at a distance s along each field line. The quantitative idea about the nature of diffusion can be obtained through the scaling exponent p by fitting the numerically calculated variance with the transport law $\sigma_x^2 \sim s^p$. The exponent p enables us to know whether the system behaves as an ordinary, diffusive medium $p = 1$, or, on the contrary, it displays anomalous features such as subdiffusion ($p < 1$) or superdiffusion ($p > 1$). Figure 3.10 shows the plots of $log_{10}\sigma_x^2$ as a function of $log_{10}s$ along

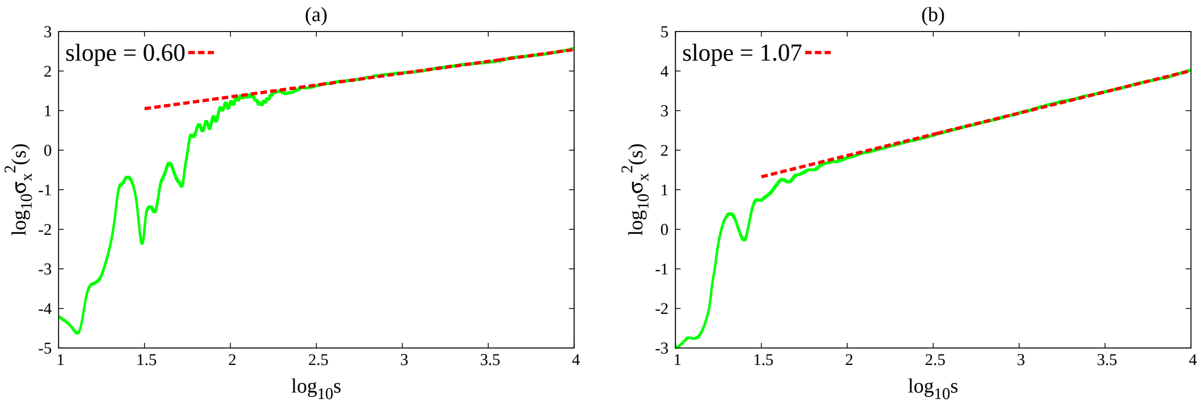

Figure 3.10: Fit of the variance of Δx between all field lines and a reference field line as a function of s for (a) $\delta B/B_0 = 0.6$ and (b) $\delta B/B_0 = 2.0$.

with their least square fits for two different values of $\delta B/B_0$. For the lower fluctuation level, σ_x^2 varies as $s^{0.60}$ indicative of a subdiffusion, whereas the higher fluctuation level leads to almost normal diffusion with the exponent $p = 1.07$.

3.4 Summary

The nonlinear dynamical characteristics of a particular double curl magnetic field in presence of a uniform mean field are studied by considering the ratio $\delta B/B_0$ as a parameter to get an understanding of the global behavior of the field lines and its effect on their perpendicular diffusion. For small values of $\delta B/B_0$, the phase space is a mixture of some islands and chaotic regions, while for larger values, there results a phase space devoid of any island like regions. Sticky behavior results from the trapping of field line trajectories at the border of islands and chaotic regions. In absence of the fluctuation, the field lines of steady mean field will not exhibit any diffusion in the perpendicular direction. The fluctuating inhomogeneous double-sine field introduces the effect of cross field diffusion. For large values of mean field, the field lines reveal dynamical traps that give support to the observation of subdiffusive scaling exponent. Finally recurrence length statistics provides global information about the phase space by showing a long-tailed distribution for smaller fluctuation level, verifying the role of stickiness, and a rapidly decaying curve for the higher fluctuation strength, signifying nearly random phase space.

CHAPTER 4

Perpendicular diffusion of field lines and charged particles in double curl Beltrami magnetic fields

In chapter 3, we analyzed the perpendicular transport characteristics of the field lines in connection with their nonlinear dynamical properties considering a particular double curl magnetic field in presence of a mean field. In this chapter, we extend the study of diffusion characteristics of the field lines taking the same magnetic field configuration. Here, the characteristics of the chaotic trajectories are studied in detail, through various statistical properties like variance, kurtosis, and probability distribution of their displacements. Finally we show the numerical results revealing the effect of field line transport on the diffusion of charged particles.

4.1 Double curl Beltrami magnetic fields and the dynamics of field lines

Again we consider double curl Beltrami magnetic field which satisfy

$$\nabla \times \nabla \times \mathbf{B} = \Lambda \mathbf{B}. \tag{4.1}$$

and consider the solution as mentioned in chapter 3:

$$B_x = a \sin \lambda z + c \sin \lambda y$$

$$B_y = b \sin \lambda x + a \sin \lambda z$$

$$B_z = c \sin \lambda y + b \sin \lambda x \tag{4.2}$$

where a, b, c are arbitrary constants and $\Lambda = \lambda^2$. Because of the presence of two *sine* functions in each component of the magnetic field, the solution represented by equation 4.2 will be referred to as double-sine field.

Here also, we take the magnetic field $\mathbf{B}$ to be the sum of a background field given by $\mathbf{B}_0 = B_0\hat{\mathbf{k}}$ and a static magnetic fluctuation $\delta\mathbf{B}(\mathbf{r})$ i.e.

$$\mathbf{B} = \delta B_x(\mathbf{r})\hat{\mathbf{i}} + \delta B_y(\mathbf{r})\hat{\mathbf{j}} + (\delta B_z(\mathbf{r}) + B_0)\hat{\mathbf{k}}. \tag{4.3}$$

The fluctuating part of the magnetic field is given by the double-sine field, presented in equation (4.2).

The field line equations are given by,

$$\frac{d\mathbf{r}}{ds} = \frac{\mathbf{B}(\mathbf{r})}{|\mathbf{B}(\mathbf{r})|} \tag{4.4}$$

where $\mathbf{r} = x\hat{\mathbf{i}} + y\hat{\mathbf{j}} + z\hat{\mathbf{k}}$, $|\mathbf{B}(\mathbf{r})|$ is the magnitude of $\mathbf{B}$ and s is the length along the field line.

To integrate equation 4.4 numerically, dimensionless variables are used where distances are normalized by constant λ and magnetic field $\mathbf{B}$ is normalized by arbitrary unit B_0'. The normalized parameters for the magnetic field are chosen as $a = 1$, $b = c = \sqrt{2/3}$ and the field line length s is taken as the integration parameter. With this choice, x and y coordinates remain in the same footing and so we consider only one perpendicular coordinate for the numerical analysis. By keeping the background field constant at $B_0 = \sqrt{7/3}(= \sqrt{a^2+b^2+c^2})$, desired values for the relative strength of fluctuation $\delta B/B_0$ with $\delta\mathbf{B}$ representing the r.m.s value of the fluctuating double-sine field, are chosen by scaling the fluctuating field by a multiplication factor.

In section 4.1.1, before considering the mean field, first we study the behavior of the field lines of double-sine field alone.

4.1.1 Spatial evolution of magnetic field lines in absence of a mean field

In the previous chapter, we plotted the $z = 0$ Poincaré section of the magnetic field lines for double-sine field in absence of any mean field. Figure 3.1 shows that the field lines are chaotic over the entire space.

Here, first we study the spatial diffusion of the field lines of double-sine field considering the evolution of an ensemble of trajectories, consisting of $N = 1001$ field lines, along the length s. The trajectories in the ensemble are chosen according to the considerations as mentioned in section 2.3 and the results remain unaffected if we consider more number of field lines. Following the ensemble of magnetic field lines, we compute the variance σ_x^2 as a function of path length s, as mentioned in section 3.3. Since x and y coordinates remain in the same footing under the choice of magnetic field parameters, only one perpendicular coordinate is considered for studying transport properties.

$$\sigma_x^2(s) = \frac{1}{N}\sum_{i=1}^{N}(\Delta x_i(s) - \mu_B(s))^2 \tag{4.5}$$

where

$$\mu_B(s) = \frac{1}{N}\sum_{i=1}^{N}\Delta x_i(s)$$

and

$$\Delta x_i(s) = |x_i(s) - x_0(s)|.$$

In order to get a quantitative idea about the nature of diffusion, the numerically calculated variance is to be fitted with the transport law $\sigma_x^2 \sim s^\alpha$. The exponent α characterizes the random walk law of the field lines. Gaussian diffusion corresponds to $\alpha = 1$, whereas for anomalous diffusive regime, $\alpha \neq 1$ with $\alpha < 1$ in case of subdiffusion and $\alpha > 1$ in case of superdiffusion. Figure 4.1(a) is a plot of the variance σ_x^2 as a function

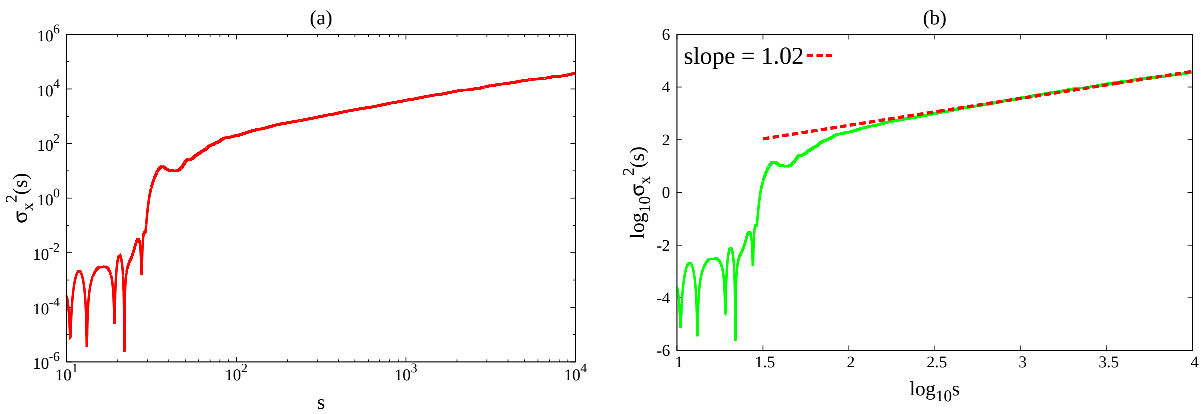

Figure 4.1: (a) Variance of Δx between all field lines and a reference field line as a function of s and (b) fit of the variance.

of length s along the field lines. This plot gives the spatial rate of spreading of the field lines from the reference one. Initial rapid growth of σ_x^2 with s suggests a correlation between the field lines. A least square fit in the range $2 < log_{10}s < 4$ is indicated by a dashed line in figure 4.1(b). The least square fit is obtained by a linear fit to the numerical data connecting $log_{10}\sigma_x^2$ and $log_{10}s$. The least square indicates that the field lines of a double-sine field are diffusive in nature with diffusion exponent $\alpha = 1.02$.

The diffusion characteristics of the field lines as obtained from the numerical analysis, can be evidenced by computing the kurtosis $K_x = \langle \Delta x^4 \rangle / \langle \Delta x^2 \rangle^2$ for the same ensemble of trajectories mentioned above. For a Gaussian probability distribution, the kurtosis is equal to 3. Kurtosis is a measure of whether the concerned distribution is peaked ($K_x > 3$) or flat ($K_x < 3$) relative to the Gaussian distribution. Figure 4.2(a) shows

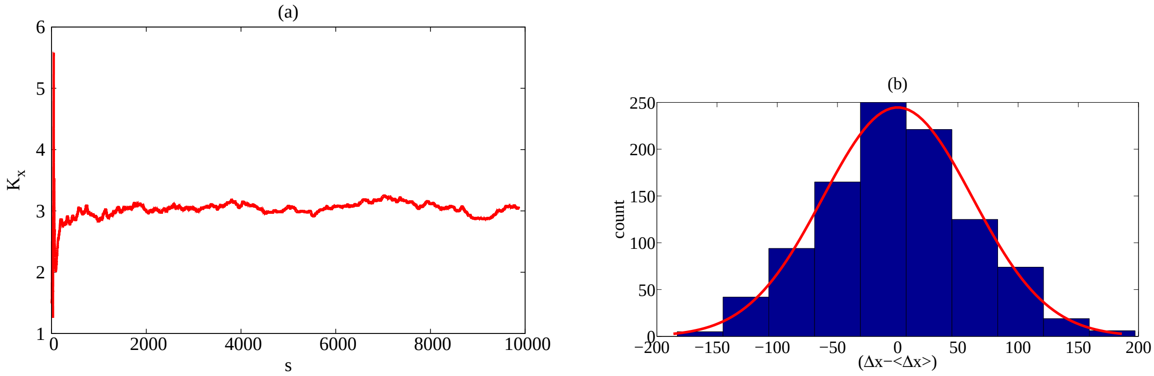

Figure 4.2: (a) Kurtosis of Δx between all field lines and a reference field line as a function of s and (b) distribution of Δx at $s = 1000$.

the plot of kurtosis as a function of length s along the field lines. It is clearly seen from the figure that the value of kurtosis nearly saturates to 3 in the asymptotic limit. The distribution of field line displacement Δx at $s = 1000$ is shown in figure 4.2(b) in which the fitted Gaussian curve is shown by the red line. The distribution of Δx when s is large enough to attain asymptotic values for the various statistical quantities, is close to Gaussian. So, for the double-sine field, the kurtosis of Δx is equal to 3, which corresponds to normal diffusion for the bunch of field lines.

4.1.2 Spatial evolution of magnetic field lines in presence of a mean field

Now we introduce the steady mean field and see how the phase space changes with increasing the relative strength of fluctuation $\delta B/B_0$. Again, in order to get a qualitative overview of the structure of field lines, we draw projections on the $x - y$ plane namely

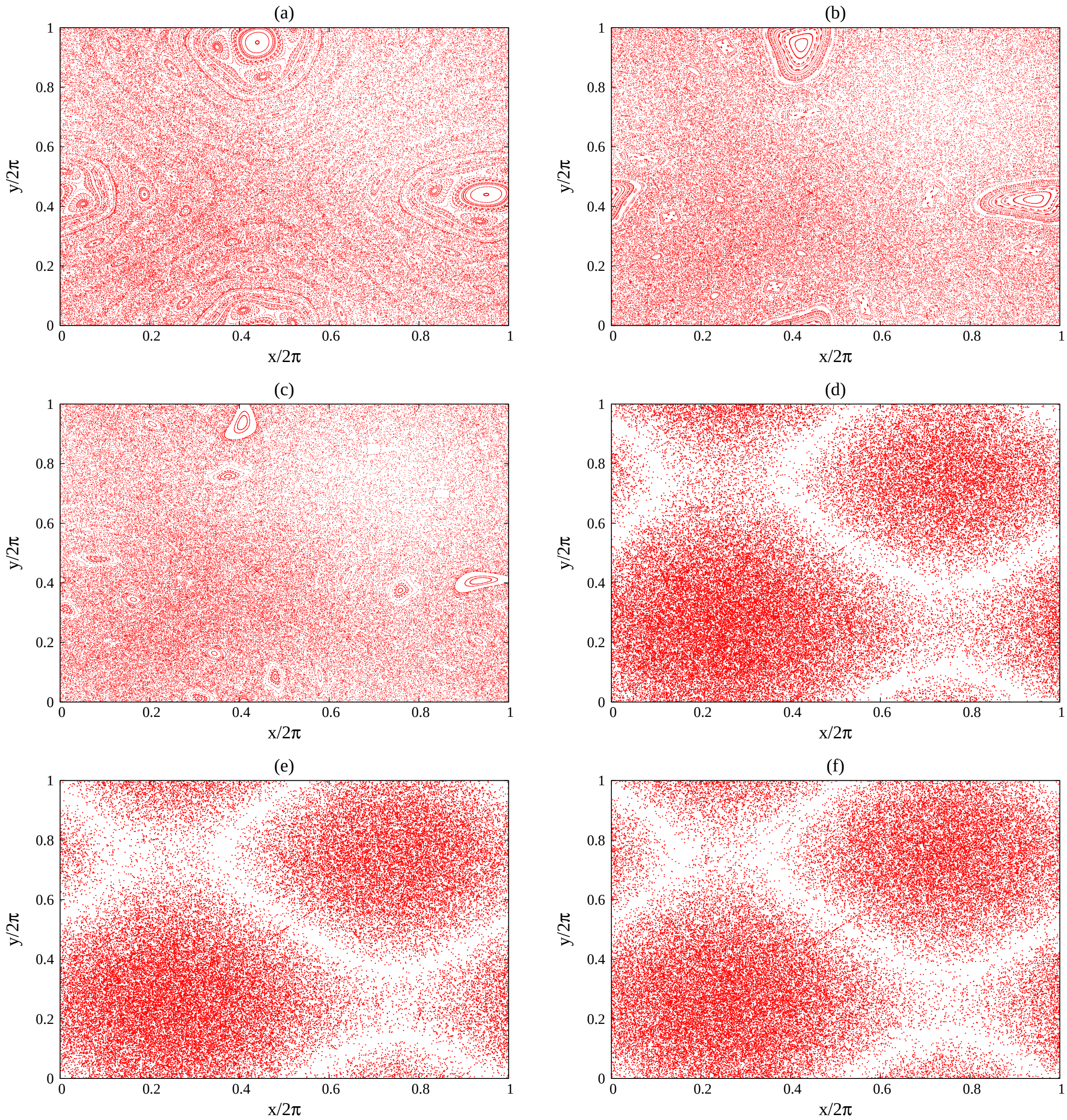

Figure 4.3: $z = 0$ Poincaré surface-of-section for (a) $\delta B/B_0 = 0.5$, (b) $\delta B/B_0 = 0.6$, (c) $\delta B/B_0 = 0.7$, (d) $\delta B/B_0 = 5.0$, (e) $\delta B/B_0 = 8.0$, and (f) $\delta B/B_0 = 10.0$.

Poincaré sections with the points of intersection of the field lines with the plane $z = 0$. Figure 4.3 shows the Poincaré sections for different levels of fluctuating magnetic field. In absence of any mean field, the double-sine field represents a fully chaotic system without any closed magnetic surfaces. The mean field introduces some regular islands in the system when fluctuation level is small compared to the mean field. The Poincaré sections for $\delta B/B_0 = 0.5$, 0.6, and 0.7 depicted in figure 4.3(a), (b) and (c) correspond to mixed phase space. The figures show that the width of the stochastic layer between the closed loops increases with increasing the fluctuation level. Figure 4.3(e), (f), and (g) correspond to globally chaotic scenario. The white regions on the Poincaré section arise when field lines move parallel to the plane of the figure.

In connection with the change of chaoticity of phase space with the level of fluctuation, it is necessary to visualize the spatial evolution pattern of a single chaotic field line. The behavior of a chaotic field line gets affected by the structure of the entire phase space. Figure 4.4 shows the spatial evolution pattern of the x component of chaotic trajectories for different levels of fluctuation. Since the two perpendicular coordinates x and y are in equal footing, y component has similar pattern of spatial evolution. Furthermore z component increases linearly with distance because of the presence of a steady field along z direction and is of no relevance here. It is clearly seen from figure 4.4(a), (b) and (c) that for mixed phase spaces, the chaotic trajectories consist of oscillations about a fixed mean value over a certain length interval during its evolution. On the other hand, for the fluctuation levels $\delta B/B_0 = 5.0$, 8.0, and 10.0, which correspond to globally chaotic phase space, the trajectories look almost random as depicted in figure 4.4(d), (e), and (f). Distribution of the field line displacements for x component of a chaotic trajectory, shown in figure 4.5(a), gives indication of Levy flights for low values of fluctuation associated with long coherent displacements. Such coherent displacements give rise to long tails in the distribution. Figure 4.5(b) shows that for higher values of fluctuations, the distribution is close to a Gaussian indicative of randomness in the field lines.

In order to visualize the phase space during the oscillation of a chaotic trajectory about a fixed mean value, the Poincaré section is plotted again for the same trajectory during the concerned length interval. Figure 4.6(a1) shows part of a chaotic trajectory previously shown in figure 4.4(a) for $\delta B/B_0 = 0.5$. Here the trajectory is plotted in two different colors red and blue to distinguish the phase space dynamics of the trajectory

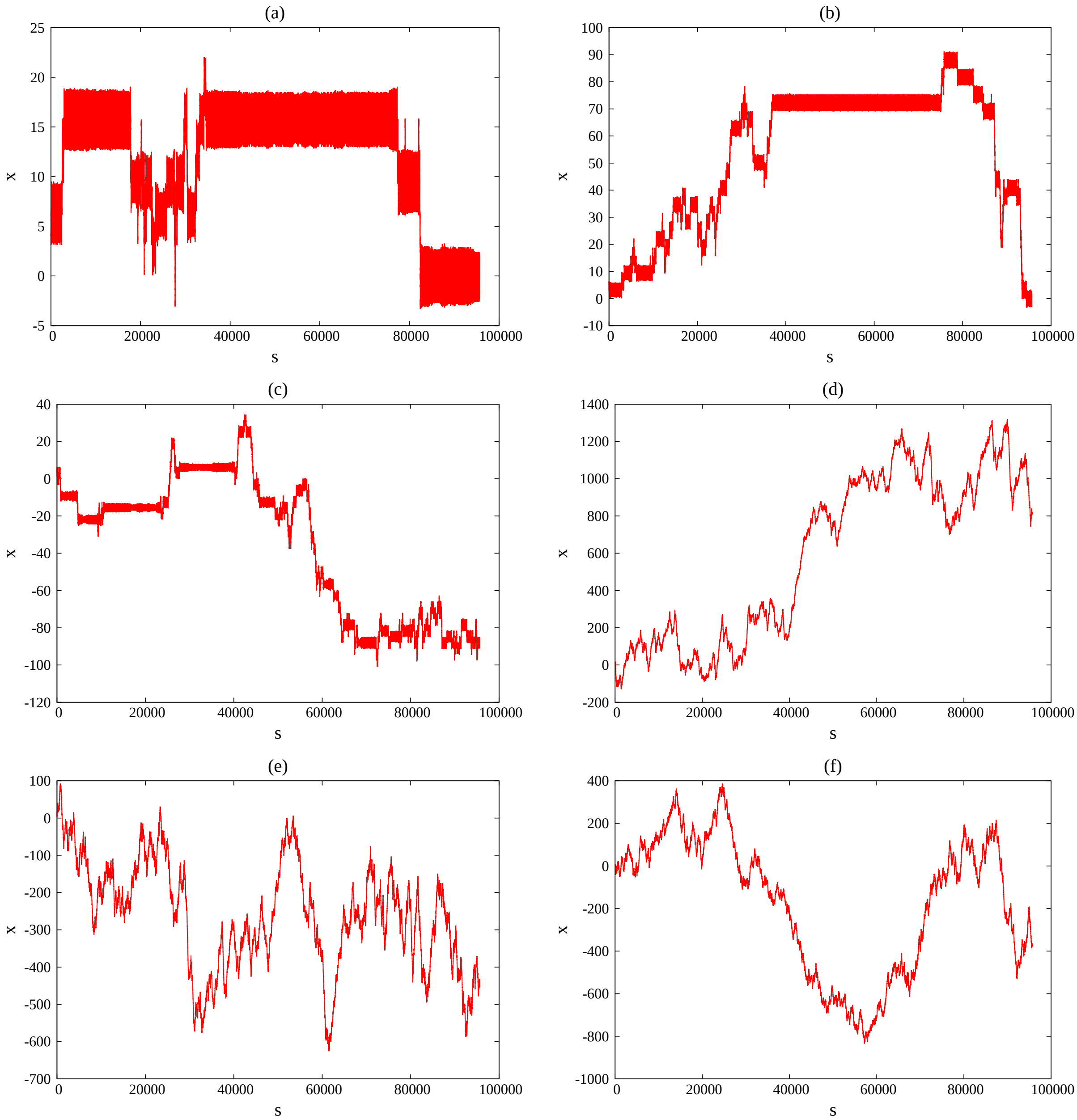

Figure 4.4: Spatial evolution of the x component of a chaotic field line for (a) $\delta B/B_0 = 0.5$, (b) $\delta B/B_0 = 0.6$, (c) $\delta B/B_0 = 0.7$, (d) $\delta B/B_0 = 5.0$, (e) $\delta B/B_0 = 8.0$, and (f) $\delta B/B_0 = 10.0$.

during the corresponding two length intervals. The Poincaré section for each part of this trajectory is plotted by the same colors in figure 4.6(b1) and (c1). A chaotic trajectory cannot enter some regions which is seen from figure 4.6(b1). Such regions are totally invariant in nature. Moreover, the oscillation of the chaotic trajectory about a fixed mean value corresponds to a localized movement in the surface-of-section, which may be called stickiness. The cluster of blue points in figure 4.6(c1) corresponds to the field line

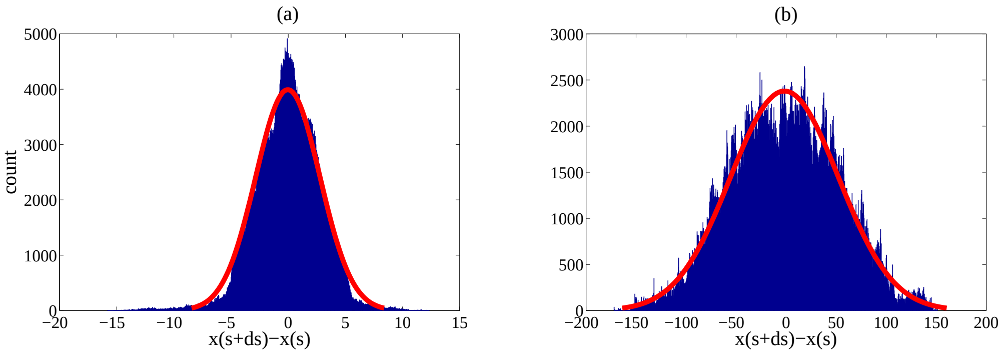

Figure 4.5: Distribution of the x component of a chaotic trajectory for (a) $\delta B/B_0 = 0.5$, and (b) $\delta B/B_0 = 10.0$.

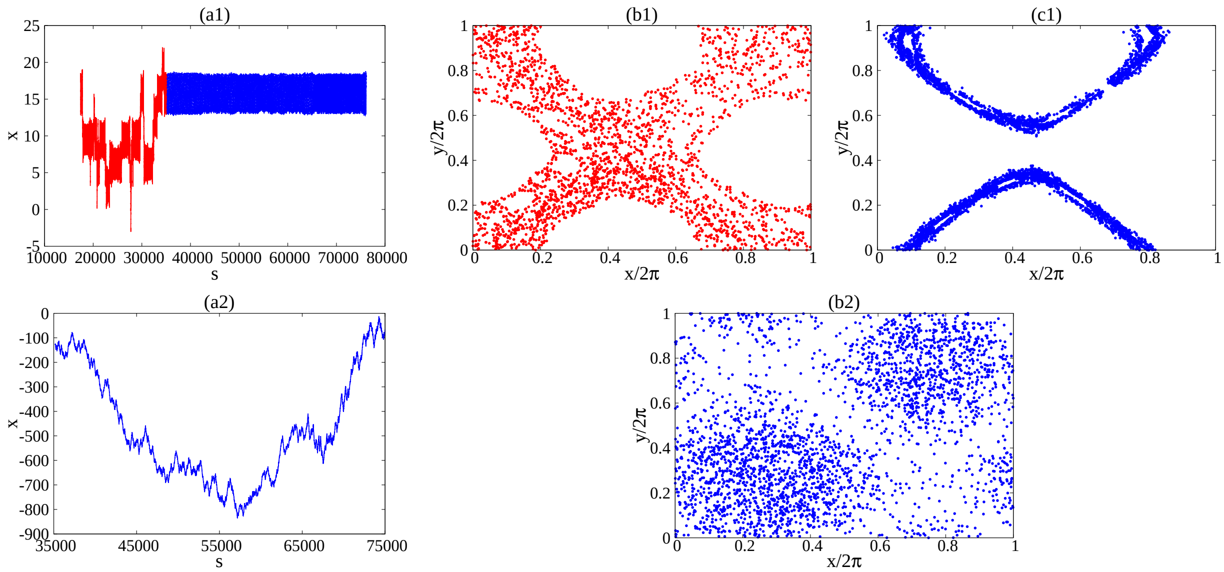

Figure 4.6: Spatial evolution of the x component of a chaotic field line for (a1) $\delta B/B_0 = 0.5$, (a2) $\delta B/B_0 = 10.0$; and corresponding $z = 0$ Poincaré surface-of-section for (b1) & (c1) $\delta B/B_0 = 0.5$, (b2) $\delta B/B_0 = 10.0$.

trapping in a small domain. Similar plots in figure 4.6(a2) and (b2) for $\delta B/B_0 = 10.0$ are given here to show the phase space dynamics of a randomly evolving trajectory in contrast to a sticky one. Here although a sticky trajectory corresponds to an oscillation about a fixed mean value and a localized movement in phase space, there is no spatial regularity in the sticky part of a chaotic field line which is also confirmed by the corresponding spatial Fourier Transform consisting of a broadband structure shown in figure .

After getting information about the phase space for different levels of fluctuation, it is necessary to characterize the field lines by studying their diffusion properties. Such

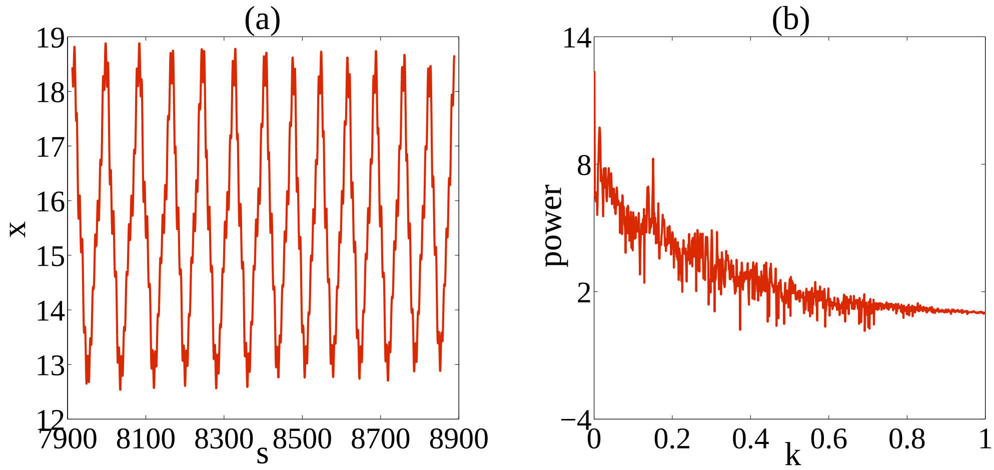

Figure 4.7: (a) Sticky part of a chaotic field line, and (b) FFT of the sticky part of the field line for $\delta B/B_0 = 0.5$.

analysis helps us to understand the global behavior of the field lines in a quantitative way. Figure 4.8 shows the plots of $log_{10}\sigma_x^2$ as a function of $log_{10}s$ along with their least square fits for different values of $\delta B/B_0$. For the numerical calculation of variance, all the field lines in an ensemble are taken from the chaotic part of the phase space. The choice of initial conditions are made by inspecting figure 4.3. The field lines for the fluctuations with $\delta B/B_0 < 1$ can be characterized by subdiffusive behavior. In the latter cases, we find nearly normal diffusion for higher values of fluctuation.

Again the results of diffusion characteristics of the field lines are supported by computing the kurtosis of field line displacement Δx as a function of s. Anomalous diffusion of field lines, for the lower values of fluctuation, corresponds to kurtosis values larger than 3 as evidenced from figure 4.9(a), (b), and (c). On the other hand, for the higher values of fluctuation, the diffusion is close to normal and the kurtosis nearly saturates to 3 in the asymptotic limit. The same behavior was observed in the previous studies of Zimbardo et al. [35]. The distribution of Δx at $s = 1000$ is shown in figure 4.10 in which two different types of distribution, one with kurtosis value larger than 3 and another nearly equal to 3, for two different fluctuation levels, are shown to distinguish their natures. Fitted Gaussian curves drawn by the red lines indicate that the distribution for lower fluctuation level is more peaked than a Gaussian one, whereas for higher

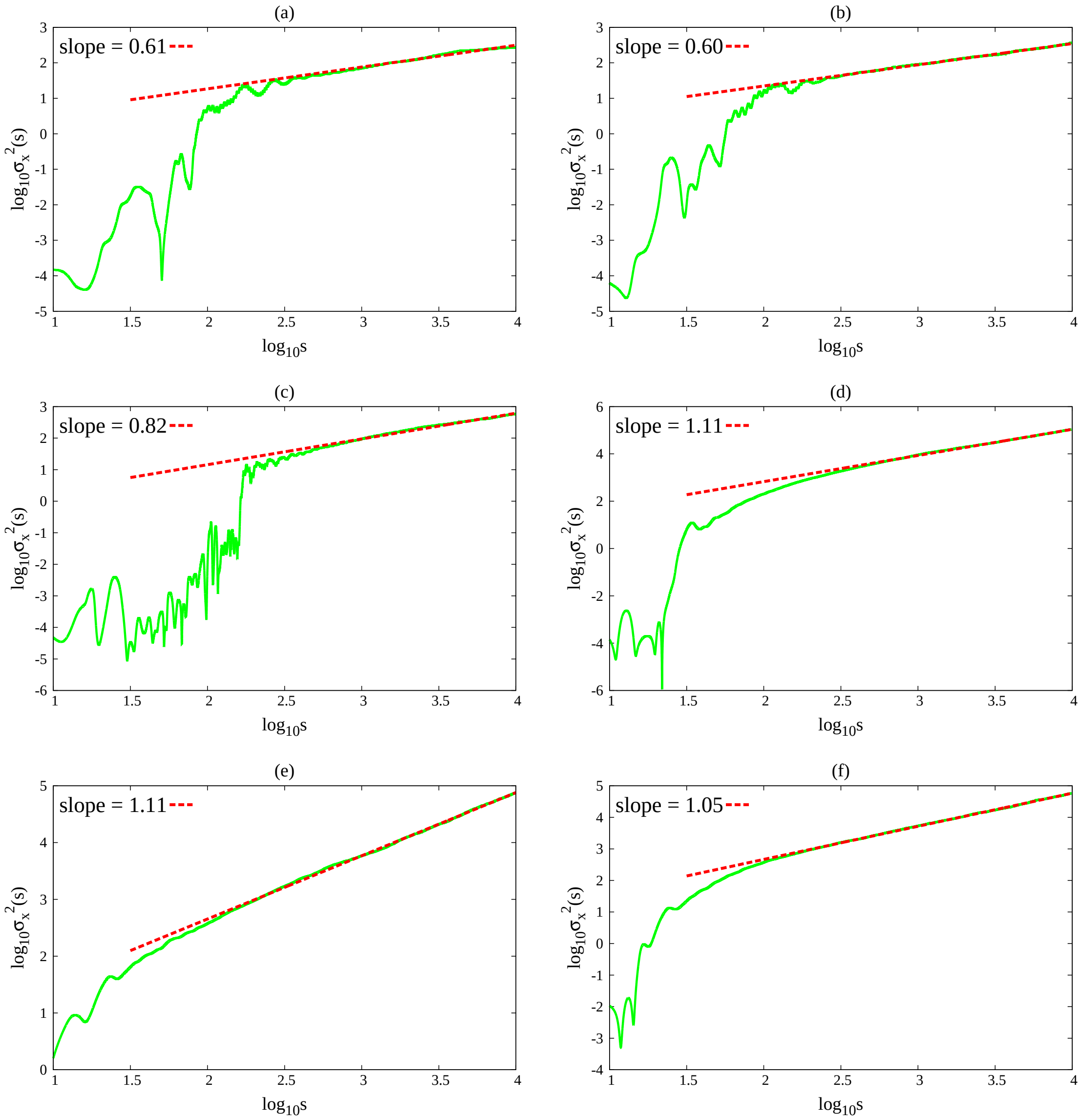

Figure 4.8: Fit of the variance of δx for (a) $\delta B/B_0 = 0.5$, (b) $\delta B/B_0 = 0.6$, (c) $\delta B/B_0 = 0.7$, (d) $\delta B/B_0 = 5.0$, (e) $\delta B/B_0 = 8.0$, and (f) $\delta B/B_0 = 10.0$.

fluctuation level, it is close to Gaussian.

4.2 Dynamics of charged particles

The motion of charged particles in complex magnetic fields is investigated in connection with magnetized plasma confinement. In order to study the dynamics of a charged particle, we consider a non relativistic particle, governed by the following equations of

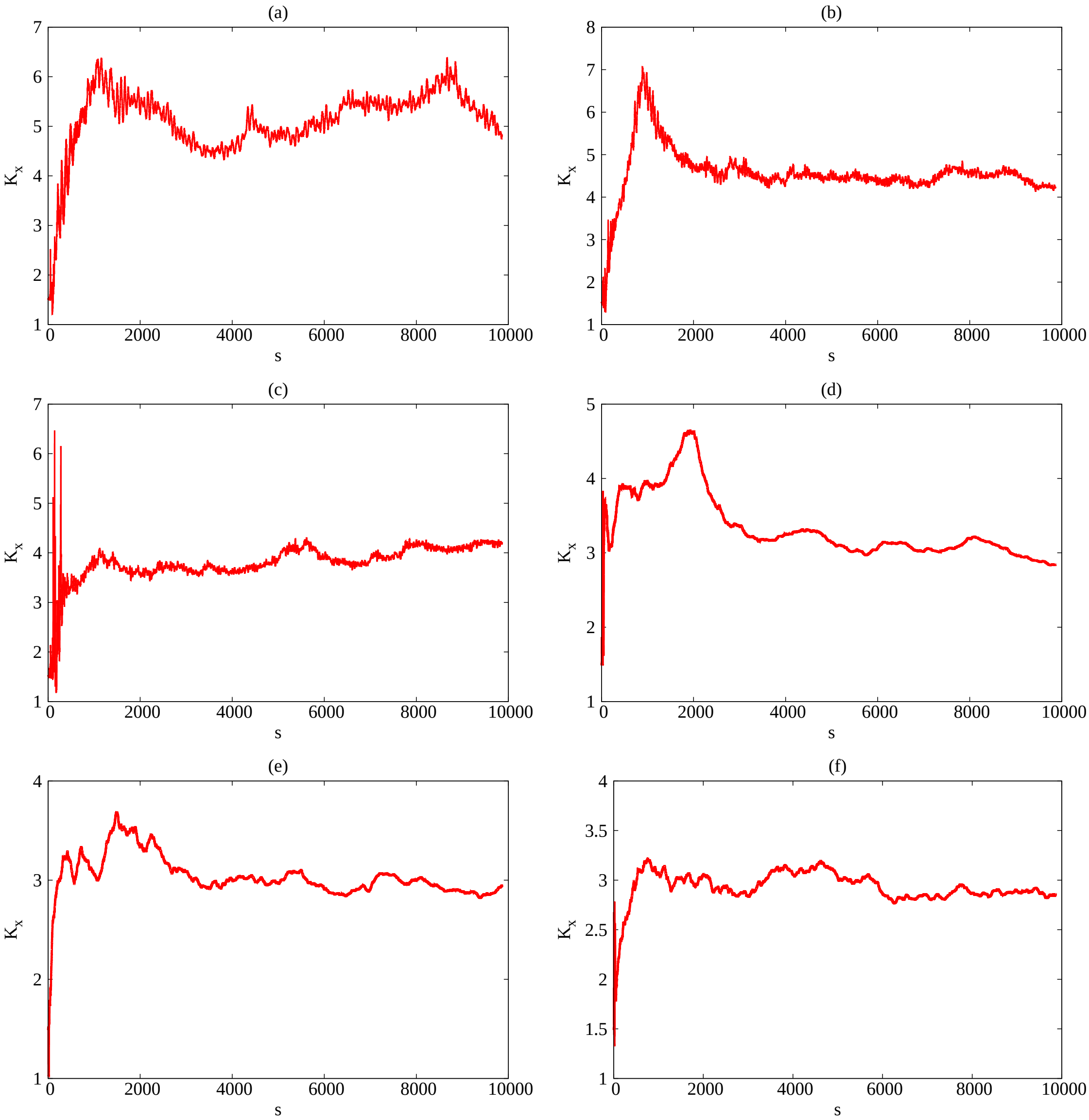

Figure 4.9: Kurtosis of Δx as a function of s for (a) $\delta B/B_0 = 0.5$, (b) $\delta B/B_0 = 0.6$, (c) $\delta B/B_0 = 0.7$, (d) $\delta B/B_0 = 5.0$, (e) $\delta B/B_0 = 8.0$, and (f) $\delta B/B_0 = 10.0$.

motion

$$\frac{d\mathbf{r}}{dt} = \mathbf{v}, \frac{d\mathbf{v}}{dt} = \frac{q}{m}\mathbf{v} \times \mathbf{B} \tag{4.6}$$

Here $\mathbf{v}$ is the velocity of a particle at time t and position $\mathbf{r}$. q and m are charge and mass of the particle respectively. Now, we normalize position coordinates by $1/\lambda$, t by $1/\Omega$ and $\mathbf{v}$ by Ω/λ where $\Omega = qB_0'/m$. In terms of dimensionless parameters, the equations

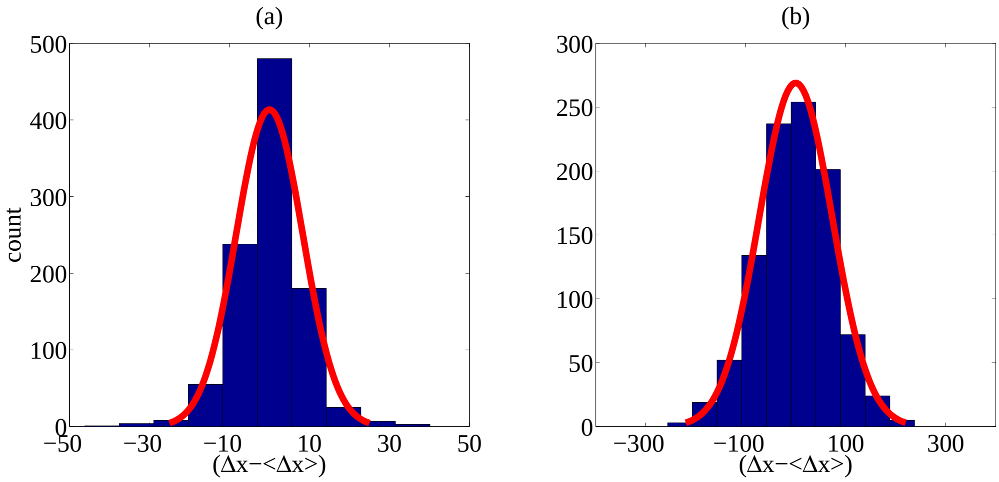

Figure 4.10: Distribution of Δx at $s = 1000$ for (a) $\delta B/B_0 = 0.5$, and (b) $\delta B/B_0 = 10.0$.

of charged particle motion take the form

$$\frac{d\mathbf{r}}{dt} = \mathbf{v}, \frac{d\mathbf{v}}{dt} = \mathbf{v} \times \mathbf{B} \tag{4.7}$$

Corresponding to the normalizations used here, v or $\sqrt{E}$ is a measure of the ratio of the Larmor radius of the particle to the scale length of magnetic field inhomogeneity.

4.2.1 Spatial diffusion of charged particles

In general, it is not possible to integrate the equations of motion (equation (4.7)) analytically. So we make use of numerical method. The particle orbit equations are integrated using fourth order Runge-Kutta scheme with fixed step size. The algorithm ensures the energy conservation over the required time interval with a relative accuracy of the order of 10^{-5}. In order to investigate the transport properties of the particles, we consider an ensemble of n_p particles. For each particle, we solve the equations of motion to construct, at regular time intervals δt, an array for the x component of position vector along the particle trajectory. For a particular p-th particle, the array is of the form $x_1^{(p)}, x_2^{(p)}, \ldots.., x_n^{(p)}$ and the particle trajectory is evolved for a time span $(n-1)\delta t$. Here, we take 100 particles ($n_p = 100$) and 4×10^5 array elements ($n = 4 \times 10^5$) for each particle, where each trajectory is evolved for 4×10^7 steps. Now we define the ensemble-averaged mean square displacement for a particular lag time $\Delta t = k\delta t$ as

$$<< \Delta x^2 >>= \frac{1}{n_p} \sum_{p=1}^{n_p} \left[\frac{1}{n-k} \sum_{i=1}^{n-k} \left(x_{i+k}^{(p)} - x_i^{(p)} \right)^2 \right] \tag{4.8}$$

where $k = 1, 2, ..., K$ with $K = 10^5$. The outer sum is the ensemble average over particles and the inner sum represents the average of mean square displacement over all pairs of points separated by a time $\Delta t = k\delta t$ for each particle. In a spatially varying magnetic field, the energy of a particle is conserved. The initial positions of the particles are chosen from the chaotic part of the Poincaré sections shown in fig. 4.3 and initial velocities are chosen in such a way that the energies of all the particles are same.

To explore the different transport regimes of charged particles, we consider two different cases. First we consider the case with particle energy less than 1 i.e. the Larmor radii of the particles are smaller than the scale length of magnetic field inhomogeneity, whereas in the second case, we consider that the normalized energy of the particles is greater than 1. Fig. 4.11 shows the spatial transport of the particles in the perpendicular

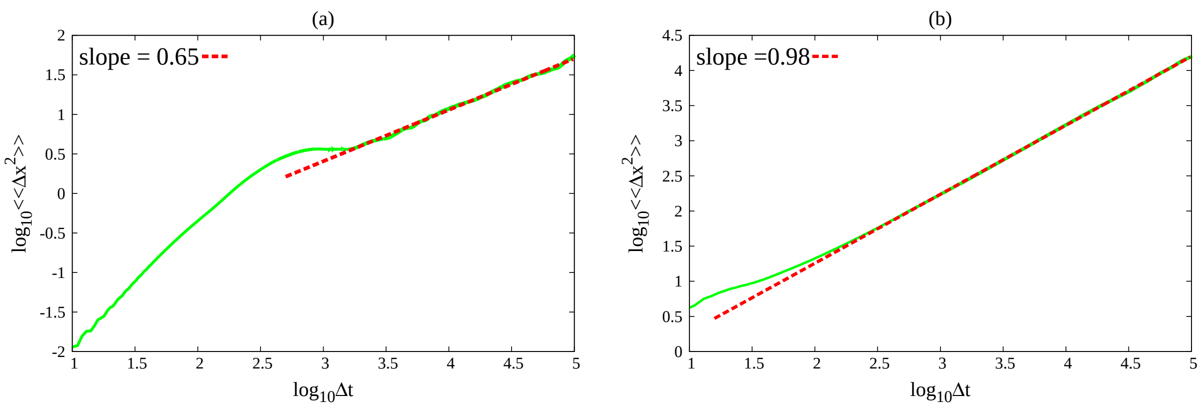

Figure 4.11: Ensemble-averaged mean square displacement $<< \Delta x^2 >>$ as a function of time lag Δt along with fit for (a) $\sqrt{E} = 0.1$ and (b) $\sqrt{E} = 2.0$ with $\delta B/B_0 = 0.5$.

direction of the mean field for two different normalized energies with relative fluctuation strength $\delta B/B_0 = 0.5$. When the Larmor radii of the particles are smaller than the scale length of magnetic field inhomogeneity, it is easier to identify the field lines associated with the particles and the transport law for the particles is consistent with that of the field lines. On the other hand, when the Larmor radii of the particles are greater than the scale length of magnetic field inhomogeneity, the particles encounter a variety of field lines during one cyclotron orbit and the transport law for the particles becomes entirely different from that of the field lines (see fig. 4.8 and 4.11). For $\delta B/B_0 = 0.5$, the particles are subdiffusive in nature when $\sqrt{E} = 0.1$, but with $\sqrt{E} = 2.0$, particles follow nearly random or Gaussian diffusion, although the field lines are subdiffusive.

4.3 Summary

The transport characteristics of a particular double curl magnetic field in presence of a uniform mean field is studied for levels of fluctuation $\delta B/B_0$. For small values of $\delta B/B_0$, the phase space is a mixture of some islands and chaotic regions, while for larger values, phase space is devoid of any island like regions. Sticky behavior results from the trapping of field line trajectories in the localized regions of phase space. For lower fluctuation levels, field lines assume the shape of spirals in various local regions for a long time causing an effect similar to trapping. In presence of such effects, the transport is subdiffusive with a scaling exponent $\alpha < 1$. With increase in the relative strength of fluctuations, the area occupied by the stochastic regions increases and finally the transport becomes diffusive at higher fluctuation levels, $\delta B/B_0 > 1$, with disappearance of all the magnetic surfaces. When the Larmor radii of the particles are smaller than the scale length of magnetic field inhomogeneity, the transport law for the field lines and the particles are almost same, while larger Larmor radii lead to different transport law for the particles from that of the magnetic field lines.

CHAPTER 5

Energization of charged particles in regular and chaotic magnetic fields

In the present chapter, we study the dynamics of charged particles in stationary inhomogeneous chaotic as well as regular magnetic fields varying in one-dimension and compare the results addressing the energization problem in the presence of a uniform electric field.

5.1 Introduction

Various descriptions of electromagnetic fields have been used in the study of charged particle dynamics such as large-scale coherent structures, spectral representation of waves to model turbulent fluctuations [52,67] or turbulent fields resulting from evolution of MHD fields [68]. Quite often, magnetic field fluctuations are governed by simple nonlinear dynamic equations obtained from fluid models [69] or otherwise. Stationary magnetic fields that are obtained as Vlasov-Maxwell equilibria also display chaotic behavior for a suitable choice [7] of single particle distribution function.

5.2 Model for chaotic magnetic fields

First we consider a magnetic field given by $\mathbf{B} = B_x(z)\hat{\mathbf{i}} + B_y(z)\hat{\mathbf{j}}$ where B_x, B_y are obtained as solutions of the following coupled differential equations with $\mathbf{B} = \nabla \times \mathbf{A}$.

$$\frac{d^2 A_{x,y}}{dz^2} + A_{x,y} + \mu A_{x,y} A_{y,x}^2 = 0 \tag{5.1}$$

Here all the variables are normalized. Magnetic field is normalized by some constant magnetic field B_0, position coordinates are normalized by a characteristic length scale L and A_x and A_y are normalized by $B_0 L$.

For $\mu = 0$, the system of equations governing the magnetic fields is integrable and corresponds to a two dimensional harmonic oscillator. For finite values of μ, the system corresponds to coupled oscillators and all cases with $\mu \neq 0$ are likely to be non integrable leading to chaotic one dimensional profiles for magnetic field. Similar equations governing the behavior of magnetic fields have also been obtained by Lee and Parks [69] using flowing MHD plasma models leading to solutions that display chaotic behavior. Figure 5.1 shows the one dimensional profiles of magnetic fields for different values of μ and figure 5.2 shows the variation of RMS values $\langle B_x^2 + B_y^2 \rangle^{1/2}$ of the fluctuating magnetic fields for different values of μ. Magnetic field line trajectories (x, y) of magnetic fields

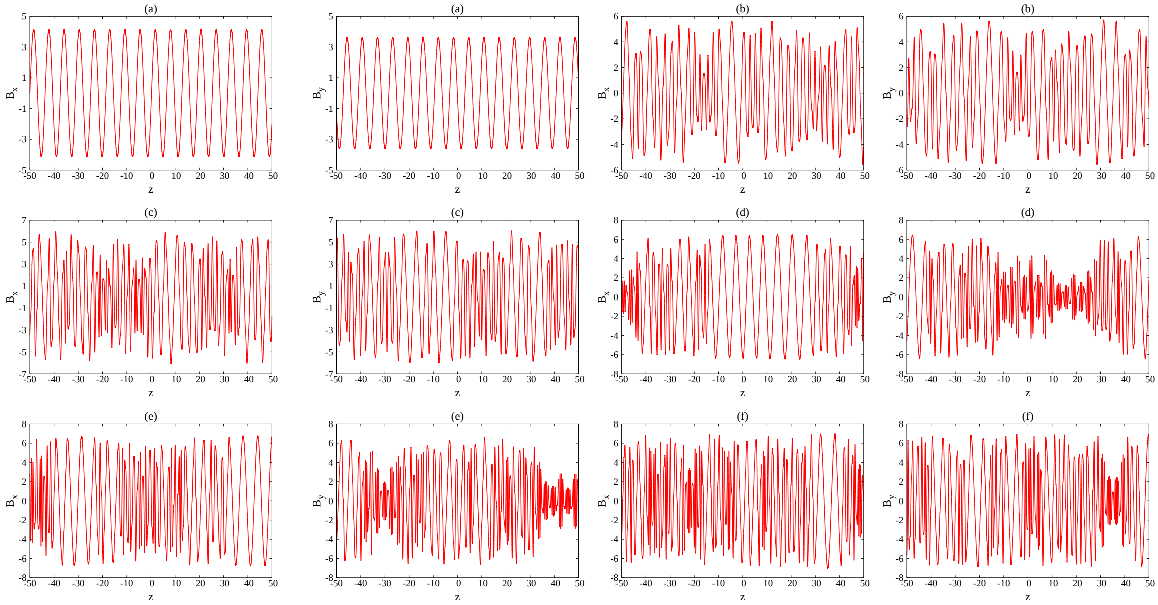

Figure 5.1: Figures showing one dimensional magnetic field profiles for (a)$\mu = 0$, (b)$\mu = 1$, (c)$\mu = 2$, (d)$\mu = 3$, (e)$\mu = 4$, and (f)$\mu = 5$.

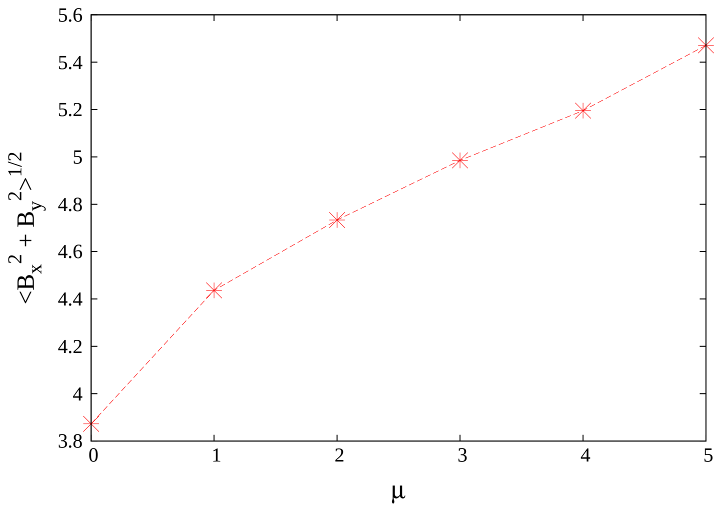

Figure 5.2: Plot of RMS values of fluctuating magnetic field against μ.

given by $(B_x(z), B_y(z))$ defined in equation (5.1) for all values of μ are obtained from

$$\frac{dx}{dy} = \frac{B_x}{B_y} \tag{5.2}$$

which are parallel straight lines in z constant plane. In order to study the chaotic dynamics, we consider the configuration $\mathbf{B} = (B_x(z), B_y(z), B_z)$ where we now include a constant magnetic field B_z in the z direction. Similar purely one-dimensional magnetostatic fields were considered by Mace et al. [67] for numerical investigation of perpendicular diffusion of charged test particles. Now field line trajectories are described by

$$\frac{dx}{dz} = \frac{B_x}{B_z}, \frac{dy}{dz} = \frac{B_y}{B_z} \tag{5.3}$$

In presence of constant B_z, magnetic field lines for zero and nonzero values of μ are shown in figure 5.3. For a particular set of fluctuating B_x and B_y, constant B_z is chosen in such a way that $\langle B_x^2 + B_y^2 \rangle^{1/2} = B_z$ throughout this work.

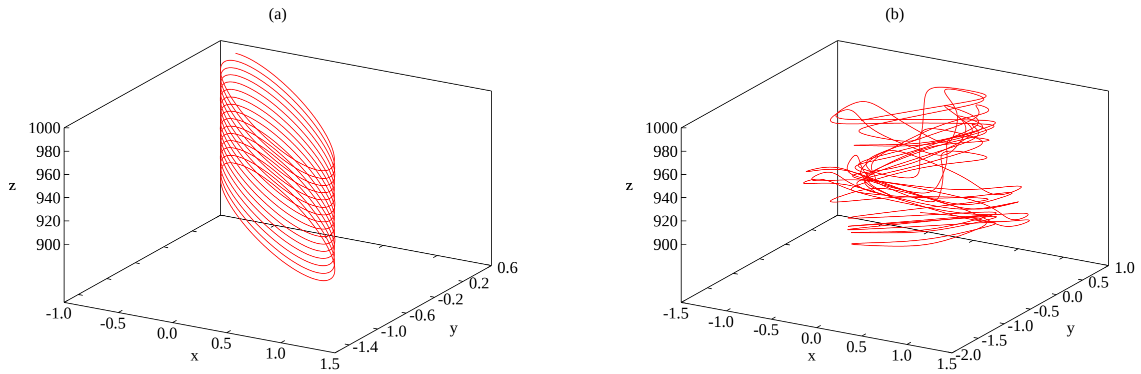

Figure 5.3: Figures showing regular and chaotic field line trajectories for (a)$\mu = 0$ and (b)$\mu = 1$.

5.3 Charged particle dynamics and energization

In order to study the dynamics of a charged particle, we consider a non relativistic particle, governed by the following equations of motion.

$$\frac{d\mathbf{r}}{dt} = \mathbf{v}, \frac{d\mathbf{v}}{dt} = \frac{q}{m}\mathbf{v} \times \mathbf{B} \tag{5.4}$$

Here $\mathbf{v}$ is the velocity of a particle at time t and position $\mathbf{r}$. q and m are charge and mass of the particle. We normalize position coordinates by a characteristic length scale L, magnetic field by a constant magnetic field strength B_0, time by $\Omega = \frac{qB_0}{m}$ and velocity by $L\Omega$.

In a magnetic field configuration $(B_x(z), B_y(z), B_z)$, the equation of charged particle motion has three constants of motion given by the Hamiltonian $H_E = v^2/2$ and two other constants $C_x = v_x + A_x(z) - B_z y$, $C_y = v_y + A_y(z) + B_z x$ associated with x and y motion respectively. The Poisson brackets of the constants of motion show that $[H_E, C_x] = [H_E, C_y] = 0$, while $[C_x, C_y] = -2B_z$, showing that C_x, C_y are not always in involution. Thus the system may possess some stochastic orbits even in the case of regular field lines, i.e., when $\mu = 0$ [51].

In order to study energization, a constant electric field is introduced in the z-direction with $\mathbf{E} = E_z\hat{\mathbf{k}}$. x and y components of chaotic magnetic field are numerically obtained by solving the coupled nonlinear differential equation with initial condition $A_x = 2$, $\frac{dA_x}{dz} = 3$, $A_y = 1$, $\frac{dA_y}{dz} = 4$. No significant change in the dynamics of the particles has been observed due to choice of a different set of initial conditions. Linear interpolation method is used to get the magnetic field components at particle positions. Particle orbit equations are solved numerically using the Dormand-Prince method with fixed step size. The step size for the numerical solution is chosen in such a way that on decreasing the step size, the results remain unaffected. Energy conservation in absence of electric field is maintained over the time interval considered here with a relative error of the order of 10^{-6}. Ensemble averaged energy gain is generated by solving 16384 copies of the following six dimensional dynamical system

$$\frac{d\mathbf{r}}{dt} = \mathbf{v}, \frac{d\mathbf{v}}{dt} = \mathbf{E} + \mathbf{v} \times \mathbf{B} \tag{5.5}$$

where electric field is normalized by $L\Omega B_0$.

Initially each component of the particle positions are randomly chosen from -1 to 1 with each normalized component of velocity randomly distributed between 0.01 to 0.03. Constraints on chosen initial values of particle velocity and electric field result from accessibility to the already fixed values of chaotic magnetic field data. Figure 5.4

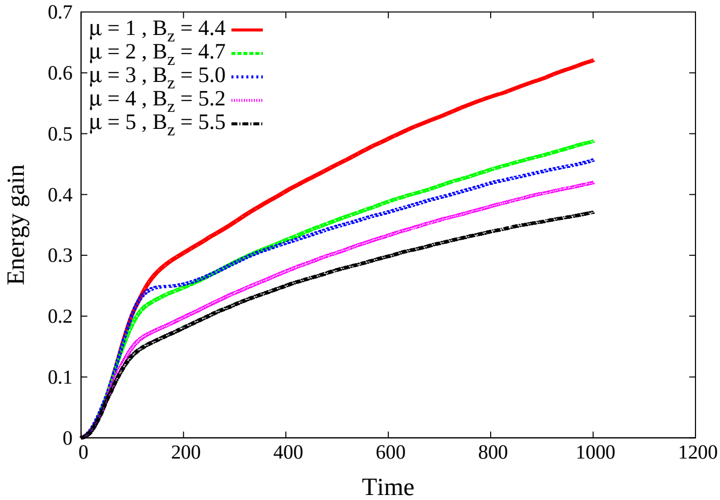

Figure 5.4: Plot of average energy gain against time in chaotic magnetic fields for different values of μ with constant B_z. The value of B_z in each case satisfies the relation $\langle B_x^2 + B_y^2 \rangle^{1/2} = B_z$. Constant electric field in each case $E_z = 0.01$.

shows the plot of average energy gain vs. time for different values of μ and B_z with $E_z = 0.01$. The figure shows decrease in energy gain with increase in the value of μ i.e. with increase in the RMS value of fluctuating components of the chaotic magnetic field. Here, the overall pattern of fluctuating components of the magnetic field changes with changing μ. In uniform electric and magnetic fields, charged particle energy gain does not change with changes in magnetic field components that have a fixed value of the ratio $\sqrt{(B_x^2 + B_y^2)}/B_z$.

The changes in energy gain is occurring due to the inhomogeneity of magnetic fields.

Now, we consider the inhomogeneous magnetic field varying in one dimension considering the coupling parameter $\mu = 0$ of equation (5.1) and a constant B_z in z direction. Equation (5.1) can then be solved analytically to give the magnetic field $B_x = B_y = a \sin z + b \cos z$. Now $\langle B_x^2 + B_y^2 \rangle^{1/2} = \sqrt{a^2 + b^2}$. So the RMS value of fluctuating components can be increased by increasing the value of the amplitude of fluctuation $\sqrt{a^2 + b^2}$. In contrast to the previous case of chaotic inhomogeneous fields, here the overall pattern of fluctuation remains same with increase in RMS value of fluctuation. The corresponding energy gain of an ensemble of particles is shown in figure 5.5 with different values of constant B_z and a fixed value of electric field $E_z = 0.01$. Here, the value of a is kept fixed and the value of b is increased in such way that the RMS values become equal to that for chaotic cases. Figure 5.5 shows that the average energy

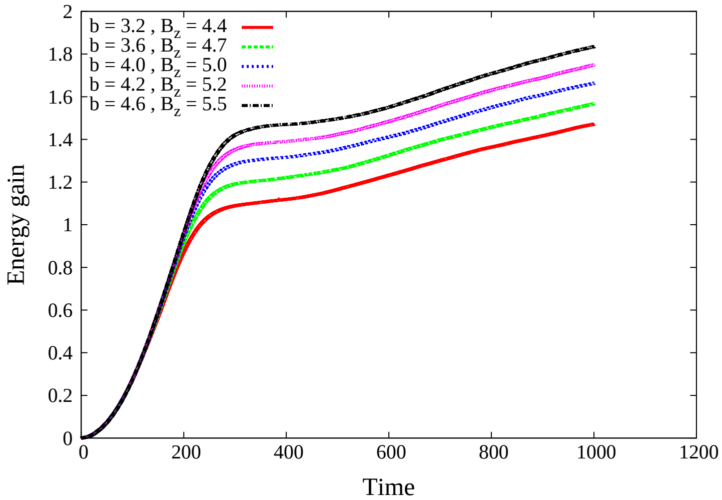

Figure 5.5: Plot of average energy gain against time in regular inhomogeneous magnetic fields with $B_x = B_y = a \sin z + b \cos z$ and constant B_z for different values of b. The value of a is kept fixed at $a = 3$. In each case, $B_z = \langle B_x^2 + B_y^2 \rangle^{1/2} = \sqrt{a^2 + b^2}$ and electric field $E_z = 0.01$.

gain in the chosen deterministic inhomogeneous magnetic fields having similar profiles increase with the increase in RMS value of fluctuation.

Now the gyroradius of a particle grows with time as energy grows. When gyroradius of a particle is very much smaller than the length scale of variation of the inhomogeneous magnetic fields, the particle encounters almost constant magnetic field. Average energy gain for $\mu = 1$ of figure 5.4 is shown in figure 5.6 and energy gain in uniform electric and magnetic field is drawn also for comparison. The red line corresponds to the energy gain in a uniform electro magnetic field whose x and y components of magnetic field are equal to the RMS values of fluctuation of the corresponding components for $\mu = 1$ case. The figure shows that for small times, the energy gain in an inhomogeneous magnetic field is same as that in a uniform field. But when the gyroradius becomes greater than the length scale of variation of inhomogeneous magnetic fields, particles encounter significant change in the magnetic field within one gyro orbit. Hence energy gain changes significantly from that in the uniform field which is shown in the figure at large times. For inhomogeneous chaotic magnetic field with $\mu = 1$ and $B_z = 4.4$, the energy gain

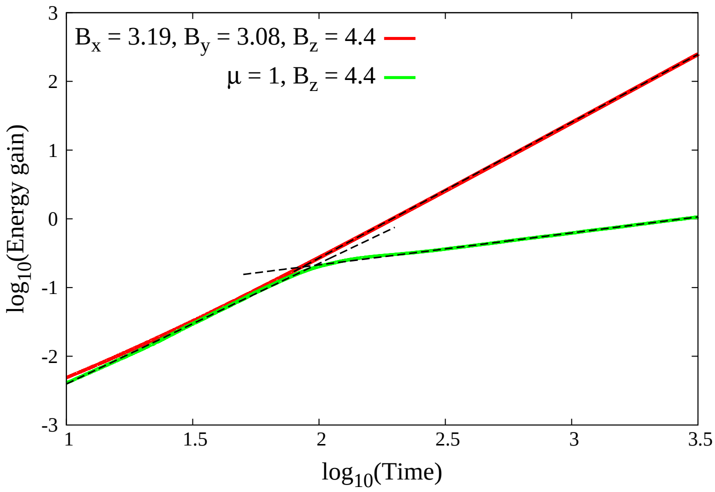

Figure 5.6: Plots of energy gain as a function of time with the broken straight lines showing the fits for small and large t. For each plot $E_z = 0.01$.

varies as $t^{1.75}$ at short times and is proportional to $t^{0.47}$ at large times. The energy gain in uniform electric and magnetic field varies as $t^{1.98}$ at large times.

5.4 Summary

In summary, we have studied the dynamics of charged particles in magnetostatic fields obtained as stationary solutions of coupled nonlinear equations with the model giving rise to both regular and chaotic magnetic fields varying in one dimension. The equations of motion of the particle become non integrable in inhomogeneous magnetic fields in the presence of a transverse uniform magnetic field component. Study of energy gain of an ensemble of charged particles is carried out in the presence of regular and chaotic magnetic fields together with a uniform electric field. The energy gain is shown to decrease with the increase in the value of the coupling parameter of the chosen equation, thereby changing the overall profile of the chaotic magnetic fields with increasing RMS values of fluctuation, whereas the same increase in RMS values by changing the amplitude of fluctuation for inhomogeneous regular magnetic fields leads to an increase in energy gain.

CHAPTER 6

Order to chaos transitions in damped KdV equation modeled as a jerk equation

This chapter deals with various dynamical aspects of KdV equation. First we study the periodic traveling wave solutions of KdV equation for both left and right moving waves. Then we introduce physically relevant dissipative type terms that lead to its formulation as a third order jerk equation whose order cannot be reduced. The rest of the chapter consists of the study of linear stability analysis and observation of Hopf bifurcation phenomena for left moving traveling wave solution for the above mentioned equation followed by numerical results.

6.1 Introduction

In the study of nonlinear waves, the KdV equation with its solitary wave solutions is of immense importance and finds applications in various branches of physics and engineering such as fluid dynamics, condensed matter, plasma physics, nonlinear optics and acoustics, quantum field theory and lattice-dynamics. The KdV theory had its origin in water waves, and it evolved to represent phenomena in many physical contexts where the steepening effect of nonlinearity is perfectly balanced by the spreading effect of dispersion. Numerical intergration of KdV equation leading to solitary wave solutions from general initial conditions was demonstrated by Zabusky et al. [70] in 1965. Like elementary particles, such waves survive collisions with other solitary waves, leading to their description by the term 'soliton'. Mathematical properties of the KdV equation demonstrate that the equation possesses infinite number of conservation laws, and is a completely integrable system that can be solved using inverse scattering transform technique. The equation is known to possess traveling wave solutions in the form of solitary waves as well as more general periodic solutions.

Various modifications and generalizations of the KdV equation have been derived over the years in order to model various physical phenomena such as the modified KdV, KdV-Burgers equation to name a few. The more complicated equations typically occur in flow of liquids containing gas bubbles [71], propagation of waves on an elastic tube filled with a viscous fluid [72], in plasmas in presence of viscous and collisional effects [23] etc. The dynamics of solitary blood waves in arteries in presence of viscosity and other perturbation parameters are described [73, 74] by evolution equations belonging to the KdV-Burgers family. In presence of a non-uniform plasma, whose concentration varies slowly and linearly in the direction of the wave, the system is described by a KdV equation with a small extra linear term [75] on the right hand side. The steady state solutions of the KdV-Burgers equation have been shown to model weak plasma shocks propagating perpendicularly to a magnetic field [76]. While diffusion dominates dispersion, the steady state solutions of the KdV-Burgers equation are monotonic shocks, and when dispersion dominates, the shocks are oscillatory. Ott and Sudan [77] modified the KdV equation to include various forms of energy dissipation and use the Kryloff-Bogoliubov asymptotic expansion technique to show that the effect of a small damping is to cause a slow decrease in the amplitude of the solitary wave.

The effect of adding a periodic Hamiltonian perturbation to the KdV equation generates a stochastic layer around the separatrix, leading to a region of chaotic dynamics in the neighborhood of the peaks of the solitons and long-period waves [78]. Such result was confirmed in experiments with ion-acoustic waves in plasma [79]. Using asymptotic methods, continuous traveling wave solutions of the periodically driven KdV-Burgers equation were represented [80] as a Poincaré map at the driver period, to show a developed chaos representing a random sequence of uncorrelated shocks. Several works [22, 81–83] have demonstrated the existence of chaotic behavior in a steady state KdV-Burgers equation perturbed by periodic forcing with the chaos occurring due to Melnikov sequence of subharmonic bifurcations as well as periodic doubling sequences. The onset of temporal chaos was demonstrated [84] for a KdV equation with zeroth order damping and periodic forcing which models ion sound waves damped by ion-neutral collisions.

Investigations of regular and chaotic motions of forced compound KdV-Burgers type equation with nonlinear terms of higher order and periodic forcing show [85] abundant dynamical phenomena such as complex bifurcation structure, a cascade of period doubling leading to chaos, intermittency behavior and interior crisis.

However, equations of the KdV family that were investigated for observation of chaos, were mostly treated as second-order equations in presence of external forcing that is responsible for generating all the complex dynamical behavior. Since the master equation that happens to be the KdV equation is a third order equation to begin with, a more judicious approach would be to study its dynamics by treating it as an autonomous system without reducing its order. It was pointed out by Gottlieb [86] that the simplest ordinary differential equation in single variable that is capable of exhibiting chaos is a third order equation. Third order autonomous differential equations in single variable that can be expressed in the form $\dddot{x} = J(x, \dot{x}, \ddot{x})$ are known as jerk equations, where the jerk function J is the time derivative of acceleration. Nonlinear forms of jerk equation are therefore important in the study of chaos. Through a numerical examination of third-order, one-dimensional, autonomous, ordinary differential equations with quadratic and cubic nonlinearities, Sprott [87, 88] has uncovered a number of algebraically simple jerk functions that are capable of exhibiting chaos. Another closely related study is in the context of Poincaré-Bendixon theorem that requires that autonomous first-order ordinary differential equations with continuous functions be at least three dimensional to have bounded chaotic solutions.

6.2 Periodic solutions of KdV Equation

The Kortweg-de Vries equation reads

$$x_\tau + x x_s + x_{sss} = 0 \tag{6.1}$$

where $x = x(s, \tau)$, with x, s, τ being real variables. The study of KdV equation finds importance in context of magnetic structures also. A possible way to explain the local formation of the small-scale magnetic structures was proposed by Ji et al. [89] based on $1 - D$ KdV equation. Now we look for traveling wave solutions of equation (6.1) considering solutions of the form $x(t) = x(s - V\tau)$ for both positive and negative traveling wave velocities [90] $(V > 0, V < 0)$ that describe right and left moving waves respectively. Substitution of this form into equation (6.1) leads to the following second and first-order equations

$$x_{tt} + \frac{1}{2}x^2 - Vx = A$$

which by one integration leads to

$$\frac{1}{2}x_t^2 = -\frac{1}{6}x^3 + \frac{1}{2}Vx^2 + Ax + B \tag{6.2}$$

where A and B are constants of integration.

Equation (6.2) can be written as

$$\int_{x(0)}^{x(t)} \frac{\sqrt{3}dx}{\sqrt{-x^3 + 3Vx^2 + 6Ax + 6B}} = t + t_0 \tag{6.3}$$

where t_0 is another constant of integration. The solutions of equation (6.3) can be written in terms of the Jacobi elliptic function as

$$x(t) = \beta_2 + (\beta_3 - \beta_2)\mathrm{cn}^2\left(\sqrt{\frac{\beta_3 - \beta_1}{12}}t; k\right) \tag{6.4}$$

where $\beta_1, \beta_2, \beta_3$ are the three real roots of

$$-x^3 + 3Vx^2 + 6Ax + 6B = 0$$

and obey the following:

$$\beta_1 < \beta_2 < \beta_3, \beta_1 + \beta_2 + \beta_3 = 3V$$

and

$$k^2 = \frac{\beta_3 - \beta_2}{\beta_3 - \beta_1}$$

The well known solitary wave solutions of the KdV equation can be obtained for zero boundary conditions in the limit $\beta_2 = \beta_1 = 0$, with the constants $A = B = 0$. These are recovered as a limiting case of cnoidal waves when $k \to 1$:

$$x = x_0 \mathrm{sech}^2\left(\frac{\sqrt{\mathrm{V}}}{2}\mathrm{t}\right)$$

and exist only when V is positive. In the limit $\beta_2 \to \beta_1$ with $k \to 1$, the hyperbolic solution $x(t)$ is retained for both positive and negative values of V in the form

$$x = x_\infty + x_0 \mathrm{sech}^2 \left(\sqrt{\frac{\beta_3 - \beta_1}{12}} \mathrm{t} \right)$$

This solution $x \to x_\infty$ as $t \to \infty$ does not satisfy the zero boundary conditions. Mancas [91] has extensively discussed the traveling wave solutions of KdV equation that are right or left moving waves for media with positive or negative dispersion respectively. Whether the traveling waves are compressive (bright) or rarefactive (dark), they are always right moving in a positive dispersive medium and left moving in a negative dispersive medium. For zero boundary conditions at $t = \pm\infty$, solitary wave solutions exist only for right moving waves. For a general boundary condition, the solutions in the form of Jacobi elliptic functions as expressed in equation (6.4), exist for both positive and negative values of V. For different choice of initial values, the value of the modulus k is shown to vary from 0 to 1, so that the nature of the solutions can vary from sinusoidal type to solitary wave type for both negative and positive traveling wave velocities as shown in figure 6.1. For conditions of positive V, the stability of cnoidal waves given by equation (6.4) was extensively dealt by Pava, Bona and Scialom [92].

6.3 KdV Equation in presence of dissipative terms

The study of weakly nonlinear, dispersive waves in many practical situations necessitate a modification of the KdV equation to the following form [93]

$$x_\tau + x x_s + x_{sss} + a x_{ss} + b x = 0 \tag{6.5}$$

where s and τ represent the space coordinate in one dimension and time respectively, and the terms involving a, b can be taken to represent terms arising due to presence of dissipative effects in the medium or an external perturbation. For negative values of a

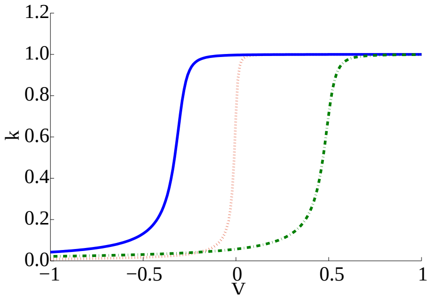

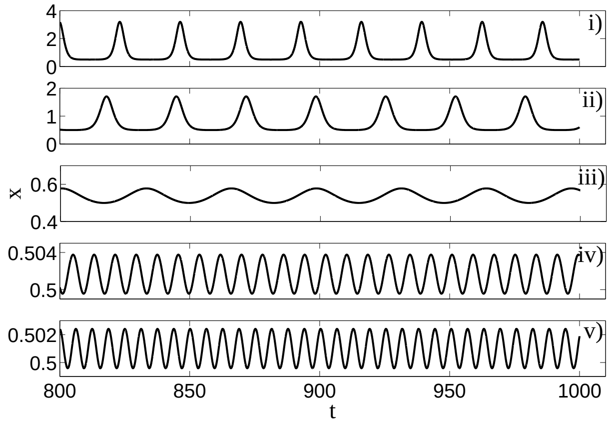

Figure 6.1: Left figure: Variation of modulus k with V for initial values $x, \dot{x}, \ddot{x}$ = i) $-0.3, 0.001, 0.001$(blue), ii)$-0.0001, 0.000061, 0.0001$ (red), iii)$0.5, 0.001, 0.001$(green). Right figure: Solutions of KdV equation for different values of V: (i) 1.4, (ii) 0.9, (iii) 0.5, (iv) -0.1, (v) -0.5 for the initial condition $(0.5, 0.001, 0.001)$.

and b, the Burger like term is known to lead to decay in the amplitude of the wave, whereas the other term is known to lead to wave steepening whereas positive values of both terms lead to opposite effects. For $a = b = 0$, equation (6.5) reduces to a second order equation which gives solitary wave solution of the form

$$x = x_0 sech^2 \left[\left(\frac{x_0}{12} \right)^{1/2} \left(s - \frac{x_0}{3} \tau \right) \right]$$

under conditions $x, x_t, x_{tt} \to 0$ as $t \to \pm\infty$ where $t = s - V\tau$ and x_0 is a constant. In presence of small but finite values of a and b, Ott and Sudan [77] use Kryloff-Bogoliubov asymptotic expansion technique with $a, b << 1$ to obtain solitary wave solution whose amplitude varies slowly with time

$$x = x_0(\tau) sech^2 \left[\left(\frac{x_0}{12} \right)^{1/2} \left(s - \frac{1}{3} \int x_0(\tau) d\tau \right) \right].$$

The slow variation of wave amplitude with time in presence of the terms a and b is given by

$$\frac{x_0(\tau)}{x_0(0)} = (1 + \nu a \tau)^{-1}, \text{ for } \ b = 0, a < 0$$

and

$$\frac{x_0(\tau)}{x_0(0)} = \exp(-4b\tau/3), \text{ when } \ a = 0, b > 0$$

where ν is a constant that signifies rate of time variation. For an unstable plasma, there exists a possibility of increase of wave amplitude with time [77].

For $b = 0$, numerical solution of equation (6.5) when solved as a third order equation, gives damped oscillatory solutions in the case of both right and left moving waves. However, KdV-Burgers equation when solved as a second order equation gives rise to shock type solutions due to the presence of two fixed points (saddle and focus or node) in the system. These features are absent in the third order equation that has a line of fixed points along the x-axis. Exact solutions for equation (6.5) have been obtained by Mancas [90] in terms for Weierstrass functions when $b = 0$.

In the present work, we consider traveling wave solutions of equation (6.5) having the form $t = s - V\tau$. Thus, new form of equation (6.5) is given by

$$x_{ttt} + (x - V)x_t + (ax_{tt} + bx) = 0 \tag{6.6}$$

where V is a constant.

Equation (6.6) is a third order jerk equation and can be rewritten as three first order ODE's as

$$\begin{aligned} \dot{x} &= y \\ \dot{y} &= z \\ \dot{z} &= -(x - V)y - az - bx \end{aligned} \tag{6.7}$$

6.4 Stability Analysis and Hopf Bifurcation

In order to understand the system dynamics, we consider the linear stability analysis for the fixed points of equation (6.7). The equilibrium or fixed points satisfy the condition $(\dot{x}, \dot{y}, \dot{z}) = (0, 0, 0)$. Here the system has only one equilibrium point obtained as $(x_0, y_0, z_0) = (0, 0, 0)$. The nature of the fixed point can be understood by analyzing the characteristic equation given by,

$$\lambda^3 + a\lambda^2 - V\lambda + b = 0 \tag{6.8}$$

The solution of the characteristic equation given in the appendix shows that one real and two complex roots can be obtained for some domain of the parameters (as mentioned in the appendix). The equilibrium point of the system will be stable if the real parts of all the roots of equation (6.8) are negative. By the Routh-Hurwitz criterion [94], this will happen if and only if the coefficients satisfy $a > 0$, $b > 0$ and $a(-V) > b$. Instability arises if the complex conjugate eigenvalues cross the imaginary axis into the right half plane. So, on the boundary of the stability, the eigenvalues will be $\lambda_1 = i\omega$, $\lambda_2 = -i\omega$ and $\lambda_3 = -a$ where $\omega > 0$. This set of complex eigenvalues leads to Hopf bifurcation. Since the system has three parameters, three cases can be considered here.

(i) a and b are fixed at 0.15 and 0.0015 respectively and V is varied as the bifurcation parameter. The critical value of V is given by $V = V_0 = -\frac{b}{a} = -0.01$. Equilibrium point will exist as a stable fixed point for $V < V_0$ and will become unstable for $V > V_0$. The parameters corresponding to Hopf bifurcation of the origin satisfy the conditions $a\omega^2 = b$ and $\omega^2 = -V_0$.

(ii) V and b are fixed at -0.005 and 0.0015 respectively and a is varied as the bifurcation parameter. The critical value of a is given by $a = a_0 = \frac{b}{(-V)} = 0.3$. Stable equilibrium of the system requires the condition $a > a_0$ and the condition $a < a_0$

makes the fixed point unstable. The parameters corresponding to Hopf bifurcation of the origin satisfy the conditions $a_0\omega^2 = b$ and $\omega^2 = -V$.

(iii) V and a are fixed at -0.007 and 0.15 respectively and b is varied as the bifurcation parameter. The critical value of b is given by $b = b_0 = a(-V) = 0.00105$ and the presence of stable and unstable fixed point requires the conditions $b < b_0$ and $b > b_0$ respectively. The parameters corresponding to Hopf bifurcation of the origin satisfy the conditions $a\omega^2 = b_0$ and $\omega^2 = -V$.

In order to make ω real, the parameter V should have negative values. So, the criteria for Hopf bifurcation will not be satisfied for traveling wave solutions moving towards right.

Now, the system of equations (6.7) can be written as

$$\dot{\mathbf{x}} = A\mathbf{x} + \mathbf{F}(\mathbf{x}), \mathbf{x} = (x, y, z)^T \in \mathbb{R}^3$$

where A is the Jacobian matrix evaluated at the fixed point. $\mathbf{F}$ is a smooth vector function starting with at least quadratic terms, $\mathbf{F}(\mathbf{x}) = \bigcirc(\|x\|^2)$ and is represented as, $\mathbf{F}(\mathbf{x}) = \frac{1}{2}B(\mathbf{x}, \mathbf{x}) + \frac{1}{6}C(\mathbf{x}, \mathbf{x}, \mathbf{x}) + \bigcirc(\|x\|^4)$.

$B(\mathbf{u}, \mathbf{v})$ and $C(\mathbf{u}, \mathbf{v}, \mathbf{w})$ are multilinear functions defined for vectors $\mathbf{u} = (u_1, u_2, u_3)^T \in \mathbb{R}^3$, $\mathbf{v} = (v_1, v_2, v_3)^T \in \mathbb{R}^3$, $\mathbf{w} = (w_1, w_2, w_3)^T \in \mathbb{R}^3$ and are given by,

$$B_i(\mathbf{u}, \mathbf{v}) = \sum_{j,k=1}^{3} \left. \frac{\partial^2 F_i(\xi)}{\partial \xi_j \partial \xi_k} \right|_{\xi=0} u_j v_k$$

$$C_i(\mathbf{u}, \mathbf{v}, \mathbf{w}) = \sum_{j,k,l=1}^{3} \left. \frac{\partial^3 F_i(\xi)}{\partial \xi_j \partial \xi_k \partial \xi_l} \right|_{\xi=0} u_j v_k w_l$$

where the matrix A is given by,

$$A = \begin{pmatrix} 0 & 1 & 0 \\ 0 & 0 & 1 \\ -b & V & -a \end{pmatrix}$$

and the parameter values correspond to Hopf bifurcation of the fixed point. If the matrix A has a pair of purely imaginary eigenvalues $\pm i\omega$ and the corresponding eigenvectors are $(\mathbf{q}, \bar{\mathbf{q}})$,

$$A\mathbf{q} = i\omega\mathbf{q},\ A\bar{\mathbf{q}} = -i\omega\bar{\mathbf{q}}$$

Also, let $\mathbf{p}$ be the adjoint eigenvector having the properties

$$A^T\mathbf{p} = -i\omega\mathbf{p},\ A^T\bar{\mathbf{p}} = i\omega\bar{\mathbf{p}}$$

with the normalization $\langle \mathbf{p}, \mathbf{q} \rangle = 1$ where

$$\langle \mathbf{p}, \mathbf{q} \rangle = \sum_{i=1}^{3} \bar{p}_i q_i$$

In order to analyze the bifurcation, we have to compute the first Lyapunov coefficient $l_1(0)$.

The expression for the first Lyapunov coefficient can be written as [95],

$$l_1(0) = \frac{1}{2\omega} Re[\langle \mathbf{p}, C(\mathbf{q}, \mathbf{q}, \bar{\mathbf{q}}) \rangle - 2\langle \mathbf{p}, B\big(\mathbf{q}, A^{-1}B(\mathbf{q}, \bar{\mathbf{q}})\big) \rangle + \langle \mathbf{p}, B\big(\bar{\mathbf{q}}, (2i\omega E - A)^{-1}B(\mathbf{q}, \mathbf{q})\big) \rangle] \tag{6.9}$$

where E is the identity matrix.

Now, the vectors $\mathbf{q}$ and $\mathbf{p}$ are

$$\mathbf{q} = \begin{pmatrix} 1 \\ i\omega \\ -\omega^2 \end{pmatrix}, \mathbf{p} = \begin{pmatrix} \frac{2b^2 + i\omega b(\omega^2 - V)}{4b^2 + \omega^2(\omega^2 - V)^2} \\ \frac{i(2b^2 + \omega^2 V^2 - w^4 V)}{\omega\left(4b^2 + \omega^2(\omega^2 - V)^2\right)} \\ \frac{-\omega^2(\omega^2 - V) + 2ib\omega}{4b^2 + \omega^2(\omega^2 - V)^2} \end{pmatrix}$$

Furthermore, the bilinear and trilinear functions $B(\mathbf{u}, \mathbf{v})$ and $C(\mathbf{u}, \mathbf{v}, \mathbf{w})$ can be expressed as,

$$B(\mathbf{u}, \mathbf{v}) = \begin{pmatrix} 0 \\ 0 \\ -(u_1 v_2 + u_2 v_1) \end{pmatrix}, C(\mathbf{u}, \mathbf{v}, \mathbf{w}) = \begin{pmatrix} 0 \\ 0 \\ 0 \end{pmatrix}$$

Then a series of algebraic manipulations gives the first Lyapunov coefficient as

$$l_1(0) = -\frac{2\omega^2 b\left(3\omega^4 - 15\omega^2 V\right)}{9\left(4b^2 + \omega^2(\omega^2 - V)^2\right)\left(b^2 + 4\omega^2 V^2\right)}$$

Now the three cases listed above can be considered separately.

(i) The roots of equation (6.8) for $a = 0.15$, $b = 0.0015$, $V = -0.01$ are $\lambda_{1,2} = \pm 0.1i$ and $\lambda_3 = -0.15$. At this point, the velocity of crossing i.e. $Re(\frac{d\lambda}{dV}\Big|_{\lambda=i\omega, V=V_0}) \neq 0$. Also, the third eigenvalue λ_3 remains negative for nearby values of the parameter V. The first Lyapunov coefficient at the above parameter values is $l_1(0) = -73.8462$.

(ii) The roots of equation (6.8) for $V = -0.005$, $b = 0.0015$, $a = 0.3$ are $\lambda_{1,2} = \pm 0.07071i$ and $\lambda_3 = -0.3$. At this point, the velocity of crossing i.e. $Re(\frac{d\lambda}{da}\Big|_{\lambda=i\omega, a=a_0}) \neq 0$. Also, the third eigenvalue λ_3 remains negative for nearby values of the parameter a. The first Lyapunov coefficient at the above parameter values is $l_1(0) = -28.7071$.

(ii) The roots of equation (6.8) for $V = -0.007$, $a = 0.15$, $b = 0.00105$ are $\lambda_{1,2} = \pm 0.083666i$ and $\lambda_3 = -0.15$. At this point, the velocity of crossing i.e. $Re(\frac{d\lambda}{db}\Big|_{\lambda=i\omega, b=b_0}) \neq 0$. Also, the third eigenvalue λ_3 remains negative for nearby values of the parameter b. The first Lyapunov coefficient at the above parameter values is $l_1(0) = -100.6880$.

So the system given by equation (6.7) undergoes a Hopf bifurcation which implies the appearance of a limit cycle in all the cases listed above. Since the first Lyapunov coefficient is negative in each case, the bifurcation is supercritical Hopf bifurcation and a unique stable limit cycle bifurcates from the origin. Now with the change of the parameters, the stable limit cycle loses stability to form limit cycles of period two, four, eight and so on giving rise to a period doubling bifurcation route to chaos.

6.5 Numerical Procedure and Results

The system of equations (6.7) is solved numerically using fourth order Runge-Kutta method with initial condition $(x, y, z) = (-0.0001, 0.000061, 0.0001)$ at $t = 0$. The region of parameter space with bounded solutions is relatively small. So the parameters are chosen accordingly.

Figure 6.2 shows the time series plots of x obtained from numerical solution of equation (6.7) for different values of V with fixed values of a and b which are equal to 0.15 and 0.0015 respectively. This figure clearly shows that the number of periods increases with increase in the value of V and the system becomes chaotic for $V > -0.00515$.

Figure 6.3 shows the phase space diagram corresponding to the time series shown in Fig. 6.2. Phase space trajectories suggest that for $V < -0.01$, the system exhibits stable fixed point dynamics and with increase in the value of V, the system exhibits limit cycle behavior as is obtained earlier from the Routh-Hurwitz criterion. Further increase in V leads the system towards chaotic regime via two period, four period, eight period cycle

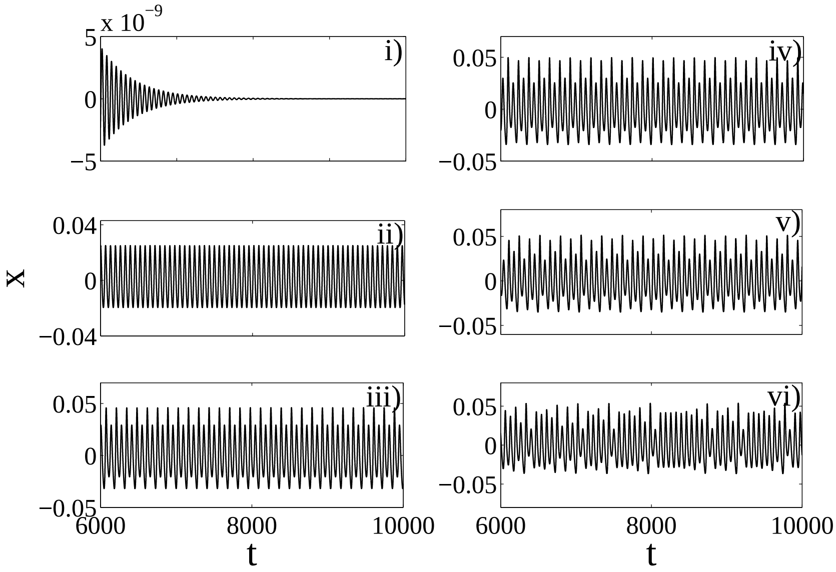

Figure 6.2: Numerically simulated time series for different values of V: (i) -0.01400, (ii) -0.00900, (iii) -0.00550, (iv) -0.00525, (v) -0.00515, and (vi) -0.00500.

and so on. This behavior is a clear signature of period doubling route to chaos.

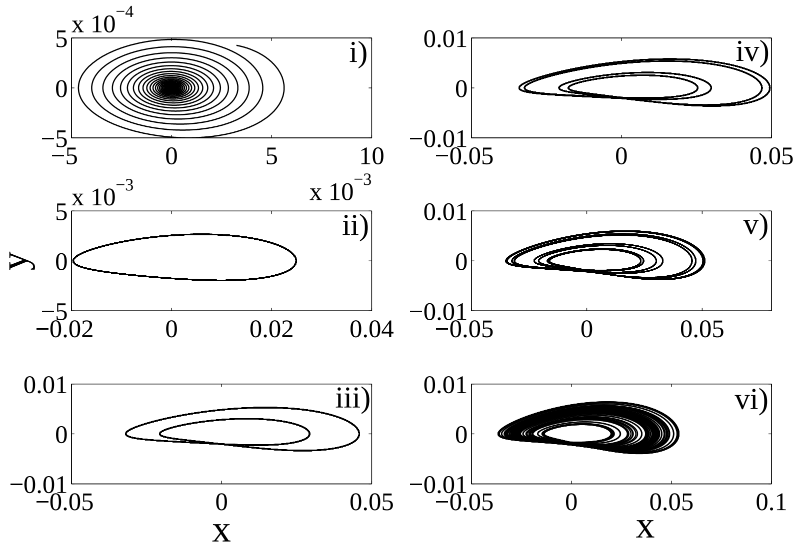

Figure 6.3: Phase space projection plots for different values of V: (i) -0.01400, (ii) -0.00900, (iii) -0.00550, (iv) -0.00525, (v) -0.00515, and (vi) -0.00500.

Now the fixed point of the system is shown in figure 6.4 as a function of parameter V with solid black circles as stable fixed point and open circles as unstable fixed point. This is shown on the basis of numerical calculation of eigenvalue λ. The fixed point (x_0, y_0, z_0)

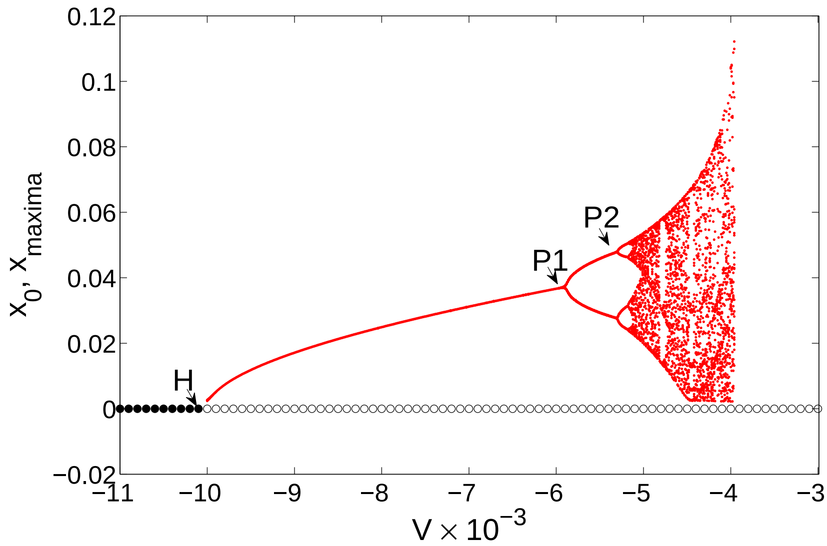

Figure 6.4: The x-component of fixed points, x_0, and the maxima of x as a function of parameter V with $a = 0.15$ and $b = 0.0015$.

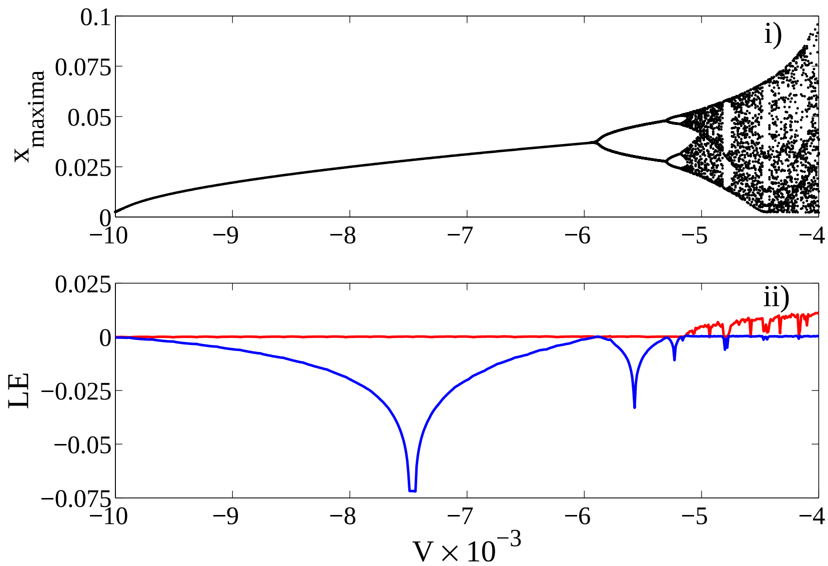

Figure 6.5: (i) Bifurcation diagram: the maxima of x as a function of parameter V and (ii) corresponding largest two Lyapunov exponents as a function of parameter V.

always exists as depicted in the figure. From numerical calculation, it is seen that real parts of complex conjugate eigenvalues change sign from negative to positive with the change of the parameter V. This indicates that a Hopf bifurcation takes place in the system. The maxima of x (x_{maxima}) are also plotted in the figure which shows that the stable fixed point becomes unstable and a limit cycle is created. The Hopf bifurcation (represented by a point H) occurs at $V = -0.01$ which is in agreement with the Routh-Hurwitz criterion discussed in section 6.4. Finally the chaotic dynamics appears due to period doubling bifurcation near P1, P2 etc.

Figure 6.5(i) exhibits an expanded view of the bifurcation diagram shown in figure 6.4. It shows x_{maxima} in the range of control parameter $V \in (-0.006, -0.004)$. The corresponding plot of Lyapunov exponents is shown in figure 6.5(ii). Lyapunov exponents clearly confirm the existence of periodic and chaotic trajectories.

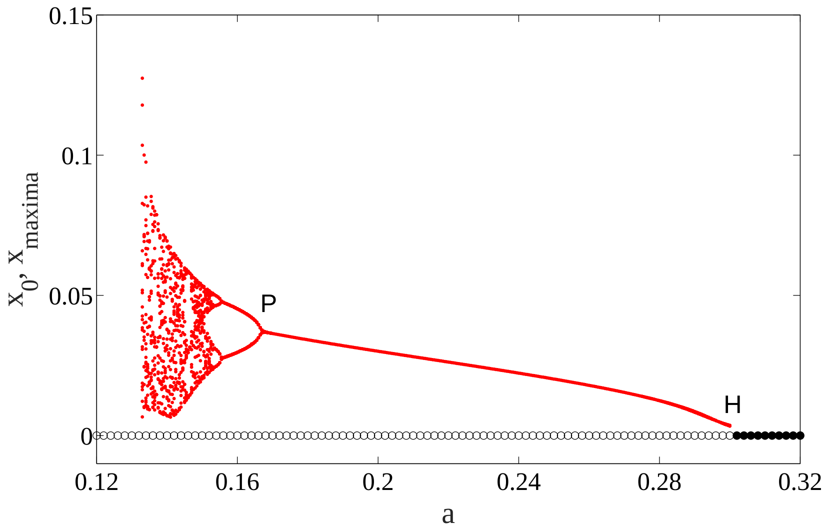

Figure 6.6: The x-component of fixed points, x_0, and the maxima of x as a function of parameter a with $V = -0.005$ and $b = 0.0015$.

For fixed values of b and V, the nature of the fixed point and the bifurcation diagram obtained using a as a control parameter is shown in figure 6.6. In this case, the system goes from chaos to order with increase in the value of a and is confirmed by plotting the corresponding Lyapunov exponents in figure 6.7.

In the search for chaotic flows of the system, another domain of the parameters is found to show a transition from chaos to order where a is used as bifurcation parameter keeping V and b constant. The nature of the equilibrium point with the bifurcation diagram is shown in figure 6.8 and the corresponding Lyapunov exponents are shown in figure 6.9.

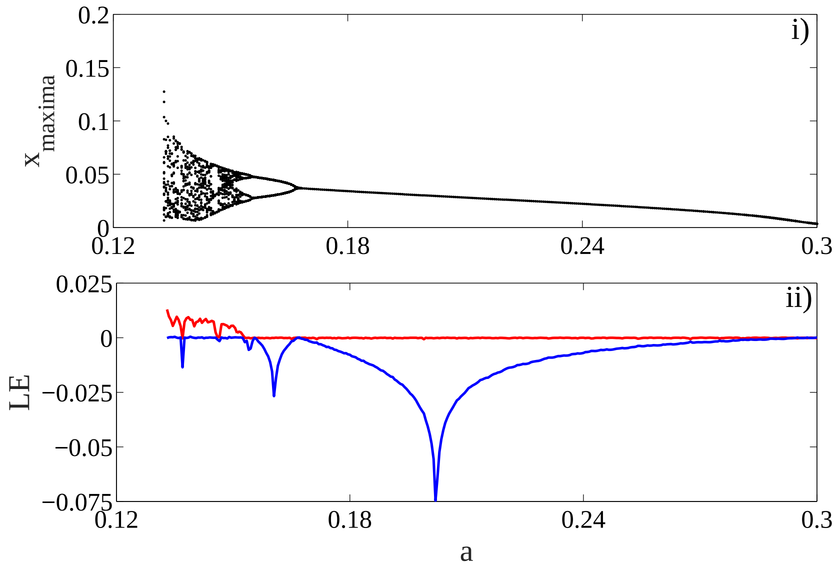

Figure 6.7: (i) Bifurcation diagram: the maxima of x as a function of parameter a and (ii) corresponding largest two Lyapunov exponents as a function of parameter a.

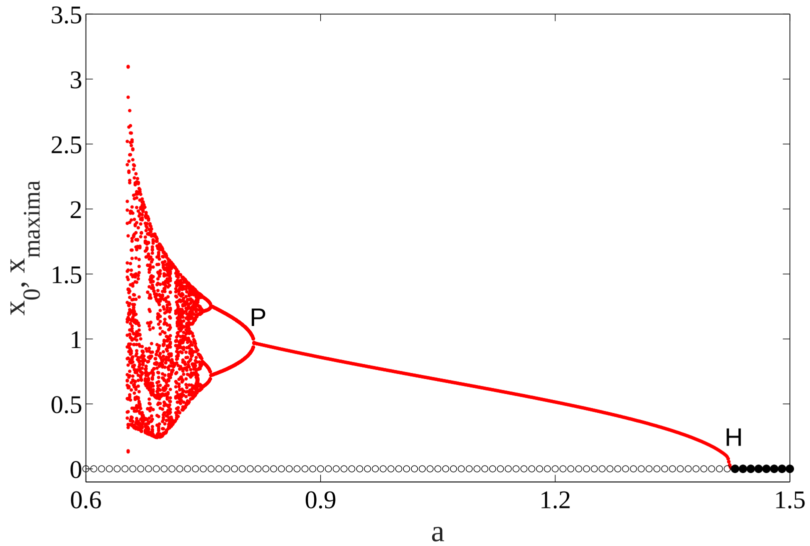

Figure 6.8: The x-component of fixed points, x_0, and the maxima of x as a function of parameter a with $V = -0.14$ and $b = 0.2$.

Figure 6.10 shows the nature of the fixed point and the bifurcation diagram obtained using b as a control parameter for fixed a and V. Here, also an order to chaos transition is observed with increase in b. Lyapunov exponents make the confirmation in figure 6.11.

The points of Hopf bifurcation in figure 6.6 and figure 6.10 are consistent with the values given in section 6.4.

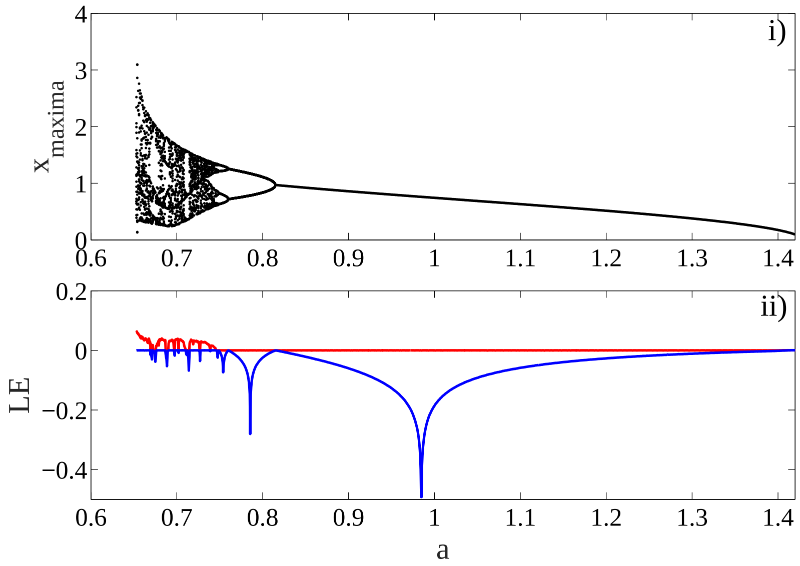

Figure 6.9: (i) Bifurcation diagram: the maxima of x as a function of parameter a and (ii) corresponding largest two Lyapunov Exponents as a function of parameter a.

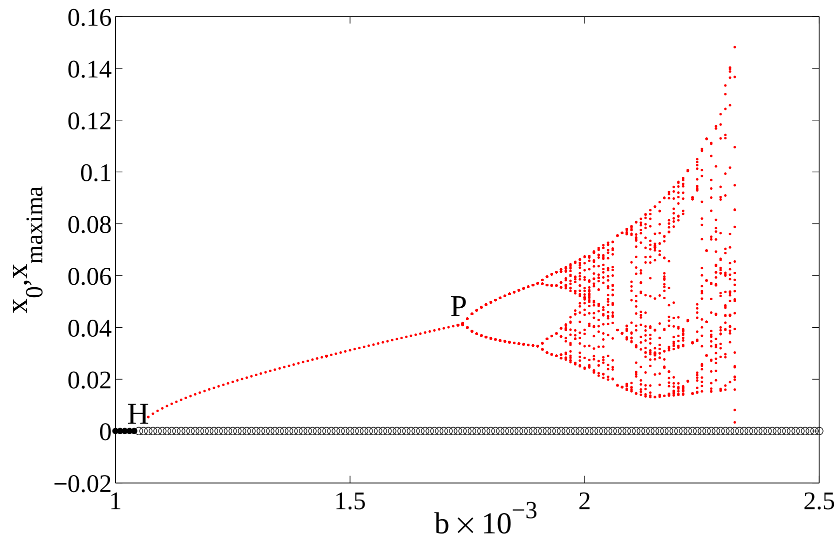

Figure 6.10: The x-component of fixed points, x_0, and the maxima of x as a function of parameter b with $V = -0.007$ and $a = 0.15$.

Figure 6.12 shows different dynamical features of the system and the corresponding bifurcation from one region to another in the a, V parameter space with constant b. Different dynamical forms are represented on this bifurcation diagram with different colors. It consists of three regions S, PD and US representing stable focus, limit cycle giving rise to order to chaos transition via period doubling route and unbound solutions

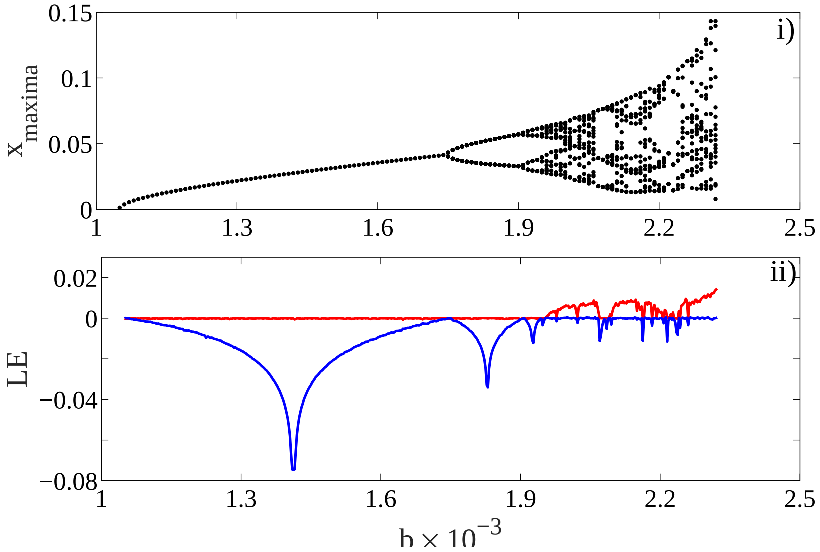

Figure 6.11: (i) Bifurcation diagram: the maxima of x as a function of parameter b and (ii) corresponding largest two Lyapunov Exponents as a function of parameter b.

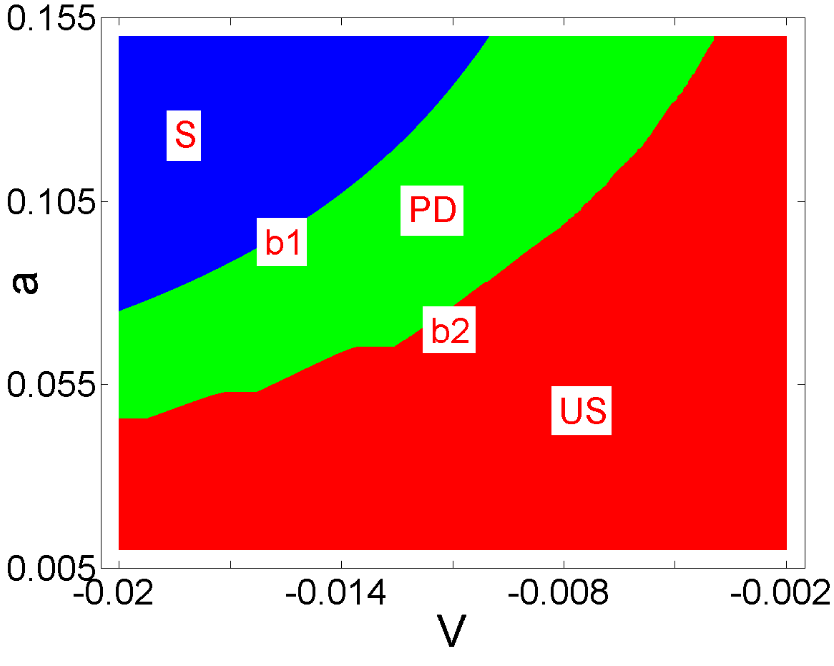

Figure 6.12: Bifurcation diagram showing different colors for different dynamical behavior in the a, V parameter space with fixed $b(= 0.0015)$.

respectively. The boundary b1 represents the transition from stable focus to limit cycle via Hopf bifurcation, whereas the boundary b2 represents the transition from bounded chaotic to unbound solution via crisis. Figure 6.13 exhibits the dynamical features and

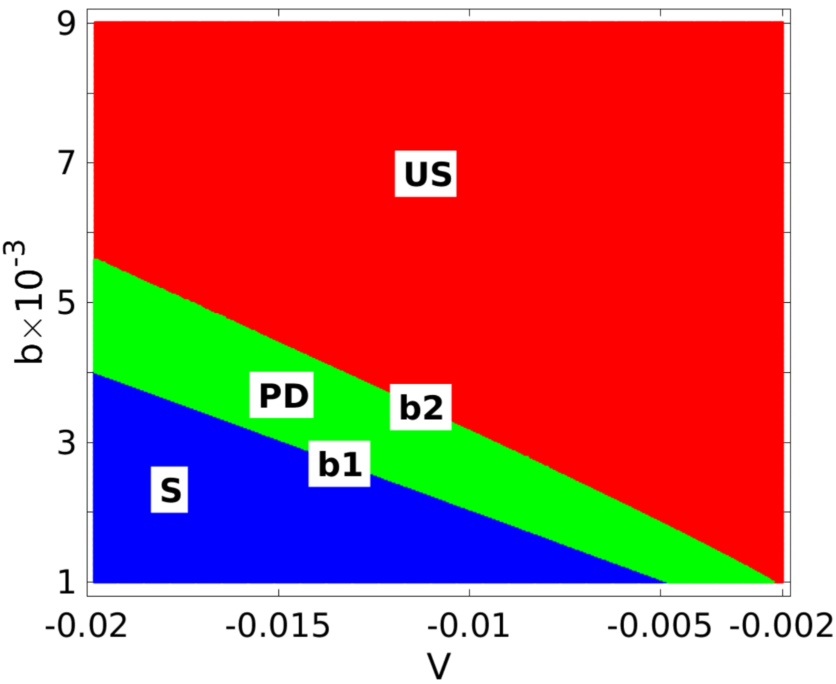

Figure 6.13: Bifurcation diagram showing different colors for different dynamical behavior in the b, V parameter space with fixed $a(= 0.15)$.

the corresponding bifurcation in the b, V parameter space with constant a.

6.6 Summary

The KdV equation in presence of Burger and a linear term that are representative of dissipative effects is treated as a third order ordinary differential equation known as the jerk equation. For general boundary conditions, the KdV equation without dissipative effects supports both left and right moving periodic traveling waves known as cnoidal waves. In presence of Burger term, when treated as a second order equation, the KdV equation supports dissipative solutions that are saddle-node heteroclinic orbits that exist due to the presence of two critical points in the system. The third order jerk equation considered in this work has only a line of fixed points along the x-axis and does not support shock like solutions for $b = 0$. The presence of collisional dissipative terms in the fluid model leads to the term with the coefficient 'b'in the jerk equation. Because of this term, it is not possible to reduce the equation to a second order one, as is done conventionally. Therefore, the traveling wave solutions of the equation are studied by using numerical methods. For left moving traveling waves, the third order system undergoes a supercritical Hopf bifurcation which implies the appearance of a limit cycle. The stable limit cycle loses stability with the change of the parameters to form limit cycles of period two, four, eight and so on giving rise to a period doubling bifurcation route to chaos, whereas the same system does not undergo a Hopf bifurcation for traveling wave solutions moving towards right.

Appendix

The characteristic equation at the equilibrium point $O(0,0,0)$ for the system [equation (6.7)] is

$$\lambda^3 + a\lambda^2 - V\lambda + b = 0 \tag{6.10}$$

Taking $\lambda = \mu - a/3$, the above equation can be written as

$$\mu^3 + p\mu + q = 0 \tag{6.11}$$

where $p = -V - \frac{a^2}{3}$, $q = b + aV/3 + 2a^3/27$.

Define

$$X = (-\frac{q}{2} + \sqrt{\Delta})^{1/3}, Y = (-\frac{q}{2} - \sqrt{\Delta})^{1/3}$$

with $\Delta = (\frac{q}{2})^2 + (\frac{p}{3})^3$. For real values of p and q, and $\Delta > 0$, the characteristic equation gives one real root and two complex roots which are given as

$$\begin{aligned}
\lambda_1 &= X + Y - \frac{a}{3} \\
\lambda_2 &= -\frac{1}{2}(X+Y) + i\frac{\sqrt{3}}{2}(X-Y) - \frac{a}{3} \\
\lambda_3 &= -\frac{1}{2}(X+Y) - i\frac{\sqrt{3}}{2}(X-Y) - \frac{a}{3}
\end{aligned} \tag{6.12}$$

CHAPTER 7

Conclusions

The characteristics of regular and chaotic magnetic fields together with their influence on the dynamics of charged particles have been studied in the present thesis with dynamical system tools. While collective effects are important in the study of magnetized plasmas, the dynamics of field lines and charged particles can also shed considerable light on the plasma behavior. In this respect, the characterization of magnetic field lines in connection with their transport from the point of view of nonlinear dynamics is an important topic. The field line equations corresponding to the deterministic Beltrami magnetic fields like those of the turbulent magnetic fields are also non-integrable in $3-D$ and lead to chaotic field lines. Although the solutions for the Beltrami magnetic fields in $3-D$ Cartesian coordinate system are monochromatic in space, the presence of chaotic field lines act as a precursor to real turbulence. A single field line of ABC field can be space filling within some subspace of a $3-D$ region. At the same time, there are ordered tube like regions embedded in the chaotic surroundings. In some regions, the magnetic field lines starting infinitesimally close to one another will diverge exponentially in future, i.e. the field lines have positive Lyapunov exponents. This behavior is also the characteristic of the turbulent flows occurring in nature. The study of Beltrami states was later extended to observe the properties of the field lines for the double curl equation. It has been found that the double curl equation can be used to model high beta magnetic configurations in the laboratory. The field lines for certain solutions of double curl Beltrami field are embedded densely in a volume leading to a fully chaotic phase space.

The random behavior of complex nonlinear processes can be governed by deterministic equations. The dynamical system which corresponds to the evolution of magnetic field lines exhibits a great variety of behaviors and thus provides a kinetic description of chaotic dynamics. There is a fundamental difference between the chaotic dynamics of uniformly chaotic systems and those possessing mixed phase space. Stickiness is an important phenomena in a mixed phase space and it corresponds to dynamical trapping during which a chaotic trajectory might show a regular behavior. Stickiness of chaotic trajectories to some specific domains in a mixed phase space leads to anomalous diffusion of field lines. In the circumstances of stickiness phenomena, analysis of asymptotic distance Lyapunov exponent for the whole trajectory may not give the correct value corresponding to the dynamics of the trajectory because of the presence of a combination of regularity and chaoticity. However, finite distance Lyapunov exponents are evaluated by dividing the entire trajectory into shorter length segments that represent either chaotic or regular behavior and is a more suitable measure for studying a sticky trajectory. On the other hand, uniform chaoticity of trajectories over the entire space leads to normal diffusion of field lines. Anomalous diffusion of field lines supports a bimodal probability distribution for a chaotic trajectory and long tail in the recurrence length distribution, whereas the probability distribution of a single trajectory in case of normal diffusion is unimodal and the recurrence length distribution consists of a rapidly decaying curve. The important aspect of the studies present in this thesis is that many of these results obtained in the context of discrete maps have also been verified in a chaotic system governed by differential equations.

The cross field diffusion is one of the most interesting aspects in a variety of magnetized astrophysical and laboratory plasmas and chaotic magnetic field lines can lead to spatial transport of particles across the ambient large scale magnetic field. Together with the presence of a uniform magnetic field, certain solutions of double curl Beltrami field display mixed as well as completely chaotic phase space with variation in the relative strength of the fluctuation. So in this respect, the present situation has some analogy with the phase space behavior of turbulent magnetic fields. Initially, when the fluctuating field is very small compared to the mean field, the field lines are mostly confined to surfaces. As the relative strength of the fluctuation increases, the field lines are no longer confined only to surface, but occupy a finite volume in space. This type of transition from order to chaos in connection with the destruction of magnetic surfaces by magnetic field irregularities [96, 97] is a well established fact in the context of plasma physics. The statistical behavior of the field lines is reflected by the diffusion scaling exponent. When the configuration leads to a mixed phase space, the trapping phenomena, which corresponds to a localized movement in the surface of section, leads to weak chaos where the chaotic field lines have smaller contribution to the transport than in case of fully chaotic scenario. In any real systems like magnetic confinement devices used in thermonuclear fusion research, stochasticity may not be often fully developed in the whole plasma volume, but with stochastic regions intermixed with islands remnants. The figures [98] of the diverted magnetic field lines of the tokamak ITER, obtained through numerical simulations, indicate that the stickiness reduces the field line transport to the divertor plates. The anomalous transport is associated with a distribution of field line displacements which is power law rather than Gaussian. The diffusion characteristics of the field lines are evidenced by computing another statistical property namely kurtosis whose asymptotic values are supportive of the transport scaling exponents. The motion of charged particles in a magnetic field is quite different from that of the field lines. The transport laws of the particles depends on their energies. When the Larmor radii of the particles are smaller than the scale length of magnetic field inhomogeneity, the particle dynamics is relatively less complex than the case with larger Larmor radii of the particles compared to the scale length of magnetic field inhomogeneity. All the above observations indicate that the deterministic ABC-type magnetic fields can form simple heuristic model for studying several transport regimes and can be used to model various realistic configurations since many results obtained in the context of turbulence, have been verified considering such fields.

Besides the $3-D$ magnetic fields, many physical systems can be modeled using simple $1-D$ magnetic fluctuations as a preliminary attempt. $1-D$ magnetic field variation in terms of slab turbulence with fluctuation of the order of mean field forms one component of the solar wind magnetic field. The slab model in which the fluctuations are transverse to a locally uniform mean magnetic field and vary only in the direction along that mean field is consistent of Alfvén waves propagating parallel to the large scale field. In this thesis, we have made an attempt of studying the energization of charged particles in presence of a slab like chaotic magnetic field configuration in which the fluctuating parts are obtained from coupled nonlinear equations varying in $1-D$. If at least one spatial coordinate is cyclic in the description of an arbitrary electromagnetic field, charged particles remain forever tied to a particular magnetic field line [99] and this fact prevent any meaningful discussion of the perpendicular diffusion of charged particles. The transport characteristics of field lines and charged particles considering more realistic fluctuating fields [100] with dependence on three spatial coordinates will be attempted in future.

The final topic of the thesis is the study of regular and chaotic magnetic fields obtained from KdV type equation. KdV equation is a paradigm equation for the formation of localized concentrations of magnetic field in a plasma. Slow and fast mode waves in electron magnetohydrodynamic plasmas can be obtained as solutions of $1-D$ KdV equation and such waves propagate as left moving magnetic holes and right moving magnetic field upsurges respectively [101]. In presence of dissipative effects, the study of KdV equation treated as a third order jerk equation, points to the existence of chaotic solutions for appropriate parameter ranges. One interesting feature of this equation is that the chaotic solutions are shown to arise in the absence of any external harmonic perturbation.

The studies carried out in the present thesis reveal that the magnetic fields resulting as solutions of various linear and nonlinear equations occurring in the context of space, astrophysical and laboratory plasmas can exhibit regular and chaotic behavior. A variety of dynamical features demonstrated by chaotic magnetic fields are investigated in the light of various phenomena observed in plasmas.

Bibliography

[1] “Self-organization processes in continuous media”, A. Hasegawa, *Advances in Physics*, **1985**, *34*, 1—42.

[2] “Relaxation of toroidal plasma and generation of reverse magnetic fields”, J. B. Taylor, *Physical Review Letters*, **1974**, *33*, 1139—1141.

[3] “Minimum dissipation rates in magnetohydrodynamics ”, D. Montgomery, L. Phillips, *Physical Review A*, **1988**, *38*, 2953—2964.

[4] “Determination of minimum-dissipation states with self-consistent resistivity in magnetized plasmas”, R. Farengo, J. R. Soběhart, *Physical Review E*, **1995**, *52*, 2102—2105.

[5] “Variational principles and self-organization in two-fluid plasmas”, Z. Yoshida, S. M. Mahajan, *Physical Review Letters*, **2002**, *88*, 095001-1—095001-4.

[6] “On a plasma sheath separating regions of oppositely directed magnetic field”, E. G. Harris, *IL Nuovo Cimento*, **1962**, *23*, 115—121.

[7] “Chaotic magnetic fields in Vlasov-Maxwell equilibria”, A. Ghosh, M. S. Janaki, B. Dasgupta, A. Bandyopadhyay, *Chaos*, **2014**, *24*, 013117-1—013117-4.

[8] “Kraftfreie Magnetfelder. Mit 4 Textabbildungen”, R. Lüst, A. Schlüter, *Zeitschrift fur Astrophysik*, **1954**, *34*, 263.

[9] "On force-free magnetic fields", S. Chandrasekhar, *Proceedings of the National Academy of Sciences of the United States of America*, **1956**, *42*, 1—5.

[10] "On force-free magnetic fields", S. Chandrasekhar, L. Woltjer, *Proceedings of the National Academy of Sciences of the United States of America*, **1958**, *44*, 285—289.

[11] "The Navier-Stokes equations: a classification of flows and exact solutions", P. G. Drazin, N. Riley, *Cambridge University Press*, **2006**.

[12] "Velocity-vorticity patterns in turbulent flow", R. B. Pelz, V. Yakhot, S. A. Orszag, L. Shtilman, E. Levich, *Physical Review Letters*, **1985**, *54*, 2505—2508.

[13] "On the helical nature of three-dimensional coherent structures in turbulent flows", A. Tsinober, E. Levich, *Physics Letters A*, **1983**, *99*, 321—324.

[14] "A theorem on force-free magnetic fields", L. Woltjer, *Proceedings of the National Academy of Sciences of the United States of America*, **1958**, *44*, 489—491.

[15] "The spectrum of the curl operator on spherically symmetric domains", J. Cantarella, D. DeTurck, H. Gluck, M. Teytel, *Physics of Plasmas*, **2000**, *7*, 2766—2775.

[16] "Eigenfunctions of the curl in cylindrical geometry", E. C. Morse, *Journal of Mathematical Physics*, **2005**, *46*, 113511-1—113511-13.

[17] "Eigenfunctions of the curl operator in spherical coordinates", G. F. Torres del Castillo, *Journal of Mathematical Physics*, **1994**, *35*, 499—507.

[18] "Heating of coronal arcades by magnetic tearing turbulence, using the Taylor-Heyvaerts hypothesis", P. K. Browning, E. R. Priest, *Astronomy and Astrophysics*, **1986**, *159*, 129—141.

[19] "Laboratory simulations of solar prominence eruptions", P. M. Bellan, J. F. Hansen, *Physics of Plasmas*, **1998**, *5*, 1991—2000.

[20] "Magnetic field generation in electrically conducting fluids", H. K. Moffatt, *Cambridge University Press*, **1978**.

[21] "Double curl Beltrami flow: diamagnetic structures", S. M. Mahajan, Z. Yoshida, *Physical Review Letters*, **1998**, *81*, 4863—4866.

[22] "On chaotic wave patterns in periodically forced steady-state KdVB and extended KdVB equations", E. A. Cox, M. P. Mortell, A. V. Pokrovskii, O. Rasskazov, *Proceedings of the Royal Society A*, **2005**, *461*, 2857—2885.

[23] "Damping of solitary waves", E. Ott, R. N. Sudan, *The Physics of Fluids*, **1970**, *13*, 1432—1434.

[24] "Sur la topologie des écoulements stationnaires des fluides parfaits", V. I. Arnold, *Vladimir I. Arnold-Collected Works*, **1965**, 15—18.

[25] "New solutions of the kinematic dynamo problem", S. Childress, *Journal of Mathematical Physics*, **1970**, *11*, 3063—3076.

[26] "Chaotic streamlines in the ABC flows", T. Dombre, U. Frisch, J. M. Greene, M. Hénon, A. Mehr, A. M. Soward, *Journal of Fluid Mechanics*, **1986**, *167*, 353—391.

[27] "Transport in chaotic magnetic fields", F. Holguin, **2016**.

[28] "Random walk of magnetic lines of force in astrophysics", J. R. Jokipii, E. N. Parker, *Physical Review Letters*, **1968**, *21*, 44—47.

[29] "Random walk of magnetic field-lines for different values of the energy range spectral index", A. Shalchi, I. Kourakis, *Physics of Plasmas*, **2007**, *14*, 112901-1—112901-6.

[30] "Random walk of magnetic field lines: subdiffusive, diffusive, and superdiffusive regimes", A. Shalchi, B. Weinhorst, *Advances in Space Research*, **2009**, *43*, 1429—1435.

[31] "Effective plasma heat conductivity in braided magnetic field-I. Quasi-linear limit", M. B. Isichenko, *Plasma Physics and Controlled Fusion*, **1991**, *33*, 795—807.

[32] "Spatial structure and field-line diffusion in transverse magnetic turbulence", W. H. Matthaeus, P. C. Gray, D. H. Pontius, Jr., J. W. Bieber, *Physical Review Letters*, **1995**, *75*, 2136—2139.

[33] "Scaling of field-line random walk in model solar wind fluctuations", P. C. Gray, D. H. Pontius, Jr., W. H. Matthaeus, *Geophysical Research Letters*, **1996**, *23*, 965—968.

[34] "Magnetic field line transport in three dimensional turbulence: Lévy random walk and spectrum models", P. Pommois, G. Zimbardo, P. Veltri, *Physics of Plasmas*, **1998**, *5*, 1288—1297.

[35] "Anomalous, quasilinear, and percolative regimes for magnetic-field-line transport in axially symmetric turbulence", G. Zimbardo, P. Veltri, P. Pommois, *Physical Review E*, **2000**, *61*, 1940—1948.

[36] "Anomalous diffusion of field lines and charged particles in Arnold-Beltrami-Childress force-free magnetic fields", A. K. Ram, B. Dasgupta, V. Krishnamurthy, D. Mitra, *Physics of Plasmas*, **2014**, *21*, 072309-1—072309-12.

[37] "Transport of cosmic rays in chaotic magnetic fields", F. Casse, M. Lemoine, G. Pelletier, *Physical Review D*, **2001**, *65*, 023002-1—023002-15.

[38] "Diffusion and drift of cosmic rays in highly turbulent magnetic fields", J. Candia, E. Roulet, *Journal of Cosmology and Astroparticle Physics*, **2004**, *2004*, 007-1—007-14.

[39] "The development of magnetic field line wander in gyrokinetic plasma turbulence: dependence on amplitude of turbulence", S. Bourouaine, G. G. Howes, *Journal of Plasma Physics*, **2017**, **83**, 905830301-1—905830301-22.

[40] "Magnetic field line random walk in isotropic turbulence with zero mean field", W. Sonsrettee, P. Subedi, D. Ruffolo, W. H. Matthaeus, A. P. Snodin, P. Wongpan, P. Chuychai, *The Astrophysical Journal*, **2014**, *798*, 59-1—59-10.

[41] "Dynamical traps", G. M. Zaslavsky, *Physica D*, **2002**, *168*, 292—304.

[42] "Weak chaos and Poincaré recurrences for area preserving maps", N. Buric, A. Rampioni, G. Turchetti, S. Vaienti, *Journal of Physics A*, **2003**, *36*, L209—L215.

[43] "Recurrence time statistics for finite size intervals", E. G. Altmann, E. C. Da Silva, I. L. Caldas, *Chaos*, **2004**, *14*, 975—981.

[44] "Hypothesis of strong chaos and anomalous diffusion in coupled symplectic maps", E. G. Altmann, H. Kantz, *EPL (Europhysics Letters)*, **2007**, *78*, 10008-p1—10008-p5.

[45] "Multifractality, stickiness, and recurrence-time statistics", C. V. Abud, R. E. de Carvalho, *Physical Review E*, **2013**, *88*, 042922-1—042922-6.

[46] "Characterizing weak chaos using time series of Lyapunov exponents", R. M. da Silva, C. Manchein, M. W. Beims, E. G. Altmann, *Physical Review E*, **2015**, *91*, 062907-1—062907-7.

[47] "Statistical characterization of discrete conservative systems: the web map", G. Ruiz, U. Tirnakli, E. P. Borges, C. Tsallis, *Physical Review E*, **2017**, *96*, 042158-1—042158-10.

[48] "Finite-time Lyapunov spectrum for chaotic orbits of non-integrable Hamiltonian systems", J. D. Szezech Jr., S. R. Lopes, R. L. Viana, *Physics Letters A*, **2005**, *335*, 394—401.

[49] "Connection between recurrence-time statistics and anomalous transport", G. M. Zaslavsky, M. K. Tippet, *Phys. Rev. Lett.*, **1991**, *67*, 3251—3254.

[50] "Introduction to plasma physics and controlled fusion", F. F. Chen, *Springer*, **1984**.

[51] "Chaos and nonlinear dynamics of single-particle orbits in a magnetotaillike magnetic field", J. Chen, P. J. Palmadesso, *Journal of Geophysical Research*, **1986**, *91*, 1499—1508.

[52] "Charged particle transport and energization by magnetic field fluctuations with Gaussian/non-Gaussian distributions", P. Shustov, A. Artemyev, E. Yushkov, *Physics Letters A*, **2015**, *379*, 590—594.

[53] "Dynamics of charged particle motion in the vicinity of three dimensional magnetic null points: energization and chaos", A. Gascoyne, *Physics of Plasmas*, **2015**, *22*, 032907-1—032907-11.

[54] "Stochastic ion heating in a field-reversed configuration geometry by rotating magnetic fields", S. A. Cohen, A. S. Landsman, A. H. Glasser, *Physics of Plasmas*, **2007**, *14*, 072508-1—072508-12.

[55] "Particle energization through time-periodic helical magnetic fields", D. Mitra, A. Brandenburg, B. Dasgupta, E. Niklasson, A. K. Ram, *Physical Review E*, **2014**, *89*, 042919-1—042919-5.

[56] "Relaxation and magnetic reconnection in plasmas", J. B. Taylor, *Reviews of Modern Physics*, **1986**, *58*, 741—763.

[57] "Magnetohydrodynamics of plasma relaxation", S. Ortolani, D. D. Schnack, *World Scientific*, **1993**.

[58] "Simultaneous Beltrami conditions in coupled vortex dynamics", Z. Yoshida, S. M. Mahajan, *Journal of Mathematical Physics*, **1999**, *40*, 5080—5091.

[59] "Relaxed states in relativistic multifluid plasmas", J. Pino, H. Li, S. Mahajan, *Physics of Plasmas*, **2010**, *17*, 112112-1—112112-7.

[60] "Multi-fluid systems—multi-Beltrami relaxed states and their implications", S. M. Mahajan, M. Lingam, *Physics of Plasmas*, **2015**, *22*, 092123-1—092123-9.

[61] "Temperature-transformed minimal coupling: magnetofluid unification", S. M. Mahajan, *Physical Review Letters*, **2003**, *90*, 035001-1—035001-4.

[62] "The relativistic electro-vortical field—revisiting magneto-genesis and allied problems", S. M. Mahajan, *Physics of Plasmas*, **2016**, *23*, 112104-1—112104-12.

[63] "Scale hierarchy created in plasma flow", Z. Yoshida, S. M. Mahajan, S. Ohsaki, *Physics of Plasmas*, **2004**, *11*, 3660—3664.

[64] "Formation and primary heating of the solar corona: theory and simulation", S. M. Mahajan, R. Miklaszewski, K. I. Nikolskaya, N. L. Shatashvili, *Physics of Plasmas*, **2001**, *8*, 1340—1357.

[65] "Quasi-stationary chaotic states in multi-dimensional Hamiltonian systems", C. Antonopoulos, T. Bountis, V. Basios, *Physica A*, **2011**, *390*, 3290—3307.

[66] "Field-reversed configuration (FRC) as a minimum-dissipative relaxed state", R. Bhattacharyya, M. S. Janaki, B. Dasgupta, *Physics Letters A*, **2001**, *291*, 291—295.

[67] "Numerical investigation of perpendicular diffusion of charged test particles in weak magnetostatic slab turbulence", R. L. Mace, W. H. Matthaeus, J. W. Bieber, *The Astrophysical Journal*, **2000**, *538*, 192—202.

[68] "Test particle energization by current sheets and nonuniform fields in magnetohydrodynamic turbulence", P. Dmitruk, W. H. Matthaeus, N. Seenu, *The Astrophysical Journal*, **2004**, *617*, 667—679.

[69] "Chaotic structures of nonlinear magnetic fields I: theory", N. C. Lee, G. K. Parks, *Geophysical Research Letters*, **1992**, *19*, 637—640.

[70] "Interaction of solitons in a collisionless plasma and the recurrence of initial states", N. J. Zabusky, M. D. Kruskal, *Physical Review Letters*, **1965**, *15*, 240—243.

[71] "One-dimensional flow of liquids containing small gas bubbles", L. v. Wijngaarden, *Annual Review of Fluid Mechanics*, **1972**, *4*, 369—396.

[72] "A non-linear equation incorporating damping and dispersion", R. S. Johnson, *Journal of Fluid Mechanics*, **1970**, *42*, 49—60.

[73] "Solitary waves in large blood vessels", S. Yomosa, *Journal of the Physical Society of Japan*, **1987**, *56*, 506—520.

[74] "Dynamics of solitary blood waves in arteries with prostheses", S. Noubissie, P. Woafo, *Physical Review E*, **2003**, *67*, 041911-1—041911-8.

[75] "Propagation of an ion-acoustic soliton in an inhomogeneous plasma", H.-Y. Chang, S. Raychaudhuri, J. Hill, E. K. Tsikis, K. E. Lonngren, *The Physics of Fluids*, **1986**, *29*, 294—297.

[76] "Unified shock profile in a plasma", H. Grad, P. N. Hu, *The Physics of Fluids*, **1967**, *10*, 2596—2602.

[77] "Nonlinear theory of ion acoustic waves with Landau damping", E. Ott, R. N. Sudan, *The Physics of Fluids*, **1969**, *12*, 2388—2394.

[78] "Chaotic behaviour of nonlinear waves and solitons of perturbed Korteweg-de Vries equation", K. B. Blyuss, *Reports on Mathematical Physics*, **2000**, *46*, 47—54.

[79] "Solitons in action", K. E. Lonngren, A. C. Scott, *New York: Academic*, **1978**.

[80] "Spatial chaos in weakly dispersive and viscous media: a nonperturbative theory of the driven KdV-Burgers equation", M. A. Malkov, *Physica D*, **1996**, *95*, 62—80.

[81] “Periodic and chaotic behaviour in a reduction of the perturbed Korteweg-de Vries equation”, R. Grimshaw, X. Tian, *Proceedings of the Royal Society of London A*, **1994**, *445*, 1—21.

[82] “Low-dimensional chaos in a perturbed Korteweg-de Vries equation”, X. Tian, R. H. J. Grimshaw, *International Journal of Bifurcation and Chaos*, **1995**, *5*, 1221—1233.

[83] “Periodic and chaotic behaviour in a reduced form of the perturbed generalized Korteweg-de Vries and Kadomtsev-Petviashvili equations”, Q. Cao, K. Djidjeli, W. G. Price, E. H. Twizell, *Physica D*, **1999**, *125*, 201—221.

[84] “Chaos for a damped and forced KdV equation”, M. Cabral, R. Rosa, *Physica D*, **2004**, *192*, 265—278.

[85] “Bifurcation and chaos in a perturbed soliton equation with higher-order nonlinearity”, J. Yu, R. Zhang, G. Jin, *Physica Scripta*, **2011**, *84*, 065004-1—065004-6.

[86] “Question # 38. What is the simplest jerk function that gives chaos?”, H. P. W. Gottlieb, *American Journal of Physics*, **1996**, *64*, 525—525.

[87] “Some simple chaotic flows”, J. C. Sprott, *Physical review E*, **1994**, *50*, R647—R650.

[88] “Some simple chaotic jerk functions”, J. C. Sprott, *American Journal of Physics*, **1997**, *65*, 537—543.

[89] “EMHD theory and observations of electron solitary waves in magnetotail plasmas”, X.-F. Ji, X.-G. Wang, W.-J. Sun, C.-J. Xiao, Q.-Q. Shi, J. Liu, Z.-Y. Pu, *Journal of Geophysical Research*, **2014**, *119*, 4281—4289.

[90] “Weierstrass traveling wave solutions for dissipative Benjamin, Bona, and Mahony (BBM) equation”, S. C. Mancas, G. Spradlin, H. Khanal, *Journal of Mathematical Physics*, **2013**, *54*, 081502-1—081502-15.

[91] "Traveling wave solutions to Kawahara and related equations", S. C. Mancas, *Differential Equations and Dynamical Systems*, **2017**, 1—19.

[92] "Stability of cnoidal waves", J. A. Pava, J. L. Bona, M. Scialom, *Advances in Differential Equations*, **2006**, *11*, 1321—1374.

[93] "A solitary-wave solution to a perturbed KdV equation", M. A. Allen, G. Rowlands, *Journal of Plasma Physics*, **2000**, *64*, 475—480.

[94] "Traveling wavetrains in the complex cubic-quintic Ginzburg-Landau equation", S. C. Mancas, S. R. Choudhury, *Chaos, Solitons and Fractals*, **2006**, *28*, 834—843.

[95] "Elements of applied bifurcation theory", Y. A. Kuznetsov, *Springer*, **1998**.

[96] "Destruction of magnetic surfaces by magnetic field irregularities", M. N. Rosenbluth, R. Z. Sagdeev, J. B. Taylor, G. M. Zaslavski, *Nuclear Fusion*, **1966**, *6*, 297—300.

[97] "Destruction of magnetic surfaces by magnetic field irregularities: part II", N. N. Filonenko, R. Z. Sagdeev, G. M. Zaslavsky, *Nuclear Fusion*, **1967**, *7*, 253—266.

[98] "Magnetic field line stickiness in tokamaks", C. G. L. Martins, M. Roberto, I. L. Caldas, *IEEE Transactions on Plasma Science*, **2014**, *42*, 2764—2765.

[99] "Charged-particle motion in electromagnetic fields having at least one ignorable spatial coordinate", F. C. Jones, J. R. Jokipii, M. G. Baring, *The Astrophysical Journal*, **1998**, *509*, 238—243.

[100] "Evidence for the presence of quasi-two-dimensional nearly incompressible fluctuations in the solar wind", W. H. Matthaeus, M. L. Goldstein, D. A. Roberts, *Journal of Geophysical Research*, **1990**, *95*, 20673—20683.

[101] "An EMHD soliton model for small-scale magnetic holes in magnetospheric plasmas", Z.-Y. Li, W.-J Sun, X.-G. Wang, Q.-Q. Shi, C.-J. Xiao, Z.-Y. Pu, X.-F. Ji, S.-T. Yao, S.-Y. Fu, *Journal of Geophysical Research*, **2016**, *121*, 4180—4190.